Fabrication of Ultra-High Molecular Weight Polyethylene by MgO-Supported Ziegler-Natta Catalyst

YUSUKE BANDO

Japan Advanced Institute of Science and Technology

Doctoral Dissertation

Fabrication of Ultra-High Molecular Weight Polyethylene by MgO-Supported Ziegler-Natta Catalyst

Yusuke Bando

Supervisor: Professor Dr. Toshiaki Taniike

Graduate School of Materials Science

Japan Advanced Institute of Science and Technology

March 2019

Referee-in-chief: **Associate Professor Dr. Toshiaki Taniike**
Japan Advanced Institute of Science and Technology

Referees: **Professor Dr. Shinya Maenosono**
Japan Advanced Institute of Science and Technology

Associate Professor Dr. Shinohara Ken-ichi
Japan Advanced Institute of Science and Technology

Senior Lecturer Dr. Shun Nisimura
Japan Advanced Institute of Science and Technology

Professor Dr. Hideki Kurokawa
Saitama University

Preface

The present dissertation is the result of the studies under the direction of Associate Professor Dr. Toshiaki Taniike during 2015 - 2019. The purpose of this dissertation is to fabrication of ultra-high molecular weight polyethylene (UHMWPE) with MgO supported Ziegler-Natta catalyst. The first chapter is a general introduction according to the object of this study. Chapter 2 shows the small size UHMWPE synthesis using $MgO/MgCl_2/TiCl_4$ core-shell nano catalyst. Chapter 3 shows the 1 μm size UHMWPE particles synthesis using nano-dispersed Ziegler-Natta catalyst. Chapter 4 shows the good moldability UHMWPE particles synthesis using a catalyst prepared with MgO as a building block. The last chapter summarizes the conclusive items of this dissertation.

Yusuke Bando

Taniike Laboratory

School of Materials Science,

Japan Advanced Institute of Science and Technology

Contents

Chapter 3

Nano-dispersed Ziegler-Natta catalysts for 1 μm-sized ultra-high molecular weight polyethylene particles

Chapter 4

Preparation of Multigrained MgO-Supported Ziegler-Natta Catalyst via Spray Dry Method

Chapter 5

General Conclusion

Chapter 1

General Introduction

1.1. Introduction

Polyolefin is one of general purpose plastics consists of only of hydrogen and carbon that does not contain any harmful substance such as chlorine and aromatic compounds. Therefore, recycling and reuse of polyolefin are easier than other materials, and they are low environmental impact materials [1]. Also, since its characteristics as a material are inexpensive, lightweight, high melting point, high chemical resistance, high strength, excellent mechanical properties, and high moldability, the application range is used automotive parts, package, and containers. It has been demanded further development of polyolefin material in the future as well [2]

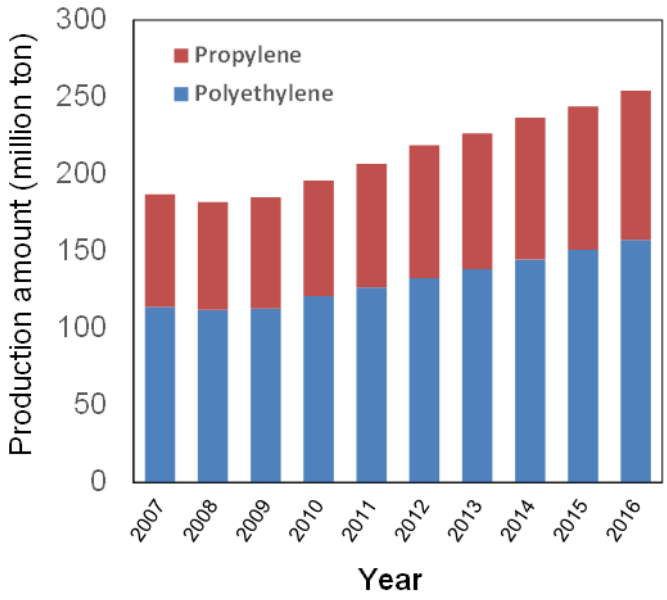

Figure 1 Production volume of polyolefin

1.2. Polyethylene

Polyethylene is a polymer having a structure, in which ethylene is basically linearly polymerized. It has the most straightforward chemical structure among polymers, and it is used for various applications in the world including containers and packaging films. The basic skeleton consists only of repeating methylene, but differences in average molecular weight, number of branches, crystallinity, *etc*. differ depending on the manufacturing method, and density, thermal properties, mechanical properties, *etc*. are also different accordingly. In general, substances with low molecular weight are swollen by hydrocarbon solvents, but those with high molecular weight are excellent in chemical resistance. It is also excellent in electric insulation.

1.2.1. History of Polyethylene

Polyethylene was adventitiously synthesized as a waxy solid from the pyrolysis of diazomethane by Pechmann in 1898 [3]. It was later confirmed by Bamberger and Tschirner to be polyethylene (low-density polyethylene).

Eric William Fawcett and Reginald Oswald Gibson of the ICI company in the United Kingdom in 1933 discovered a way to polymerize ethylene by heating ethylene to high temperature and pressure [4]. After that, industrial production began at the beginning

of 1940 by the du Pont Company and UCC Company of the United States. This polymerizes ethylene at a pressure as high as 1000 atmospheres or higher, so it is called high pressure polyethylene. Polyethylene obtained by this production method is also called low density polyethylene (LDPE) because of its low density [5].

Meanwhile, in the early 1950s Robert Banks of Philips Petroleum of America and J. Paul Hogan developed a method to polymerize ethylene at 30-100 atm. In 1953, ethylene polymerization at atmospheric pressure became possible by Karl Ziegler of the Max Planck petroleum coal research institute in West Germany, and the production cost drastically decreased. Polyethylene synthesized by these two production methods is collectively called medium and low pressure polyethylene. It is also called high density polyethylene (HDPE) because it can obtain high density compared to low density polyethylene.

Later on, Mitsui Petrochemical (1970) and, by UCC in the United States (1977) synthesized polyethylene different from conventional medium and low pressure polyethylene. Since this polyethylene is called a third polyethylene and is a low density polyethylene obtained by copolymerizing a large amount of linear polyethylene with an α-olefin containing a large amount of short side chain, thus called linear low density (LLDPE) It is also called.

1.2.2. Types and Characteristics of Polyethylene

The molecular structure of polyethylene is greatly affected by its production method. Polyethylene has a simple crystal structure, but characteristics are greatly affected by the number and structure of branches of the polymer chain. Therefore, it is mainly classified into LDPE, HDPE, and LLDPE (Figure 2).

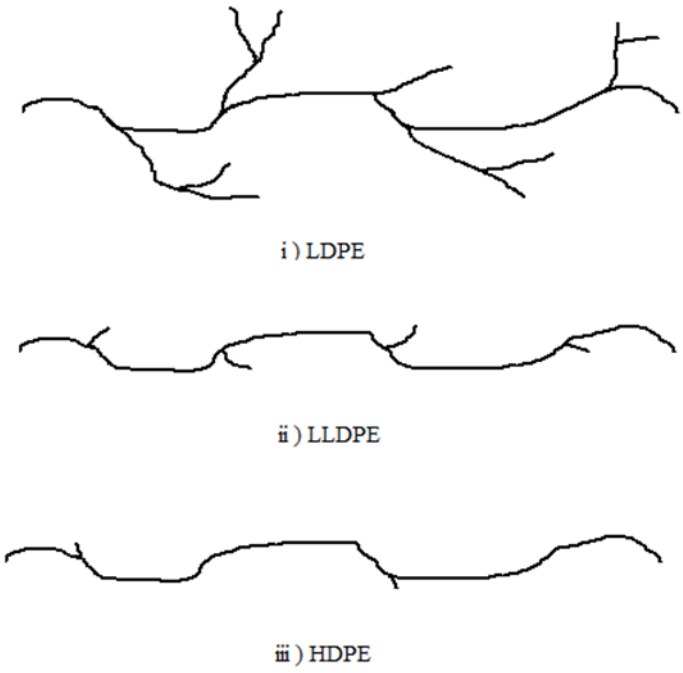

Figure 2 Structure of polyethylene

Table 1 Characteristics of various PE [6]

	Density ($g \cdot cm^{-3}$)	Melting point (°C)	Crystallinity (%)
LDPE	0.915-0.930	106-120	40-60
LLDPE	0.910-0.940	120-125	40-60
HDPE	0.940-0.965	125-135	65-80

LDPE has a structure with many long chain branching, and its degree of crystallinity is low, and the spread of molecules in solution is small. On the other hand, HDPE is linear with few branches, and therefore has a higher degree of crystallinity than LDPE and widens the molecule in solution. Unlike LDPE, LLDPE has a low density but a linear structure and is synthesized by copolymerization with an α-olefin, so that it is possible to control the number and length of branching with α-olefin. Therefore, it is an intermediate structure between LDPE and HDPE. Since the LLDPE is linear, the spread of molecules in solution is about as wide as HDPE.

Generally, polyethylene having a molecular weight of several hundred to several hundreds of thousands are produced on an industrial scale. Those whose molecular weight has been increased to several million or more will be distinguished from each other, they are classified as ultra-high molecular weight polyethylene (UHMWPE).

UHMWPE is structurally similar to HDPE and is a linear polymer with few branches, but its molecular weight has been increased to several million or more. Therefore, the entanglement of the molecular chains is large, the melt viscosity is extremely high, and the fluidity is poor.

1.2.3. Ultra-High Molecule Weight Polyethylene

UHMWPE has excellent properties such as high chemical resistance and light weight of polyethylene, improved impact resistance, high wear resistance, and self-lubricating property [7]. Therefore, it is classified as an engineering plastic. Because of having such excellent properties, it is added to rubber, cosmetics, *etc.*, and it is used for artificial implants, bulletproof vests, chemical pumps, and the like [8]. However, since UHMWPE has a very high molecular weight, entanglement of molecular chains is large, it shows extremely high melt viscosity and low fluidity. As a result, it is impossible to be peretallized. Moreover, general molding methods such as extrusion and blowing cannot be used for UHMWPE, requiring special molding methods such as compression and ram extrusion [8]. In these molding methods, the polymer particles directly obtained by the polymerization are thermally fused as they are. However, since UHMWPE melts the surface of the particles even when heat is applied, delamination due

to uneven structure formed by grain boundary formed at the time of molding and bonding failure between particles is problematic [9]. Industrially, UHMWPE is synthesized by slurry polymerization with Ziegler-Natta catalyst [10,11].

1.2.4. Chain Entanglement of UHMWPE

The molding process of UHMWPE is almost impossible to use conventional methods such as injection molding due to the very high melt viscosity [12]. Therefore, it is processed by powder metallurgy such as sintering. This process requires knowledge of the diffusion mechanism of very long molecules and is necessary to improve the mechanical properties and durability of the sintered part. In the sintering of the polymer powder, initially, densification of the powder concerning particle wetting takes place. In the case of a semi crystalline polymer, it is efficiently carried out below the melting temperature [13]. Next, cross-crystallization is performed by re-crossing due to diffusion of polymer chains at the particle interface. At this stage, the polymer particles melt and time and temperature play an important role [14].

The diffusion mechanism of polymer chains is generally explained by reptation [15]. Reptation is also used to explain the mechanism of crack sealing and polymer chain diffusion of welding [16–19]. Reptation strongly depends on the molecular weight of

the polymer. Also, it is influenced by the mutual penetration distance of polymer chains during fusion, which depends on the temperature and time of sintering. Co-crystallization is the growth of new microcrystals across the interface bonding the original powder particles. The final mechanical properties of the semicrystalline sintered body depend on the reconfiguration of the entwining network and the formation of the crystal network in the interface region of the sintered powder [20–22].

In the case of UHMWPE, there is the consequence that sintering depends much more on temperature than time. Also, it is said that a long diffusion time is not necessary in order to impart high ductility to the bonding interface and sintered powder. The ultimate mechanical properties of the sintered UHMWPE are dominated by the formation of crystal networks in the interfacial region of the sintered powder rather than a reconfiguration of the entangled network. These results indicate that there is a phenomenon that enables polymer chain diffusion and crossing in a much shorter time than Reptation [23–26]. It is explained by the melting explosion phenomenon which actively promotes the diffusion of polymer chains. This phenomenon has been demonstrated by molding UHMWPE crystallized in a solvent, and it has been shown that the bulk properties recover much sooner than the predicted time. It has been confirmed that this phenomenon also appears in UHMWPE powder. During the melt explosion

process, the entanglement of chains from adjacent particles due to the lateral movement of the initially entangled polymer chain loops is much faster than the encounters of the ends at both ends along that tube, It promotes recovery of the bulk properties at a much shorter time scale than the long chain reaction time [27–29].

1.3. Polymerization Catalyst

Current polyolefin industry consists of various technologies such as catalyst, manufacturing process, molding process, additives etc. The catalyst for polymerizing olefins is a heterogeneous catalyst such as a Ziegler-Natta catalyst and a Phillips catalyst, and a homogeneous catalyst such as a metallocene catalyst, which is an organometallic complex containing cyclopentadienyl anion. Among them, Ziegler-Natta catalyst, in particular, has excellent characteristics such as high activity, high stereo specificity, wide molecular weight distribution, excellent polymer morphology, low cost. Therefore, it is an important catalyst not only used for many propylene polymerizations but also for a synthesis of high-density polyethylene and linear low-density polyethylene.

Table 2 Characteristic of HDPE

Catalyst type	M_w/M_n	Number of long chain branches (/10000 carbon)
Phillips catalyst	6-15	*ca.* 1
Ziegler-Natta catalyst	3-6	0
Metallocene catalyst	2-3	0-1

However, the correlation between the structure and performance of Ziegler-Natta catalyst is not well understood, and the guiding principle of development is difficult to stand. Therefore, catalyst development is carried out by preparing a catalyst and conducting a polymerization performance test. Repeated try-and-error is being carried out in an inefficient way of obtaining a catalyst with good performance. Therefore, it is strongly desired industrially to elucidate the correlation between the structure and performance of the catalyst. Ziegler-Natta catalyst has been developed for nearly 60 years, but related technological development and basic research are vigorously carried out.

1.3.1. Ethylene Polymerization Catalyst

Polyethylene is classified according to its density and production method. LDPE is polymerized by ethylene polymerization using a chromium catalyst or Ziegler-Natta catalyst or copolymerization of a small amount of comonomer with ethylene by LDPE by radical polymerization under high temperature and pressure, and HDPE is added and more comonomer is added to copolymerize LLDPE is obtained. A Phillips catalyst which is one of the chromium based catalysts is prepared by depositing chromium oxide on a silica · alumina carrier and heating it in a gas flow of oxygen, nitrogen, carbon

dioxide or the like to activate it. Ziegler-Natta catalyst uses titanium as an active species, and magnesium chloride is used as a carrier.

1.3.2. History of Ziegler-Natta Catalyst

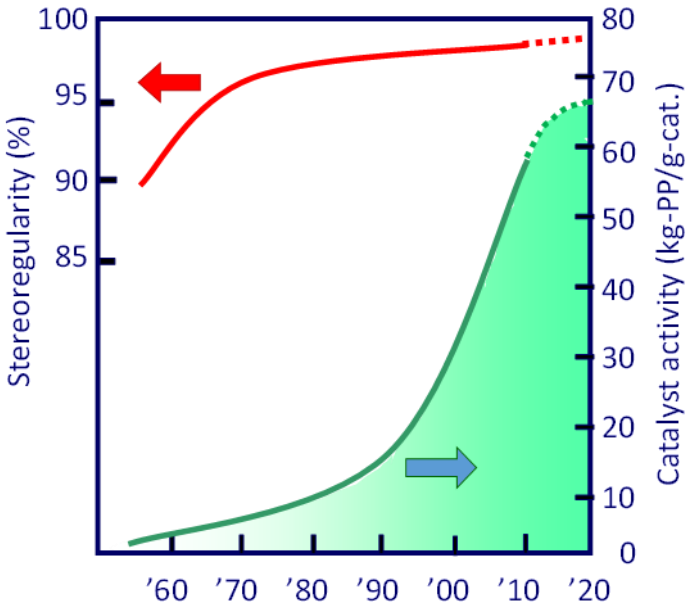

Figure 3 History of performance improvement of Ziegler-Natta catalyst

In 1953, Karl Ziegler succeeded ethylene polymerization under normal temperature and pressure by using $TiCl_4/AlR_3$ which is a mixture of titanium tetrachloride and an organoaluminum compound as a catalyst [30]. Then in 1954 Giulio Natta successfully synthesized a polypropylene with an isotactic content of 30 to 40% with a similar catalyst

system [31]. Synthesis of polypropylene with a high isotactic content of 80 to 90% was achieved by $TiCl_3/AlR_3$ catalyst using titanium trichloride instead of soluble titanium tetrachloride. The $TiCl_3/AlEt_2Cl$ catalyst initially used in ethylene polymerization had activity of about 2 to 3 kg-PE/g-Ti

In 1963 Solvay Company in Belgium succeeded in greatly improving the activity by immobilizing and supporting titanium tetrachloride utilizing the surface hydroxyl group of hydroxy chloride magnesium chloride [32]. This made it possible to omit the catalyst removal step. It was realized for the first time when the decalcification process was placed on an industrial plant. Then in the late 1960s Magnesium chloride-loaded Ziegler-Natta catalyst was developed by Montecatini of Italy and Mitsui Petrochemical. This catalyst is still used for polyethylene production.

In the case of polymerization of propylene, control of stereospecificity and regiospecificity other than polymerization activity is required for the catalyst. When the active species is titanium Propylene polymerization usually proceeds with 1,2-addition. Therefore, the 2,1-addition hardly progressed and it is not necessary to consider position specificity. On the other hand, about 10% of atactic polypropylene is formed as a by-product. For this reason, research to improve stereospecificity was done from the late 1950's. As a result, in 1972 Solvay Company extracted β-type titanium trichloride with

isoamyl ether and reacted with titanium tetrachloride to obtain δ-type titanium trichloride. It succeeded in obtaining a catalyst complex having a large surface area, porosity and very high activity. This catalyst is called Solvay $TiCl_3$, the polymerization activity is improved, and by-production of atactic polypropylene can also be suppressed to about 3 to 4%. Solvay $TiCl_3$ is the first example of a second generation catalyst. Improvements have been repeated thereafter, and it is still used in some manufacturing processes now.

The third generation Ziegler-Natta catalyst has combined an electron donating compound typified by ethyl benzoate as a third component, was developed by Montecatini and Mitsui Petrochemical Industries in 1971-1974. As a method for preparing this catalyst, there is a method of co-grinding magnesium chloride, titanium tetrachloride and an external donor complex, and a method of treating a co-pulverized product of $MgCl_2$ and ED with $TiCl_4$ heated and then washing with an organic solvent. The characteristic of this catalyst system is that there is no need decalcification because of its high activity. $AlEt_3$-ED-based activators come to be used instead of $AlEt_2Cl$ for propylene polymerization. From 1980 to 1981 it was found that the specific combination of ED used for solid catalyst preparation and ED used during polymerization is important. As an example it was found that introduction of organic acid diester into

$MgCl_2/TiCl_4$ catalyst and addition of alkoxysilane compound during polymerization gave excellent stereospecificity. However, it was necessary to remove atactic polypropylene by 6 to 10% of the whole depending on usage conditions. Therefore, catalyst development has focused on finding a more efficient combination of catalyst preparation and a more effective combination of electron donating compounds.

Later, in the early 1980s a new combination of electron donor compounds was discovered. Catalyst preparation is carried out using an alkyl phthalate compound as an internal donor. The catalyst was developed in which alkoxysilane compounds or silyl ether compounds are added as external donors during polymerization. This catalyst system had better balance between productivity and stereospecificity than ethylbenzoate system. This catalyst system was originally called ultra-high activity third generation type catalyst. However, it was later called the fourth-generation Ziegler-Natta catalyst because it used a completely different electron-donating compound from the third-generation Ziegler-Natta catalyst. In the latter half of the 1980's, a new type of electron donor compound, 1,3-diether compound, was used. When used as an internal donor component, it exhibits extremely high activity and stereospecificity without requiring any external Lewis base. This catalyst system is called a fifth generation catalyst.

1.3.3. Catalyst Preparation Method

Since 1970, $MgCl_2$-supported Ziegler-Natta catalyst had been developed, not only aiming for higher activity catalyst but also stabilization of active behavior and morphology control of obtained polymer had become required. Therefore, a method of preparing a catalyst having a better form was developed. The method for preparing $MgCl_2$ -based Ziegler-Natta catalyst can be broadly divided into three main preparation methods. They are called co-grinding method, dissolution precipitation method and chemical reaction method, respectively.

In the co-grinding method, a catalyst component is pulverized using a ball mill. As the characteristics of the particles obtained by the co-grinding method, the catalyst form cannot be controlled because it is pulverized, it has a nonuniform and irregular form, and a catalyst with a wide particle size distribution can be obtained. In addition, the polymerization performance of this catalyst behaves such that the activity immediately decreases after rapid activation at the beginning of polymerization. Since the form of the catalyst is heterogeneous, there is a feature that the polymer form obtained becomes worse. However, since it is simple and inexpensive compared to other preparation methods, it had been mainly used in the early stage of development of $MgCl_2$ supported Ziegler-Natta catalyst. Since the problem of the form of a polymer obtained and the

activity behavior are not stable, it was possible to use it in slurry polymerization, but because it is not suitable for gas phase polymerization or bulk polymerization with higher productivity, the frequency of use was diminished. It is currently used industrially as a very small part of slurry polymerization.

In the dissolution-precipitation method, a solution of a magnesium compound such as $MgCl_2$ or $Mg(OR)_2$, $Mg(OCOR)_3$, MgR, magnesium silylamide compound is prepared using alcohol, trialkyl phosphate or the like as a solvent [33]. Treating the solution with a halogenating agent to precipitate $MgCl_2$, treating it with an internal donor and $TiCl_4$, or mixing an internal donor with a solution and treating it with $TiCl_4$ to obtain a catalyst component. It is possible to obtain catalysts whose morphology is controlled by this method. Further, by halogenating the solution with $TiCl_4$, the catalyst component can be obtained in one step, which is a cost saving and saving process. The characteristic of this catalyst is that the surface is smooth and the bulk density is high. Polymer particles having a high bulk density and a small amount of fine powder can be obtained. Since this catalyst has strong particle strength, it retains its particle shape even when it is used for high productivity polymerization methods such as gas phase polymerization and bulk polymerization. Therefore, it is used industrially favorably and is one of the most used catalyst preparation methods. The chemical reaction method treats solid $Mg(OR)_2$ or

Mg(OR)Cl and an internal donor in aromatic or halogenated solvent with an excess of $TiCl_4$. $MgCl_2$ is produced by the reaction of the magnesium compound with $TiCl_4$ [34]. The by-product $Ti(OR)_4$ is removed by washing to obtain a catalyst component. It is possible to obtain catalysts whose morphology is controlled by this method. The form of the Mg compound as the reaction precursor become the form of catalyst particles. Therefore, the catalyst form can be controlled by controlling the form of the Mg compound used. Industrially, $Mg(OEt)_2$ is prepared by a method of converting $Mg(OEt)_2$ to $MgCl_2$ with a halogenating agent. The catalyst obtained by this method has a form of $Mg(OEt)_2$ as a catalyst form. Therefore, it is easy to control the form of the catalyst particle. This catalyst has high activity and excellent copolymerization performance. Further, since it is easy to control the form, it is often used for study of catalyst form. Industrially, prepolymerization is necessary, but it can be used for gas phase polymerization and bulk polymerization. It is often used when copolymerization performance is required as compared with dissolution precipitation method.

1.4. Structure of $MgCl_2$ Supported Ziegler-Natta Catalyst

The Ziegler-Natta catalyst is generally composed of $MgCl_2$ as a carrier, $TiCl_4$ as a catalyst, and a donor for controlling stereoregularity. From the 3rd generation Ziegler-Natta catalyst and later, $MgCl_2$ has used as a carrier material to achieve a drastic improvement in activity. This is because not only an increase in the active surface like the general catalyst system but also an electron donating effect on the active species has been exerted.

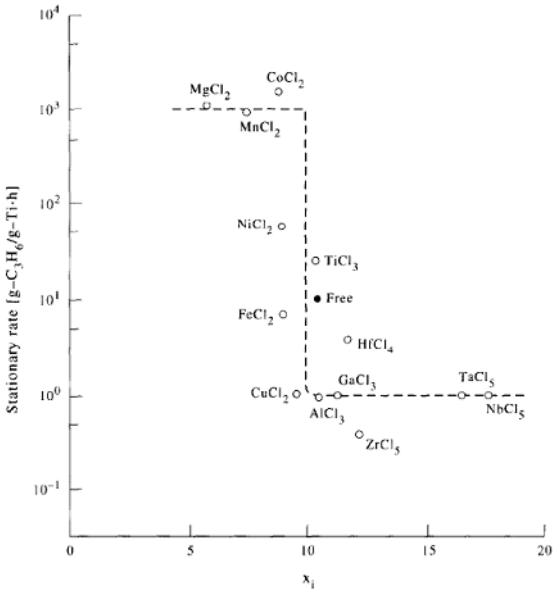

Figure 4 Relationship between activity of polymerization and electronegativity of support [35]

Soga investigated the influence on the activity of various metal chlorides in propylene polymerization, indicating that there is a correlation between electronegativity and activity. Among the metal chlorides, $MgCl_2$ has the lowest electronegativity and high activity. From this fact, magnesium chloride is most frequently used as a carrier in the Ziegler-Natta catalyst. The crystal structure of $TiCl_4$ and $MgCl_2$ are similar in hexagonal system and the ion radii of Ti_4^+ (0.68 Å) and Mg_2^+ (0.65 Å) are about the same. It is believed that Ti, Cl atom enters the defective part of the $MgCl_2$ crystal of the catalyst.

1.4.1. Structure of $MgCl_2$

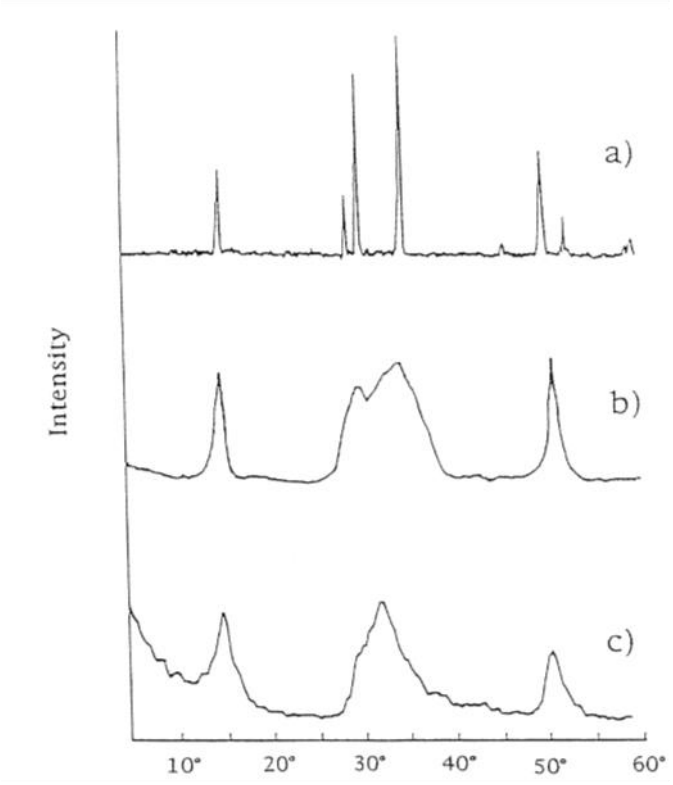

Figure 5 XRD pattern of various $MgCl_2$;

(a) α -$MgCl_2$ (b) δ-$MgCl_2$ activated from α -$MgCl_2$ by ballmilling,

(c) δ-$MgCl_2$ activated α -$MgCl_2$ by chemical reaction method [36]

$MgCl_2$ has two kinds of crystal structures, a commercial α type, and an unstable β type . The α type has a $CdCl_2$ type crystal structure. A structure in which magnesium ions are arranged in gaps of octahedrons in which chlorine ions are arranged in a face centered cubic lattice structure, takes a layered structure in which a layer of magnesium ions is

sandwiched between layers of chloride ions. The β type has a hexagonal close-packed packing structure [37]. Actually, the crystal structure of magnesium chloride used for Ziegler-Natta catalyst is activated to δ-$MgCl_2$ [38,39]. In this crystal structure, the layer of the Cl-Mg-Cl structure shows an irregular structure due to the transition and rotation, and the crystal size is about several tens of nm [40]. In the X-ray spectrum, a halo pattern is shown between the cubic structure and the hexagonal close-packed structure.

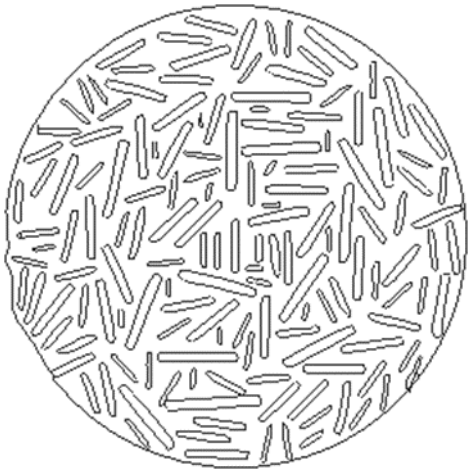

Figure 6 Structure model of MgCl2-supported ZN catalysts

Zannetti showed a model of metal chloride which was closely packed with Cl ions in the layered structure which was continuously disordered and overlapped [41]. This model is compatible with the experimental X-ray spectrum and it can be considered that the activated $MgCl_2$ is composed of very small lamella. It is known that (100) and (110)

planes are preferentially exposed on the catalyst surface, and Mg_2^+ ions having various degrees of coordination unsaturation exist. Therefore, activated $MgCl_2$ is considered to be aggregates of very small crystallites.

1.4.2. Catalyst Active Site

$TiCl_4$ is alkylated with TEA in the preparation of the catalytic system consisting of the first discovered TEA and $TiCl_4$. The produced ethyltitanium compound is unstable and releases ethane and ethylene to be reduced to $TiCl_3$ which is a trivalent titanium compound. Further, the generated $TiCl_3$ is similarly alkylated, the reduction reaction proceeds, and a divalent titanium compound is produced. Therefore, it is known that 4, 3, and 2 valence titanium compounds were produced. In this way, it is thought that a very complicated reaction is occurring in the Ziegler catalyst formation reaction process.

Activation of $MgCl_2$ supported Ziegler-Natta catalyst using TEA produces various atomically dispersed Ti(II) and Ti(III) species containing 3 to 5 ligands, these ligands being chloride and a mixture of ethyl ligands and contains 1 to 3 vacancies. In addition, it is known that small clusters of reduced Ti(III)XClY are formed during interaction with TEA. Among these species, catalytic sites containing Ti(II) have also been proposed for ethylene polymerization. The pentacoordinated Ti(III) atom fixed on the 110 face

characterized by the ethyl ligand and the open orientation is widely considered to be the active site of olefin polymerization [42–46].

1.4.3. Mechanism of Catalyst Reaction

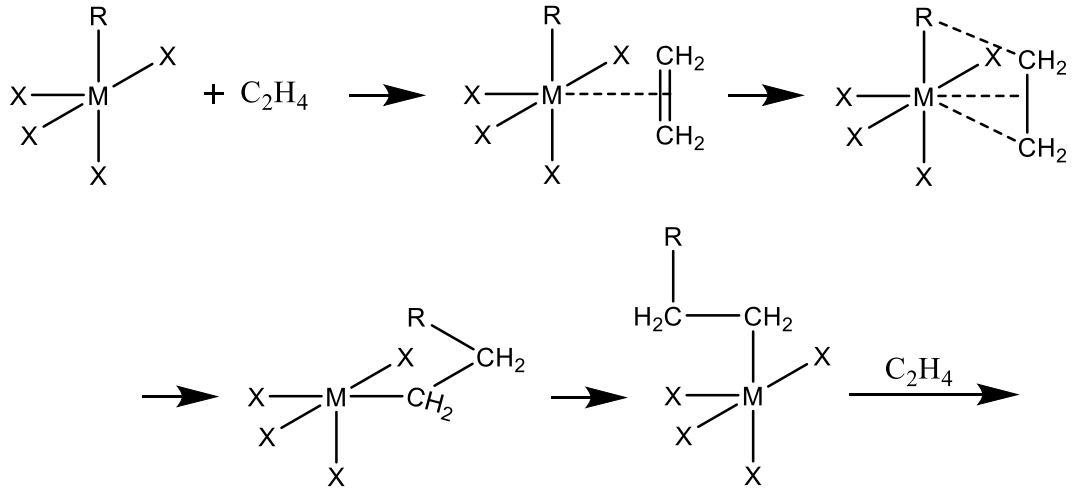

Figure 7 Ethylene polymerization

where M and R are Active metal and alkyl group, respectively

Chain growth reaction

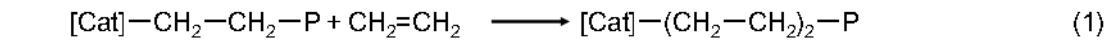

Chain termination and transfer reaction

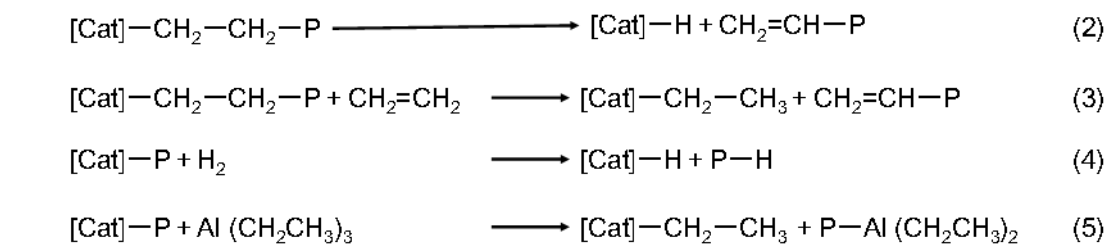

Figure 8　Elementary reactions of ethylene polymerization

The mechanism of the polymerization reaction is known as the mechanism of Coossee, and ethylene is first activated by coordinating to the ethylethane compound [47,48]. Next, it is thought that new ethylene is inserted between the ethyl group and titanium and the reaction starts.　Polymerization occurs by repeating new ethylene insertion again. As a termination reaction, there is a method by β-hydrogen elimination reaction, but the active point is not inactivated, new ethylene is added again and a new reaction is started. In addition, although it may be stopped by chain transfer reaction to ethylene, also in this case, new ethylene is inserted again and the reaction is started.　In addition to ethylene, hydrogen and alkylaluminum cause chain transfer reaction.　Chain transfer reaction by hydrogen is mainly used for controlling the molecular weight of polyethylene.

1.4.4. Polymer Particle Growth and Fragmentation of Catalyst

The growth of the polymer particles progresses by exposing the activation site by fragmentation of the catalyst particles. Therefore, it is possible to control the shape and size of polymer particles to some extent through the catalyst. Mainly, when homogeneous crushing of a catalyst or growth of a polymer occurs at each catalyst surface at a stable speed, it is well known as a replica phenomenon in which polymer particles reproduce physical properties such as the shape and structure of catalyst particles [49]. This phenomenon is related to how catalyst particles collapse and diffuse as polymerization progresses. Such growth is possible only when several conditions are met. The conditions are a high surface area, homogeneous high porosity, good mechanical strength enough to disintegrate during polymerization, homogeneous activity distribution, the fact that the monomer easily reaches the interior reaching the interior. Several single particle growth models are shown to understand the growth process of polymer particles [50–55]. The most common of these models is the multi grain model.

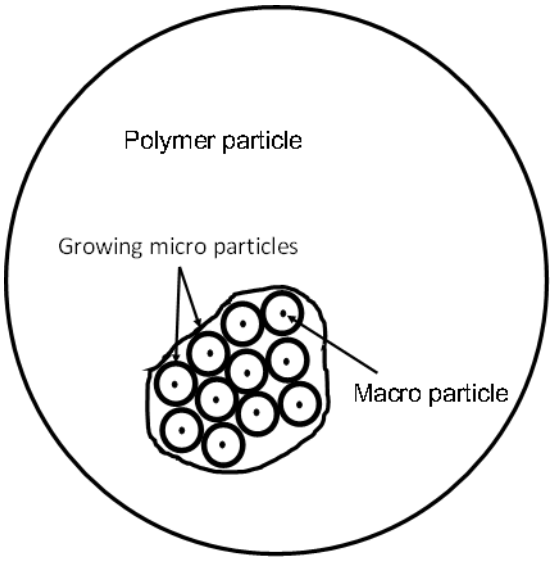

Figure 9　Schematic drawing multi grain model

Nagel first showed the multigrain model [56]. It was later expanded to include fragmentation by Laurence and Chiovetta, and mass and heat transfer were taken into account [57]. In this model catalyst particles are formed by aggregates of macro particles. Polymerization begins at the activation site on the macro particle surface and is surrounded by growing polymer. The growing polymer pushes out the previously generated polymer particles from within the microparticles. In this way, the polymer particles grow.

Many studies have been done to understand the process of fragmentation of catalyst particles. Regarding the porous carrier, catalytic activity abruptly increases at the start of polymerization, and a polymer is formed in the pores. As a result, monomer transport

to the catalytically active site is delayed, and a decrease in activity is caused. This deactivates may also occur due to inactivation of the catalyst by heating of the catalyst particles due to reaction heat at the beginning of the polymerization. It is known that fragmentation is affected by polymerization temperature. When the temperature is raised, the initial activity increases but persistence decreases. Fragmentation is observed to depend on the structure of the catalyst carrier. However, due to its complicated catalyst structure, it has not been fully elucidated yet.

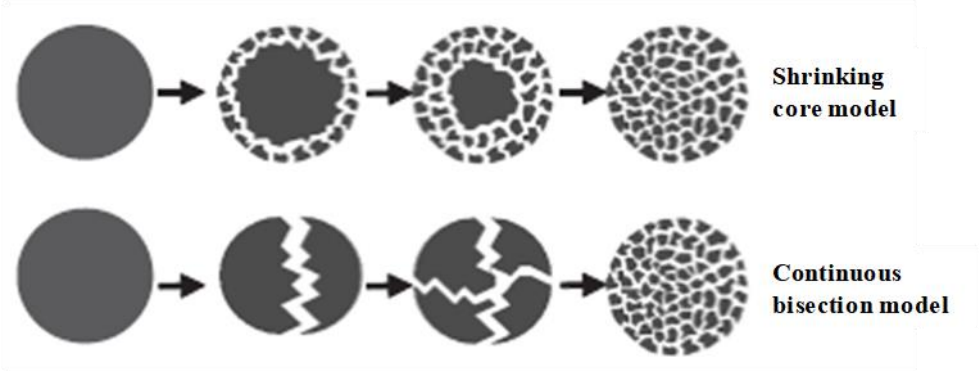

Figure 10 Two types of the fragmentation of catalyst [58]

It has been observed that the catalyst having low mechanical strength is mainly cracked, the distribution of fragmented size becomes uniform, and the form of the catalyst particle is sufficiently replicated. This mechanism of fragmentation is called Continuous bisection model. In this mechanism, since the porous catalyst can be broken easily, the

resistance of monomer transport is not essential, and almost no polymer is clogged in the pores. On the other hand, a catalyst having a relatively high mechanical strength using silica or a polymer as a carrier has low activity. This mechanism of fragmentation is called Shrinking core model. In this case, the catalyst particles are not easily broken, and the maximum of the outer layer pore is clogged with the polymer so that the spread of the monomer is delayed. Actual fragmentation is considered to progress simultaneously in these two models, and it is considered to be affected by monomers and polymerization conditions.

1.5. Objective of This Study

UHMWPE is excellent in impact strength, sliding property and abrasion resistance, and it is used for artificial hip joints and machine parts. In molding process of UHMWPE which is inferior in fluidity at the time of melting, a special method (compression or ram extrusion) using polymer powder is required, and defects due to particle interface are a problem. Also, the produced UHMWPE particles are hard and difficult to crush further finely by grinding. Therefore, UHMWPE with small particle size can only be obtained by controlling the particle size during polymerization. In the case of heterogeneous catalysts, it is known that the morphology of the polymer depends on the catalyst particles, and the size of the polymer is proportional to the catalyst particle size and polymerization activity used. Reducing the particle size of the polymer and narrowing the particle size distribution is one of the methods to solve problems such as defective joining of grain boundaries when performing compression molding. However, at present, there are many processes for preparing the Ziegler-Natta catalyst, and advanced techniques are necessary because the catalyst form changes due to multivariate factors. Catalyst preparation using magnesium oxide (MgO) nanoparticles can be easily prepared only by chlorinating the surface of MgO particles, and the particle morphology does not change before and after treatment. In addition, MgO nanoparticles are prepared by a build-up

method, and can obtain a nanometer size particle with narrow particle size distribution. Therefore, it is possible to obtain a catalyst having a small particle size and a narrow particle size distribution without going through complicated steps such as conventional Ziegler-Natta catalyst preparation. Hence, the MgO-supported Ziegler-Natta catalyst can be a very excellent catalyst which can easily obtain UHMWPE particles having a small particle size and narrow particle size distribution. In chapter 2, the agglomeration of the catalyst particles in the polymerization solvent was partially suppressed by treating the MgO surface with methyloleate. Polymerization using the catalyst successfully obtained UHMWPE particles, which shows a catalyst system featuring simpler and simpler preparation methods than conventional catalyst systems for synthesis of UHMWPE. In Chapter 3, successfully prepared a truly nano-dispersed Ziegler-Natta catalyst in a polymerization solvent by adding an appropriate organic modifier to the MgO surface. UHMWPE synthesized by this catalyst was 1-2 μm fine particles. The UHMWPE particles had significantly lower melting temperatures, resulting in several advantages in processing, such as enhanced bonding in compression molding. In Chapter 4, secondary aggregates of catalyst particles were formed using spray drying in order to improve catalyst handling. Two kinds of catalysts of different forms were prepared. Spherical particles could be obtained.

Reference

[1] C. Vasile, Handbook of Polyolefins, **2000**.

[2] P. Galli, G. Vecellio, *J. Polym. Sci. Part A Polym. Chem.*, **2004**, *42*, 396–415.

[3] H. v. Pechmann, *Berichte Der Dtsch. Chem. Gesellschaft*, **1898**, *31*, 2950–2951.

[4] E. W. Fawcett, R. O. Gibson, M. W. Perrin, J. G. Paton, E. G. Williams, GB 471590 19370906, **1937**.

[5] K.B. Sinclair, in:, Macromol. Symp., Wiley-Blackwell, **2001**, pp. 237–261.

[6] P.S. Chum, K.W. Swogger, *Prog. Polym. Sci.*, **2008**, *33*, 797–819.

[7] J. M. Kelly, *J. Macromol. Sci. Part C*, **2002**, *42*, 355–371.

[8] J. Furmanski, L.A. Pruitt, *Polymer*, **2007**, *48*, 3512–3519.

[9] T. Morikawa, F. Xu, K. Ninomiya, H. Matsuda, M. Yoshikawa, *Chem. Pharm. Bull. (Tokyo).*, **2004**, *52*, 494–497.

[10] R.L. Jones, M. Armoush, *Macromol. Symp.*, **2009**, *283–284*, 88–95.

[11] J.C. Somberg, J. Molnar, *Am. J. Ther.*, **2008**, *15*, 292–295.

[12] A.E. Likhtman, T.C.B. McLeish, *Macromolecules*, **2002**, *35*, 6332–6343.

[13] K. Al Jebawi, B. Sixou, R. Séguéla, G. Vigier, C. Chervin, *J. Appl. Polym. Sci.*, **2006**, *102*, 1274–1284.

[14] M. Bousmina, H. Qiu, M. Grmela, J.E. Klemberg-Sapieha, *Macromolecules*,

1998, *31*, 8273–8280.

[15] P.G. De Gennes, *J. Chem. Phys.*, **1971**, *55*, 572–579.

[16] P.G. De Gennes, *Tribol. Ser.*, **1981**, *7*, 355–367.

[17] R.P. Wool, K.M. O'Connor, *J. Appl. Phys.*, **1981**, *52*, 5953–5963.

[18] S. Prager, M. Tirrell, *J. Chem. Phys.*, **1981**, *75*, 5194–5198.

[19] K. Jud, H.H. Kausch, J.G. Williams, *J. Mater. Sci.*, **1981**, *16*, 204–210.

[20] S. Rastogi, D.R. Lippits, G.W.M. Peters, R. Graf, Y. Yao, H.W. Spiess, *Nat. Mater.*, **2005**, *4*, 635–641.

[21] D. Romano, N. Tops, E. Andablo-Reyes, S. Ronca, S. Rastogi, *Macromolecules*, **2014**, *47*, 4750–4760.

[22] Z. Bartczak, P.F.M. Beris, K. Wasilewski, A. Galeski, P.J. Lemstra, in:, J. Appl. Polym. Sci., Wiley-Blackwell, **2012**, pp. 4155–4168.

[23] Y.-Q. Xue, *, and T. A. Tervoort, P.J. Lemstra, **1998**,.

[24] C.W.M. Bastiaansen, H.E.H. Meyer, P.J. Lemstra, *Polymer*, **1990**, *31*, 1435–1440.

[25] P.J. Barham, D.M. Sadler, *Polymer*, **1991**, *32*, 393–395.

[26] T. Deplancke, O. Lame, F. Rousset, I. Aguili, R. Seguela, G. Vigier, *Macromolecules*, **2014**, *47*, 197–207.

[27] B.P. Rotzinger, H.D. Chanzy, P. Smith, *Polymer*, **1989**, *30*, 1814–1819.

[28] J. Loos, M. Arndt-Rosenau, U. Weingarten, W. Kaminsky, P.J. Lemstra, *Polym. Bull.*, **2002**, *48*, 191–198.

[29] P. Smith, H.D. Chanzy, B.P. Rotzinger, *J. Mater. Sci.*, **1987**, *22*, 523–531.

[30] K. Ziegler, E. Holzkamp, H. Breil, H. Martin, *Angew. Chem.*, **1955**, *67*, 541–547.

[31] G. Natta, P. Pino, P. Corradini, F. Danusso, G. Moraglio, E. Mantica, G. Mazzanti, *J. Am. Chem. Soc.*, **1955**, *77*, 1708–1710.

[32] J. P. Hermans, P. Henrioulle, US 3769233, **1973**.

[33] M. Ferraris, F. Rosati, S. Parodi, E. Giannetti, E. Albizzati, US 4399054, **1983**.

[34] M. Kioka, N. Kashiwa, JP 2537506, **1996**.

[35] Y. Doi, K. Soga, M. Murata, E. Suzuki, Y. Ono, T. Keii, *Polym. Commun.*, **1983**, *24*, 244–246.

[36] V.D. Noto, S. Lavina, D. Longo, M. Vidali, *Electrochim. Acta*, **1998**, *43*, 1225–1237.

[37] I.W. Bassi, F. Polato, M. Calcaterra, J.C.J. Bart, *Zeitschrift Fur Krist. - New Cryst. Struct.*, **1982**, *159*, 297–302.

[38] M. Vittadello, P.E. Stallworth, F.M. Alamgir, S. Suarez, S. Abbrent, C.M. Drain, V. Di Noto, S.G. Greenbaum, *Inorganica Chim. Acta*, **2006**, *359*, 2513–2518.

[39] V. Di Noto, S. Bresadola, *Macromol. Chem. Phys.*, **1996**, *197*, 3827–3835.

[40] U. Giannini, *Makromol. Chem., Suppl*, **1981**, *5*, 216–229.

[41] R. Zannetti, C. Marega, A. Marigo, A. Martorana, *J. Polym. Sci. Part B Polym. Phys.*, **1988**, *26*, 2399–2412.

[42] E. Groppo, K. Seenivasan, C. Barzan, *Catal. Sci. Technol.*, **2013**, *3*, 858–878.

[43] E. Morra, E. Giamello, S. Van Doorslaer, G. Antinucci, M. D'Amore, V. Busico, M. Chiesa, *Angew. Chemie - Int. Ed.*, **2015**, *54*, 4857–4860.

[44] R. Mülhaupt, *Macromol. Chem. Phys.*, **2003**, *204*, 289–327.

[45] L.L. Böhm, *Angew. Chemie - Int. Ed.*, **2003**, *42*, 5010–5030.

[46] K. Ziegler, E. Holzkamp, H. Breil, H. Martin, *Angew. Chem. Int. Ed. Engl.*, **1955**, *67*, 426–426.

[47] P. Cossee, *J. Catal.*, **1964**, *3*, 80–88.

[48] P. Cossee, *Tetrahedron Lett.*, **1960**, *1*, 12–16.

[49] P. Galli, P.C. Barbè, L. Noristi, *Die Angew. Makromol. Chemie*, **1984**, *120*, 73–90.

[50] E.L. Hoel, C. Cozewith, G.D. Byrne, *AIChE J.*, **1994**, *40*, 1669–1684.

[51] R. Galvan, M. Tirrell, *Chem. Eng. Sci.*, **1986**, *41*, 2385–2393.

[52] D. Singh, R.P. Merrill, *Macromolecules*, **1971**, *4*, 599–604.

[53] W.R. Schmeal, J.R. Street, *AIChE J.*, **1971**, *17*, 1188–1197.

[54] J.W. Begley, *J. Polym. Sci. Part A-1 Polym. Chem.*, **1966**, *4*, 319–336.

[55] T. F. McKenna, J. B. P. Soares, *Chem. Eng. Sci.*, **2001**, *56*, 3931–3949.

[56] E. J. Nagel, V. A. Kirillov, W. H. Ray, *Ind. Eng. Chem. Prod. Res. Dev.*, **1980**, *19*, 372–379.

[57] R. L. Laurence, M. G. Chiovetta, PolymIn Polymer Reaction Engineering: Influence of Reaction Engineering on Polymer Properties, Wiley-Blackwell, **1985**.

[58] B. Horáčková, Z. Grof, J. Kosek, *Chem. Eng. Sci.*, **2007**, *62*, 5264–5270.

Chapter 2

Synthesis of $MgO/MgCl_2/TiCl_4$ Core-Shell Nano Catalyst Using MgO Particles

Abstract

In this chapter, $MgO/MgCl_2/TiCl_4$ core–shell catalysts are employed for the production of ultrahigh molecular weight polyethylene (UHMWPE) particles, motivated by their advantages including simple preparation, ease of morphology control, and a dramatically reduced Cl content. It is found that the $MgO/MgCl_2/TiCl_4$ core–shell catalysts can provide UHMWPE at a reasonable activity, but the agglomeration of the catalyst particles leads to poor morphology of the UHMWPE. The dispersion problem is largely alleviated by modifying MgO nanoparticles with methyl oleate (MO). Thus, the MO-modified $MgO/MgCl_2/TiCl_4$ core–shell catalyst successfully affords UHMWPE particles of 100–200 μm at a high yield of 8670 g-PE g-Cat^{-1}.

2.1. Introduction

Heterogeneous olefin polymerization catalysts have been widely used to manufacture a wide variety of polyolefins owing to their economic advantages and the ease of polymer morphology control. The morphology of polymer particles, for instance, the particle size, the particle size distribution and shape, is important for the efficiency of the polymer production in plants. In particular, polymer particles with a narrow particle size distribution are desirable to improve the flow ability in the transportation line and to prevent the reactor fouling. It is well-known that the morphology of polymer particles can be controlled through the morphology of catalyst particles [1–3]. Polymerization initiates at active sites that are located on accessible surfaces of the catalyst particles. Once the polymer is formed, it forces the catalyst to fragment, leading to the exposure of fresh active sites. The repetition of this process within multigrained particles lets the morphology of polymer replicate that of the catalyst particles, known as "replicating phenomena" [4–6].

In the past decade, the synthesis of fine particles of polyolefins has gained increasing attention due to potential applications: unlike a typical pellet form, fine particles are mainly used as a modifying additive, in which a large specific surface area and fine structure of polymer particles contribute to improve properties of other materials. For

example, micron-sized polyethylene wax is used as an additive for paints, inks, and powder coatings to enhance the esthetics of a protective finish [7], slip properties, and scratch resistance, while the addition of micron-sized ultrahigh molecular weight polyethylene (UHMWPE) enhances the self-lubricating properties and abrasion resistance of matrix polymers [8]. Though emulsion polymerization is most widely employed for accessing polymer fine particles [9], it is hardly applicable in the case of olefin polymerization owing to the catalyst deactivation in the presence of a polar solvent. Fine particles are also formed by a solvent deposition technique, where a polymer solution is brought to a supersaturated state either by adding a poor solvent or by rapid quenching [10–12]. The process is applicable to many types of polymers and easy to control the morphology of resultant fine particles by process conditions, but a required large volume of solvents is not economically viable. Consequently, a method to directly obtain polyolefin fine particles in catalyzed olefin polymerization is most preferred in industry.

Under the assumption of the replication in olefin polymerization, the size of polymer particles obtained is expressed in proportion to $Y^{1/3} \cdot D_{Cat}$, where Y and D_{Cat} represent the polymer yield per gram-catalyst and the size of catalyst particles, respectively. Considering the productivity of a plant as well as the factor of 1/3 for Y relative to unity for D_{Cat}, the size of catalyst particles, D_{Cat}, must be the main parameter to manipulate the

polymer particle size. Likewise, reduction in the catalyst particle size without scarifying the activity and morphological integrity during polymerization becomes a key target to obtain fine polymer particles. In general, commodity grades of UHMWPE have particle sizes of 140–300 μm, and produced using Ziegler–Natta catalysts possessing particle sizes around 5–20 μm. While microfine grades of UHMWPE below 80 μm can be accessed by catalysts with the sizes of a few-to-several micrometers. In obtaining size- and morphology-controlled Ziegler–Natta catalysts, a number of preparation protocols have been developed, most frequently based on reprecipitation of a Mg precursor solution under a controlled condition. Various types of Mg precursor solutions have been proposed such as a $MgCl_2 \cdot n AlRCl_2 \cdot m AlCl_3$ solution prepared from the dissolution of magnesium chloride, alkyl aluminum dichloride, and aluminum trichloride at high temperature [13], a Mg- and Ti-alkoxide solution prepared from the dissolution of magnesium ethoxide with titanium tetrabuthoxide followed by the dilution in hydrocarbon solvent [14], a sort of a Grignard compound with a formula of $MgPh_2 \cdot n MgCl_2 \cdot m Bu_2O$ that was obtained by reacting metallic Mg with chlorobenzene and dibutyl ether in the presence of iodine as an initiator [15], and *etc.* The reprecipitation of a solution and subsequent or simultaneous titanation can be performed in single or multiple steps, using a halogenating agent and/or a Ti-containing halogen

compound to form a solid catalyst. The chlorination at a low temperature [15], step-wise heating [16], and the application of a special mixer [17] are typical strategy to control the morphology of catalyst particles during the reprecipitation. Furthermore, a high speed shearing treatment (>10 000 rpm) either during the formation of a solid support [18] or after forming a solid catalyst [19] is additionally required, when the particle size down to a few-to-several micrometers is desired. Likewise, existing protocols can more or less afford catalysts with controlled morphology and particle sizes suitable for the production of UHMWPE fine particles, but reduction in the particle size has necessitated complicated chemical formulas as well as technically demanding and/or elaborate processes.

In previous study, a simple preparation route for Ziegler–Natta catalysts was reported, in which magnesium oxide (MgO) crystalline nanoparticles were treated with $TiCl_4$ to form $MgO/MgCl_2/TiCl_4$ core–shell catalysts for studying the structure–performance relationship between the surface area and activity in propylene polymerization [20,21]. This catalyst system was considered as promising for the production of UHMWPE particles based on the following reasons:

(i). The particle size of the catalysts can be easily controlled through the size of original MgO nanoparticles.

(ii). The catalyst preparation is quite simple, *i.e.*, only the chlorination of preformed MgO nanoparticles with $TiCl_4$.

(iii). Even though the catalyst behaves similar to conventional Ziegler–Natta catalysts, the chlorine content per gram-catalyst is dramatically reduced.

In this chapter, I report the first application of the $MgO/MgCl_2/TiCl_4$ core–shell catalysts in ethylene polymerization, especially focusing on the production of UHMWPE particles. It was found that the $MgO/MgCl_2/TiCl_4$ core–shell catalysts were able to produce UHMWPE at a reasonable activity, and that the modification of MgO supports with methyl oleate largely improved the dispersibility of the catalyst particles in a hydrocarbon medium, thus affording UHMWPE particles of 100–200 μm.

2.2. Experimental

2.2.1. Materials

MgO samples with the particle size of 50, 60, and 200 nm were obtained from Wako Pure Chemical Industries Ltd. They were used after dehydration in vacuo at 160°C for 2 h. Titanium tetrachloride ($TiCl_4$), kerosene, methyl oleate (MO), *o*-dichlorobenzene (ODCB), and decahydronaphthalene of research grades were used without further purification. Ethylene of a polymerization grade was purchased from Hokurikuekikasangyou Co., Ltd. and used as received. Triisobutylaluminium (TiBA) and triethylaluminium (TEA) were donated by Tosoh Finechem Co. *n*-Heptane was used after dehydration by passing through a column of molecular sieve 4A and N_2 bubbling for 2 h.

2.2.2. Catalyst Preparation

Pre-dehydrated MgO (2.0 g) powder was reacted with 30 mL of $TiCl_4$ at 140°C for 2 h under stirring at 250 rpm. The obtained solid was washed with 100 mL of heptane for ten times and kept as a slurry in heptane. The catalysts were named as Cat50, Cat60, and Cat200, where the numbers specified the particle size of the employed MgO samples. In another set of experiments, MgO powder was treated with MO prior to the catalyst

preparation. MgO (10.0 g) was sonicated in 25 mL of kerosene at room temperature for 10 min. Thereafter, 8.0 mL of MO was added to the suspension followed by refluxing at 160°C for 1 h. The obtained solid was washed with 100 mL of ODCB for five times to obtain MO-treated MgO samples (denoted as MO-MgO50 and MO-MgO200). The catalyzation was performed as described above, except 50 mL of ODCB was co-added together with $TiCl_4$. The catalysts were named as MO-Cat50 and MO-Cat200, which corresponded to the use of MO-MgO50 and MO-MgO200, respectively.

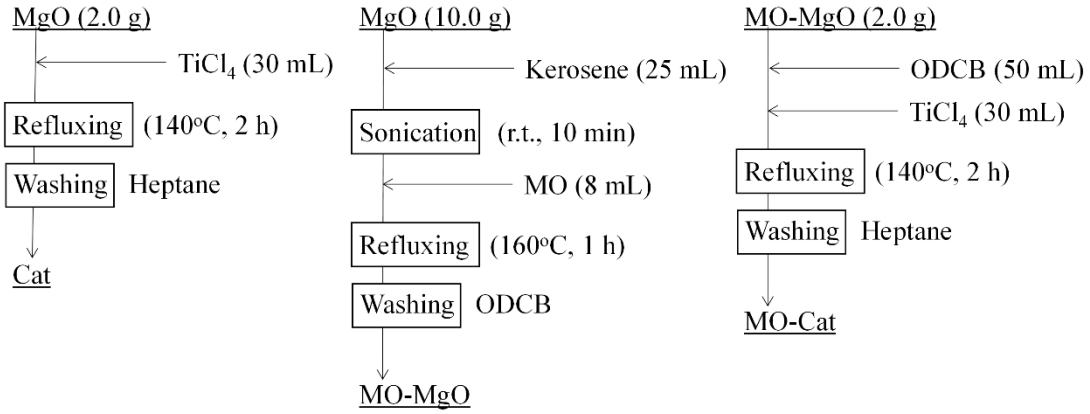

Scheme 1 Catalyst preparation

2.2.3. Polymerization

Slurry polymerization of ethylene was first performed in a 1 L stainless steel reactor equipped with a mechanical stirrer. Heptane (200 mL) as a solvent was injected into the

reactor under N_2 and then saturated with 0.5 MPa of ethylene at 50°C for 30 min. Following the addition of 2.0 mmol of TiBA as an activator, 30 mg of a catalyst was introduced to the reactor to start polymerization. The polymerization was continued for 30 min at 50°C and 0.5 MPa of ethylene pressure, and finally terminated by the addition of acidic ethanol. The obtained polymer samples were named as PE50, PE60, and PE200, which corresponded to the use of Cat50, Cat60, and Cat200, respectively.

The polymerization using the MO-treated catalysts was conducted at an optimized condition to obtain a reasonable polymer yield: using the same reactor, heptane was introduced into the reactor under N_2 blanking. TEA was then introduced at the concentration of 2.0 mmol L^{-1}. The solvent was saturated with 0.8 MPa of ethylene at 70°C for 30 min before charging the catalyst slurry to start polymerization. The catalyst amount was fixed at 10 mg with the total solvent volume kept at 500 mL. The polymerization was carried out at 70°C under 0.8 MPa of ethylene pressure for 2 h. The obtained polymer was filtered and dried in vacuum at 60°C for 6 h. The polymer samples were named as MO-PE50 and MO-PE200, which corresponded to the use of MO-Cat50 and MO-Cat200, respectively.

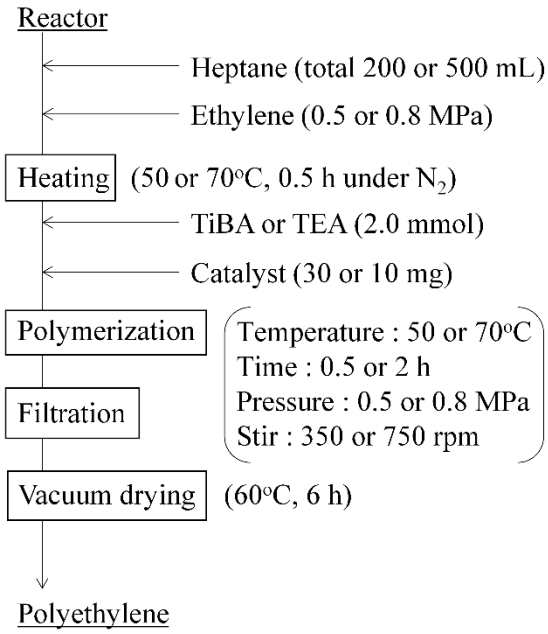

Scheme 2 Polymerization condition

2.2.4. Characterization

The morphology of MgO and catalyst particles was observed by transmission electron microscopy (TEM, Hitachi H-7100) operated at an accelerating voltage of 100 kV. TEM samples were prepared by dropping a suspension of samples in ethanol or heptane to a carbon film reinforced copper grid and subsequent drying. The particle size and the particle size distribution of MgO and catalyst samples were analyzed by light scattering (Horiba Partica LA-950V2) in a suspension form using ethanol or heptane as a solvent. The particle size was reported as D_{10}, D_{50}, and D_{90}, which corresponded to the particle size at 10%, 50%, and 90% of the cumulative volume [6]. The particle size distribution

was reported as a relative span factor (RSF) [6] calculated based on

$$\mathrm{RSF} = \frac{D_{90} - D_{10}}{D_{50}} \quad (1)$$

N_2 adsorption/desorption isotherms of the catalyst were acquired using BELSORP-max at 77 K. The sample was out gassed at 80°C for 3 h prior to the measurement [20,21]. The surface area of the sample was calculated by the Brunauer–Emmett–Teller (BET) equation. The presence of MO on MgO nanoparticles was observed by attenuated total reflectance infrared spectroscopy (ATR-IR, Perkin Elmer Spectrum 100 FT-IR) in the range of 500–4000 cm^{-1}. After repetitive washing of MO-MgO with ODCB, the powder was dried under vacuum and subjected to the measurement. The Ti content of the catalyst was analyzed by ultraviolet–visible spectrometry (UV–vis, Jasco V670). The catalyst (50 mg) was dissolved in an aqueous solution of hydrochloric acid and sulfuric acid. Thereafter, 200 µL of hydrogen peroxide was added to form a peroxotitanium complex that exhibited the absorption band at 410 nm. The Ti content was determined based on the intensity at 410 nm, using an externally acquired standard curve.

The morphology of polymer powder was observed by scanning electron microscopy (SEM, Hitachi S-4100) operated at an accelerating voltage of 20 kV. Polymer powder was dispersed on a carbon tape and subjected to Pd–Pt sputtering for 100 s before the

measurement. The viscosity-average molecular weight (M_v) of polymer samples was obtained based on ASTM 4020D, except the fact that the relative viscosity of a polymer solution was measured using an electromagnetically spinning viscometer (EMS, Kyoto Electronics Manufacturing, EMS-100). In the EMS measurement, a polymer sample was dissolved in decahydronaphthalene at 0.02 g L^{-1} and at 150°C. Subsequently, 300 μL of the solution was transferred to a glass vial containing an aluminum ball. The viscosity of the polymer solution was measured at 135°C based on the frustrated rotation of the aluminum ball in the viscous solution. The relative viscosity (η_{rel}), specific viscosity (η_{sp}), intrinsic viscosity ([η]), and M_v were derived according to **Equations (2)–(5)**

$$\eta_{rel} = \frac{\eta_{solution}}{\eta_{solvent}} \quad (2)$$

$$\eta_{sp} = \eta_{rel} - 1 \quad (3)$$

$$[\eta] = \frac{\sqrt{2\eta_{sp} - 2\ln\eta_{rel}}}{C} \quad (4)$$

$$M_v = 5.34 \times 10^4 [\eta]^{1.37} \quad (5)$$

where C is the concentration of the polymer dissolved in decahydronaphthalene.

The melting temperature (T_m) of the obtained polymer in the nascent form and melt-crystallized form was acquired using differential scanning calorimetry (Mettler Toledo DSC 822). In the case of the nascent form, T_m was obtained from the melting endotherm

in the first heat cycle, where a sample was heated to 180°C at the heating rate of 10°C min^{-1} under N_2 flow. After cooling to 50°C at the cooling rate of 10°C min^{-1}, the second heat cycle was applied at the same heating rate to acquire T_m in the melt-crystallized form.

The polymer particle size was analyzed by light scattering in ethanol suspension. The theoretical size of polymer particles was estimated according to **Equation (6)**

$$D_{PE} = \left(\frac{d_{Cat}}{d_{PE}} Y\right)^{\frac{1}{3}} D_{Cat} \quad (6)$$

where d_{Cat} and d_{PE} are the densities of the catalyst and polymer, respectively. Y is the polymerization yield. D_{PE} and D_{Cat} are the particle sizes of the polymer and catalyst, respectively.

2.3. Results and Discussion

The $MgO/MgCl_2/TiCl_4$ core–shell catalysts comprise of a thin $MgCl_2/TiCl_4$ catalytic layer covering MgO crystalline cores. As the catalyzation proceeds on the outermost surfaces of MgO cores, the morphology of catalyst particles well retains that of the original MgO particles. In addition to this, nonporous and nonfragmentable characters assure the correspondence between the BET surface area and practically available surface area of the catalysts during polymerization [22]. In the previous papers, a series of $MgO/MgCl_2/TiCl_4$ core–shell catalysts were had prepared to have different surface areas using MgO nanoparticles of different sizes so as to clarify a linear relationship between the surface area and propylene polymerization activity.

Here, a similar attempt was extended to ethylene polymerization. Three $MgO/MgCl_2/TiCl_4$ core–shell catalysts were synthesized using MgO samples with the particle sizes of 50, 60, and 200 nm. MgO nanoparticles utilized in this work are commercially available samples having relatively broad particle size distributions. In TEM images, it was confirmed that the morphology of the catalyst samples well preserved that of the original MgO samples, *i.e.*, polygonal and cubic nanoparticles for MgO50 and Cat50, and for MgO200 and Cat200, respectively (Figure 1).

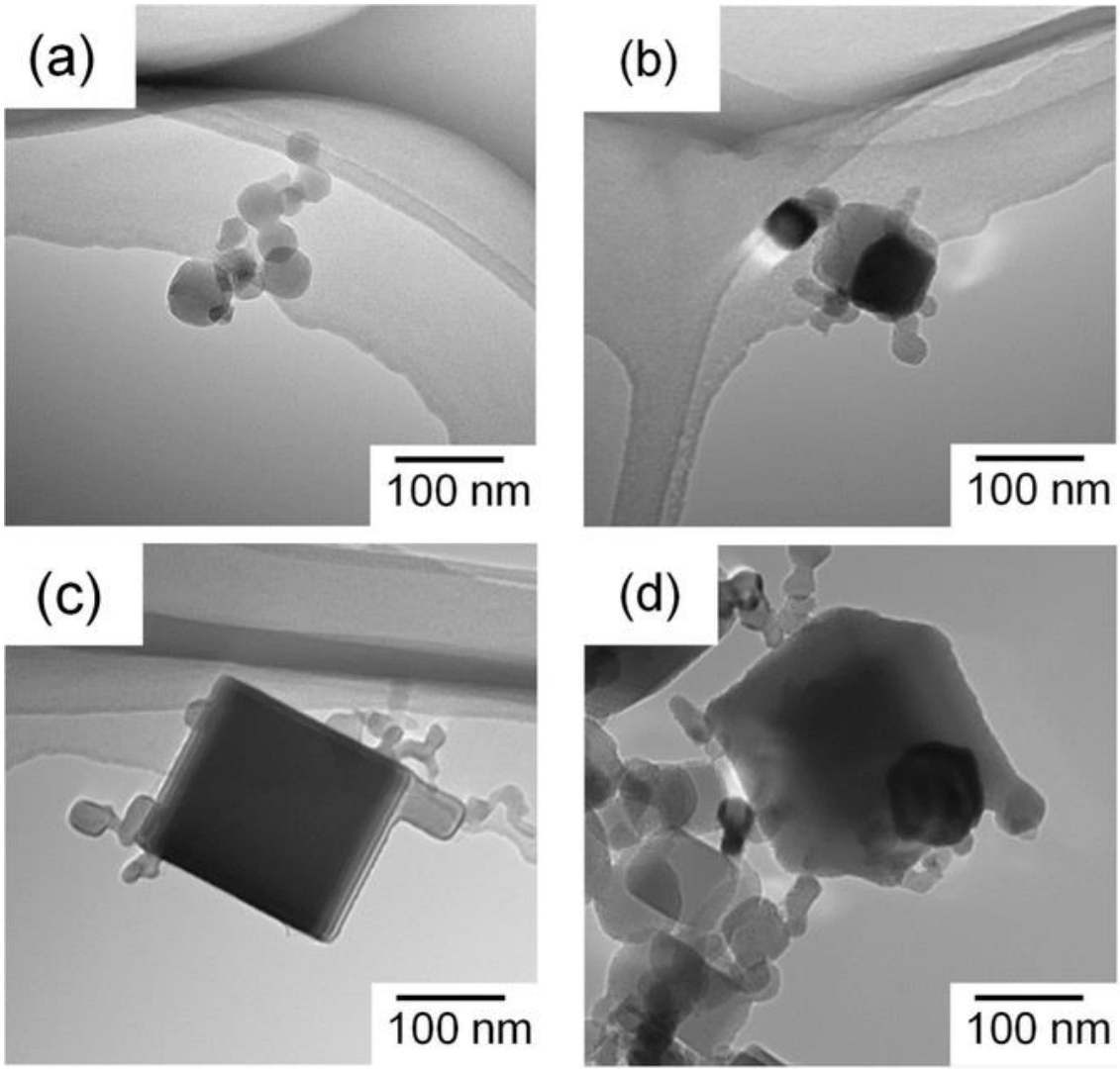

Figure 1 TEM images of MgO and catalyst particles:

a) MgO50, b) Cat50, c) MgO200, and d) Cat200

In Figure 2, N_2 adsorption/desorption isotherms for the MgO and catalyst samples were featured with a plateau of an adsorption profile at low relative pressure and an unrestricted sorption at high relative pressure, which can be classified as a type II adsorption isotherm for nonporous materials based on the IUPAC classification [23].

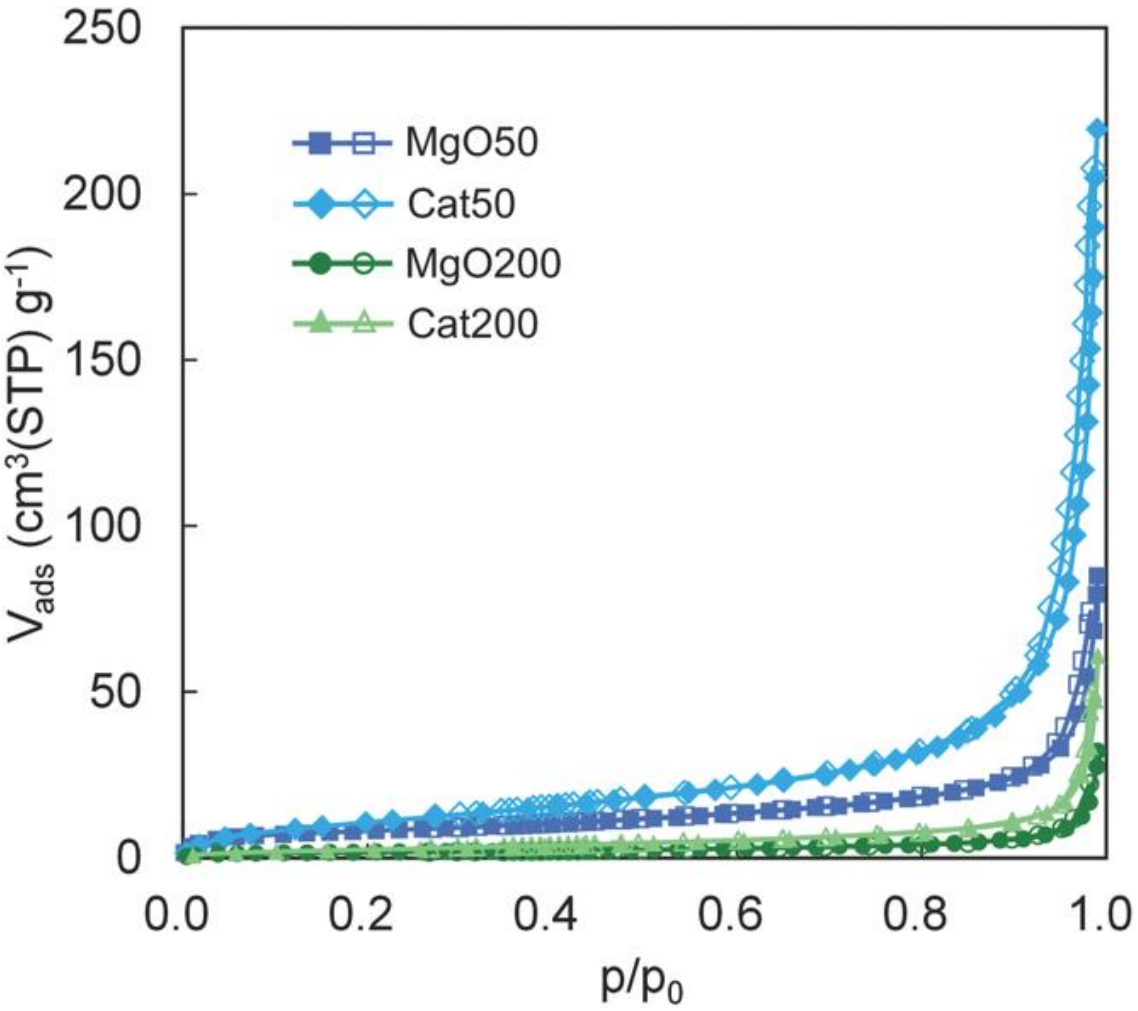

Figure 2 N_2 adsorption/desorption isotherms for MgO50, Cat50, MgO200, and Cat200

The plateau at low relative pressure results from the transition from mono to multilayer adsorption of N_2 on the outermost surfaces of the nanoparticles, while the unrestricted adsorption at high relative pressure attributes to the N_2 condensation in interparticle voids among the nanoparticles. Below $p/p_0 = 0.3$, the isotherms for the catalyst samples fully overlapped with those of the corresponding MgO samples, indicating that the catalyzation

hardly affected the surface area of the nanoparticles. Meanwhile, the upward deviation of the isotherms for the catalysts with respect to those of the MgO samples suggested that the formation of the catalyst overlayer affected the agglomeration structure of the nanoparticles. It is notable that the flowability of the catalyst samples in a dry state was much lower than that of the corresponding MgO samples. Obviously, the ionic nature of the catalyst overlayer enhanced the attraction among the nanoparticles. Table 1 summarizes the results of the characterization. As explained above, the BET surface areas were almost identical between the MgO and catalyst samples of the corresponding sizes, and the Ti content tended to increase along the surface area.

Table 1 Characteristics and ethylene polymerization performance of $MgO/MgCl_2/TiCl_4$ samples

Sample	BET surface area[a] ($m^2\ g^{-1}$)	Ti content[b] (wt%)	Yield[c] (g-PE g-Cat^{-1})	M_v[d] ($\times 10^6$)
Cat50	33.5 (34.3)[e]	0.47	1270	3.4
Cat60	29.1 (29.8)[e]	0.43	1100	3.1
Cat200	8.4 (8.1)[e]	0.17	5.44	3.0

[a]Acquired from the N_2 adsorption isotherm.

[b]Determined based on UV-vis spectroscopy.

[c]Polymerization conditions: Ethylene pressure = 0.5 MPa, heptane = 300 mL, TiBA = 2.0 mmol, catalyst = 30 mg, T = 50°C, t = 0.5 h.

[d]Calculated based on **Equations (1)–(4)** using the relative viscosity measured by an EMS viscometer.

[e]The values in parentheses are the BET surface areas of original MgO samples.

A relationship between the surface area and the productivity of the catalysts in ethylene polymerization is plotted in Figure 3, together with the same relationship for propylene polymerization (acquired under the same condition).

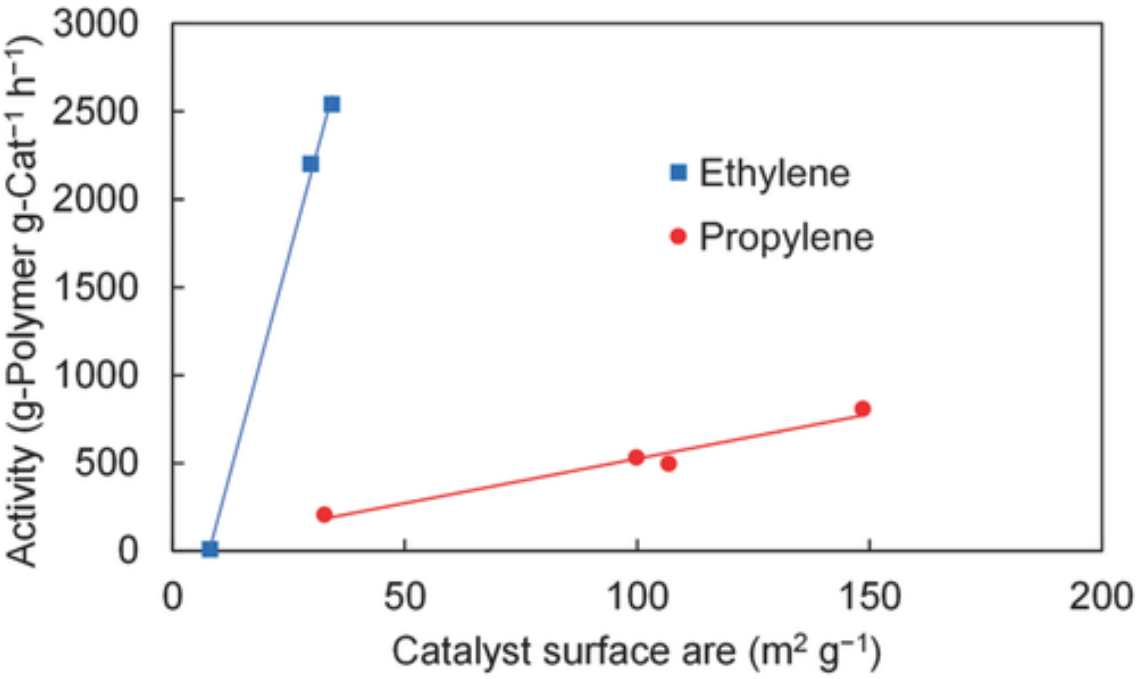

Figure 3　Relationships between the catalyst surface area and activity of the catalysts in ethylene and propylene polymerization.　Note that the propylene polymerization results are taken from previous work [21]

It was found that the productivity of the catalysts increased in a completely linear fashion to the surface area in both of the ethylene and propylene polymerization.　This fact suggested that the amount of the polymer producible per catalyst surface area was somewhat constant for each of the monomers.　Interestingly, the slope of the line for the

ethylene polymerization was ≈19 times greater than that for the propylene polymerization. The molecular weight of the obtained polyethylene was evaluated based on ASTM 4020D. It was found that the $MgO/MgCl_2/TiCl_4$ core–shell catalysts were able to produce UHMWPE with M_v of 3.0–3.4 × 10^6 (Table 1).

As the molecular weight of produced polyethylene fell in the range of an ultrahigh molecular weight region independently from the catalyst particle size, it was considered that the $MgO/MgCl_2/TiCl_4$ catalysts would provide a great advantage for synthesizing micron- or even submicron-sized UHMWPE polymer particles.

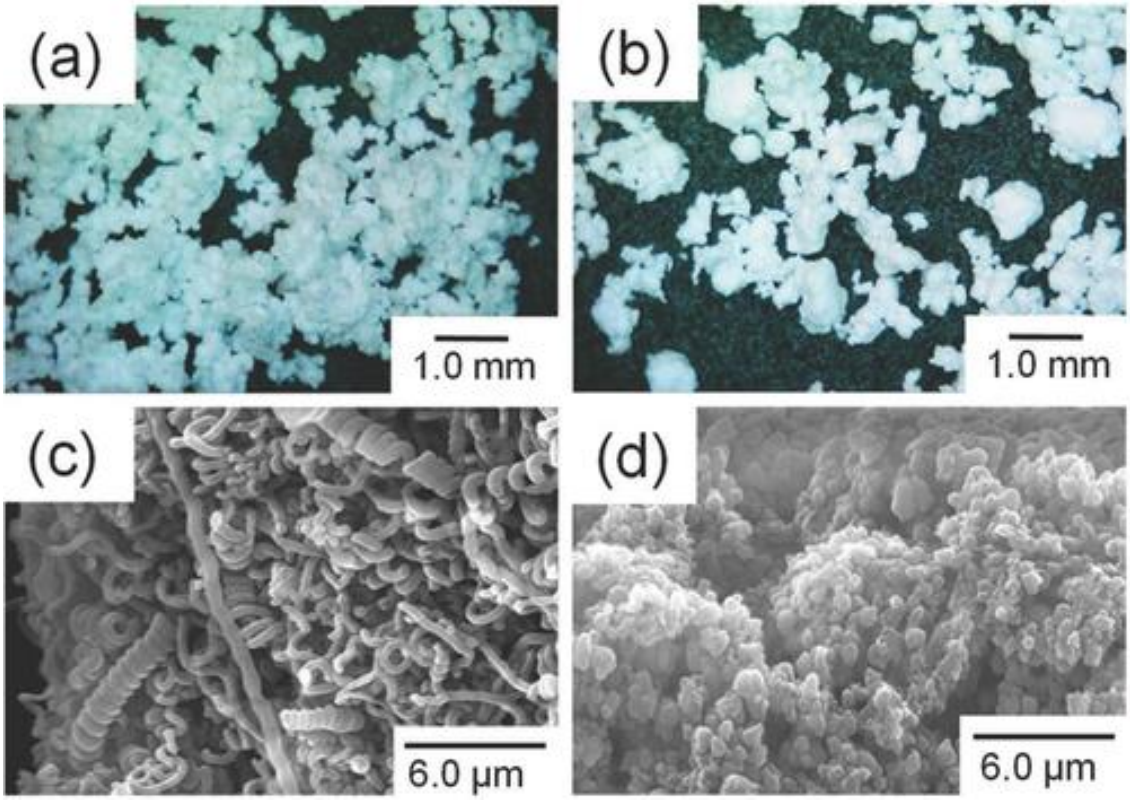

Figure 4　Optical and SEM images of obtained UHMWPE samples:

a,c) PE50 and b,d) PE200

Consequently, ethylene polymerization was performed at a more practical condition using TEA as an activator instead of TiBA.　The appearance of the obtained polymer is shown in Figure 4a, b.　Unlike the expectation, the morphology of the obtained polymer was far from that of fine particles, where polymer particles seemingly agglomerated with each other to form a coarse body.　SEM images of the polymer samples revealed heavily agglomerated structures for both of PE50 and PE200, while their morphologies were found to be very different: in the case of PE200, the globular morphology was obtained,

which is typical for a low polymerization rate [24]. As the size of each globule was consistent with the size expected from **Equation (5)**, it was supposed that the polymerization was performed with the catalyst nanoparticles heavily agglomerated in the polymerization medium. Contrary to PE200, the surfaces of PE50 represented full of coil structures. Such a coli-like morphology is often observed when many active sites are located close to each other [25], or when the growth of polymer is sterically restricted by surroundings such as pore walls of nonfragmentable supports [26,27]. Considering that the Ti content of $MgO/MgCl_2/TiCl_4$ catalysts was roughly proportional to the surface area, it was unlikely that Cat50 and Cat200 possessed greatly different active site densities. Hence, it was presumed that stronger agglomeration among the nanoparticles of Cat50 sterically forced growing polymer to be extruded out of interparticle voids, and a twisted conformation of the coils appeared as a result of the internal stress relaxation [28]. It must be mentioned that the aggregation of catalyst particles hardly affected the linear relationship between the surface area and the productivity of the catalysts, as long as the particles are nonfragmentable and free from inaccessible pores [20].

In order to improve the dispersibility of the catalyst nanoparticles not only in the polymerization but also during catalyst preparation, MgO nanoparticles were modified with MO as a nonprotic surfactant. Figure 5 shows the ATR-IR spectrum of a MO-

treated MgO sample, referenced to those of untreated MgO and MO molecules. In the spectrum of MO, an intense peak at 1742 cm^{-1} and a broader band at 1171 cm^{-1}, respectively correspond to the C−O and C−O stretching vibrations of carboxylic acid ester [29,30]. The other peaks at 3006, 2964, 2923, 2854, 1461, and 723 cm^{-1} are assigned as the stretching mode of C−H bond adjacent to the C−C group [31], asymmetric stretching of CH_3, asymmetric stretching of CH_2, symmetric stretching of CH_2, CH_2 deformation, and bending vibration of RCH−CHR, respectively [32,33]. In the spectrum of untreated MgO, a sharp peak at 3700 cm^{-1} indicates the presence of physisorbed water [34,35], which accompanies the band of the O−H bending mode at 1632 cm^{-1} [35]. The bands at 526 and 648 cm^{-1} are due to the Mg−O stretching vibrations [35,36]. In the spectrum of MO–MgO50, the peaks relevant to the ester group of MO were unseen. Instead, broad bands were newly observed between 1600 and 1300 cm^{-1}. According to Thistlethwaite *et al.* [37], the peaks at 1564 and 1394 cm^{-1} are respectively associated with the asymmetric and symmetric stretching vibrations of COO^- (the latter was overlapped with the absorption by the CH_2 deformation). Similar results, in particular, the replacement of the C−O stretching vibration of the carboxylic acid ester by ν_{as} (COO^-) and ν_s (COO^-), have been reported for the dissociative adsorption of a long chain carboxylic acid on a metal atom [38]. It was plausible that the carboxylate head

group of MO was directly bonded to surface Mg atoms (COO−Mg) as a result of the dealcoholization reaction with surface hydroxyl groups. The peak separation (Δ) between ν_{as} (COO^{-}) and ν_{s} (COO^{-}) can be utilized to distinguish the type of interaction [39]. The Δ value of 170 cm^{-1} for the MO−MgO sample was associated with interaction in a bridging mode [39,40], where comparable intensities for ν_{as} (COO^{-}) and ν_{s} (COO^{-}) further suggested that the carboxylate head group coordinated on Mg atoms with its orientation outward from the surfaces [41]. After chlorination using $TiCl_4$, the peaks belonging to ν_{as} (COO^{-}) and ν_{s} (COO^{-}) disappeared, while the peaks at 1262, 1094–1019, and 801 cm^{-1}, corresponding to the stretching vibration of C−O [42], the stretching vibration of terminal and bridging C−O(−Ti), [40,42,43] and the stretching vibration of Ti−O, [42,43] became evident. Since the bands for the aliphatic chain of the surfactant remained after the catalyzation, it was believed that the reaction between $TiCl_4$ and the carboxylate head group of the surfactant caused the dissociation of Mg−O−C bonds to form titanium alkoxide complexes (most possibly as titanium oleate) attached on the catalyst surfaces.

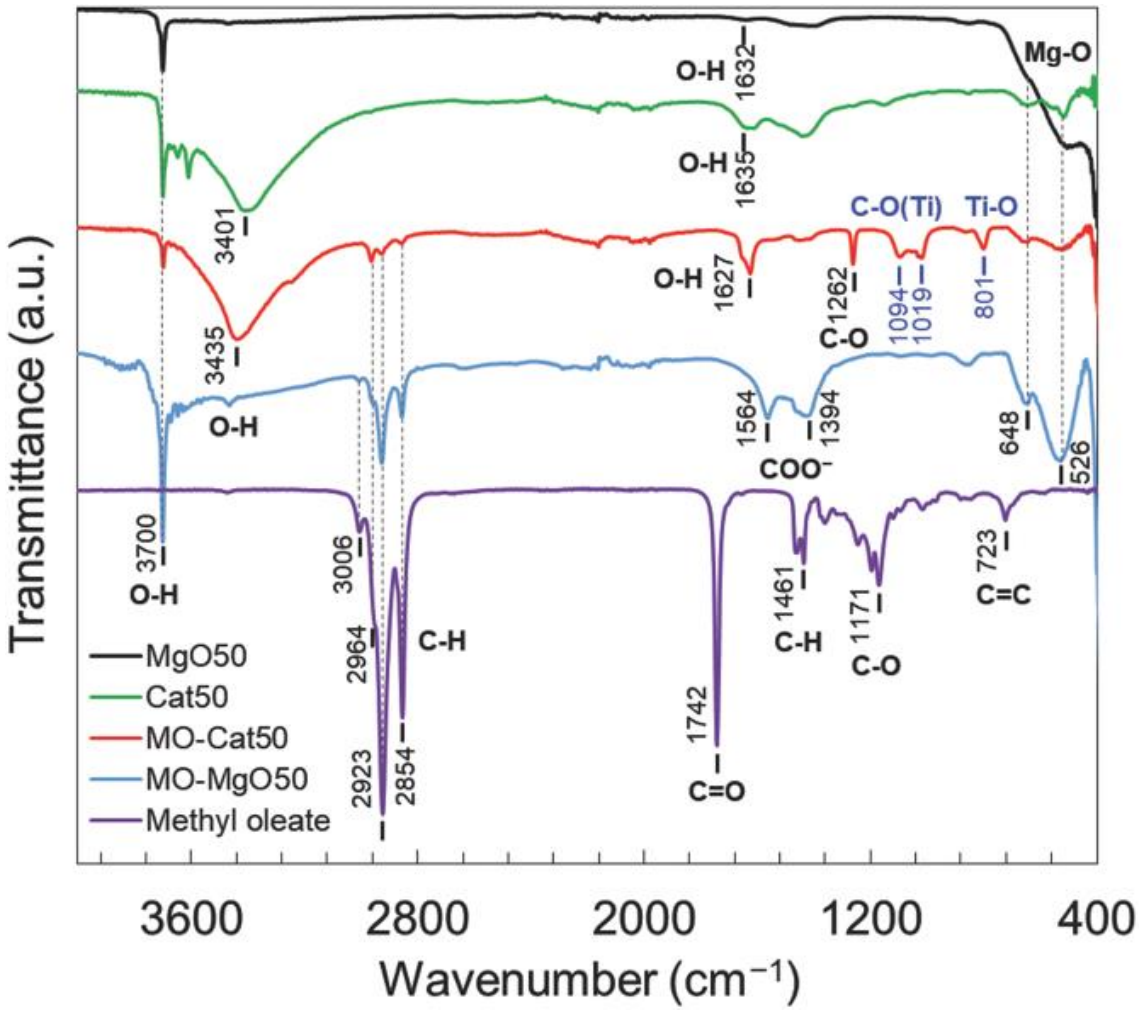

Figure 5 ATR-IR spectra of MO-MgO50 and MO-Cat50. The spectra of pristine MgO50, Cat50, and methyl oleate are also shown as references

The morphology of the MO-treated MgO and catalyst samples was observed by TEM (Figure 6). It can be seen that the MO treatment and subsequent catalyzation hardly affected the morphology of the original MgO nanoparticles. Figure 7a illustrates the particle size distributions of the MgO50 and relevant catalyst samples in heptane, measured by light scattering.

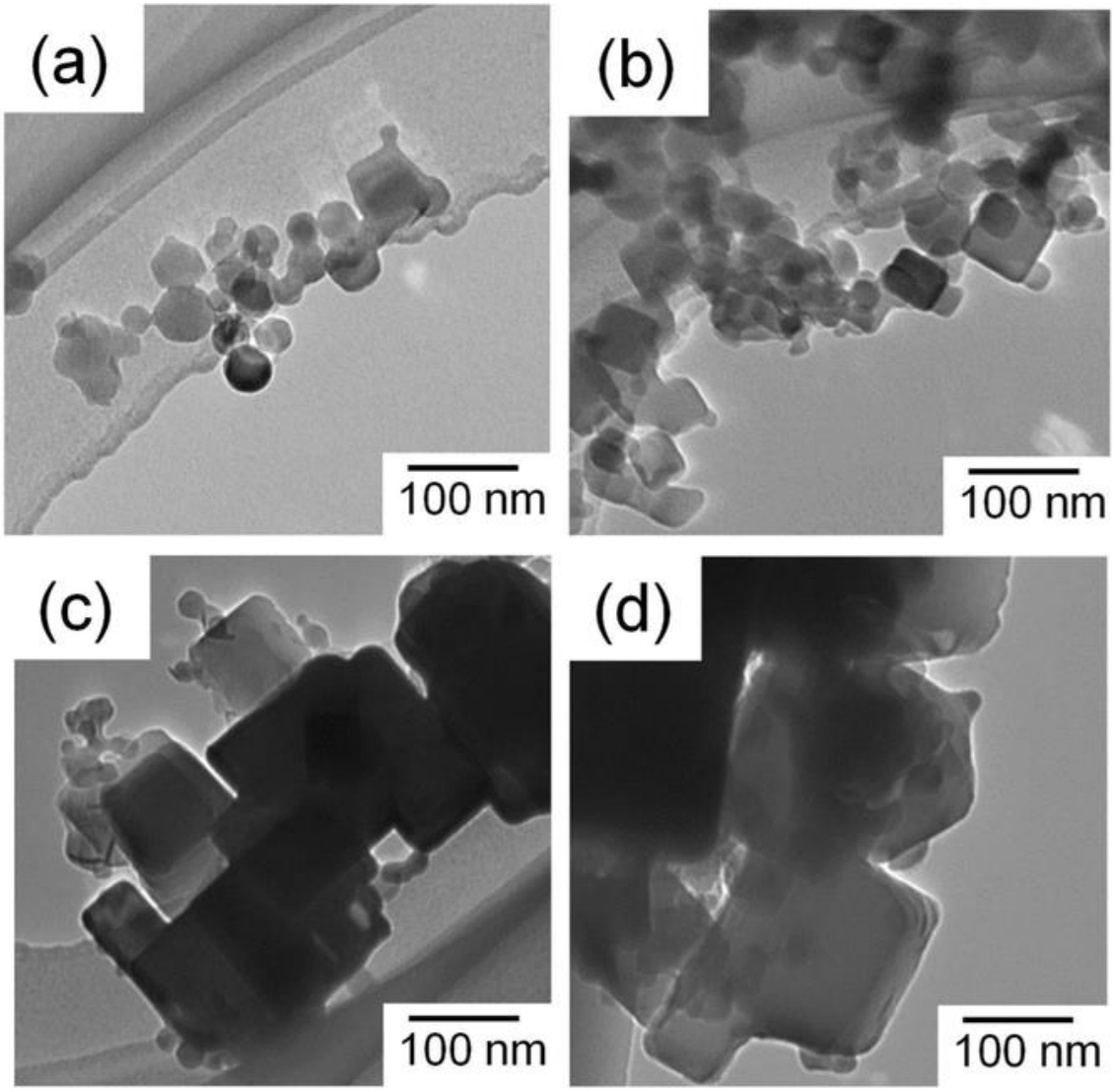

Figure 6 TEM images of MO-treated MgO and catalyst particles:

a) MO-MgO50, b) MO-Cat50, c) MO-MgO200, and d) MO-Cat200

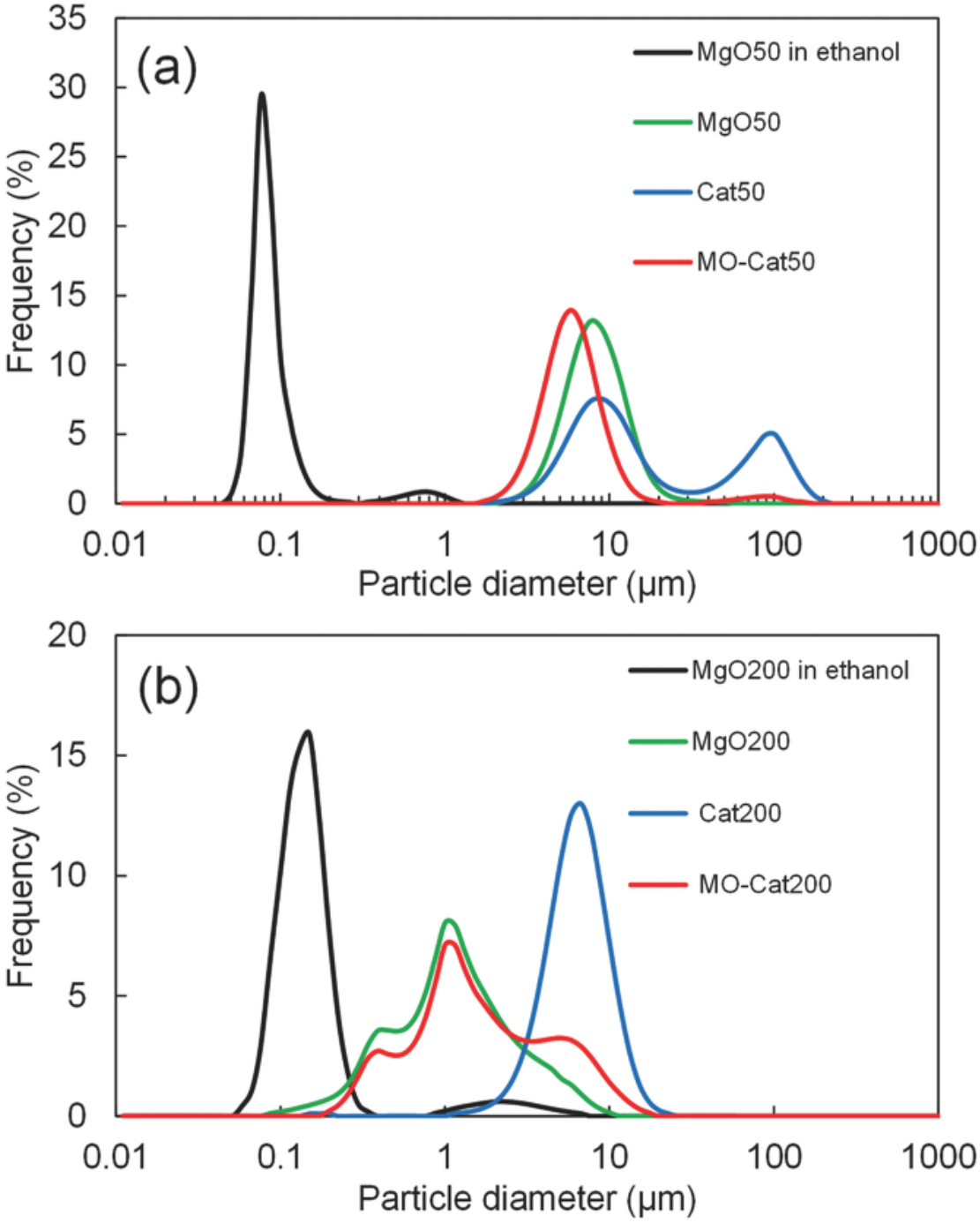

Figure 7 Particle size distribution for

a) MgO50-related samples and b) MgO200-related samples

The analysis was conducted as a suspension in heptane unless specified.

Table 2 Particle size characteristics of MgO and catalyst samples

Sample	D_{10}[a] (μm)	D_{50}[a] (μm)	D_{90}[a] (μm)	RSF[b]
MgO50 in ethanol	0.061	0.077	0.12	0.77
MgO200 in ethanol	0.086	0.13	0.23	1.1
MgO50	4.5	7.6	13	1.1
MgO200	0.34	1.0	3.2	2.8
Cat50	5.0	11	98	8.3
Cat200	3.3	6.0	10	1.1
MO-Cat50	3.3	5.5	9.6	1.2
MO-Cat200	0.43	2.3	6.0	2.4

[a]Analyzed by light scattering as a suspension in heptane unless specified.
[b]Calculated based on **Equation (1)**.

Table 2 summarizes the particle size characteristics derived from these distributions. The original MgO nanoparticles were highly dispersible in ethanol: a sharp size distribution was obtained, and the mode size of ≈80 nm was small enough to be regarded as the dispersion of primary particles. Contrary, the MgO nanoparticles were not dispersible in heptane, as demonstrated in the mode size of around 10 μm. The catalyzation further promoted the agglomeration unless modified (Cat50), where the second maxima appeared at around 100 μm. It was believed that this poorest dispersion

of the catalyst particles in heptane led to the above-mentioned coarse morphology of UHMWPE. When the surface modification was applied (MO-Cat50), the dispersion at the primary particle level was not attained but the promotion of the agglomeration during the catalyzation was successfully suppressed: the second agglomeration peak disappeared from the distribution. Similar results were obtained for MgO200 (Figure 7b and Table 2).

The BET surface area and the Ti content of MO-Cat samples are listed in Table 3 together with their polymerization performance.

Table 3 Characteristics and ethylene polymerization performance of methyl oleate-modified MgO/MgCl2/TiCl4 samples

Sample	BET surface area[a] ($m^2\ g^{-1}$)	Ti content[b] (wt%)	Yield[c] (g-PE g-Cat^{-1})	M_v[d] ($\times 10^6$)	D_{50}[e] (μm)	Theoretical size[f] (μm)
MO-Cat50	33.1	3.42	8670	3.1	191	177
MO-Cat200	8.2	1.83	770	2.8	106	33

[a]Acquired from the N_2 adsorption isotherm.

[b]Determined based on UV-vis spectroscopy

[c]Polymerization conditions: Ethylene pressure = 0.8 MPa, heptane = 500 mL, TEA = 1.0 mmol, catalyst = 10 mg, T = 70 °C, t = 2 h.

[d]Calculated based on **Equations (2)–(5)** using the relative viscosity measured by an EMS viscometer.

[e]Polymer particle size measured by light scattering in ethanol

[f]Theoretical polymer particle size calculated based on **Equation (6)**. The densities of the polymer and catalysts were set to 0.97 g cm^{-3} of high-density PE and 3.65 g cm^{-3} of MgO, respectively. The catalyst particle size was set to the D_{50} value measured in light scattering (*cf.* Table 2).

While the catalyst surface area was unaffected by the MO treatment, the Ti content greatly increased as compared to the nontreatment one. Considering that not only the Ti content but also the polymerization activity were not anymore correlated with the surface area in the MO-treated catalysts, it was presumed that the MO modification greatly altered the nature of active sites or surfaces as compared with those of the original catalysts. Reaction between $TiCl_4$ and the carboxylate head group of MO might explain this deviation. Nonetheless, the molecular weight of all the obtained polymers still fell in

the ultrahigh range. The melting endotherms as well as the T_m values of UHMWPE in the nascent form and melt-crystallized are shown in Figure 8 and Table 3.

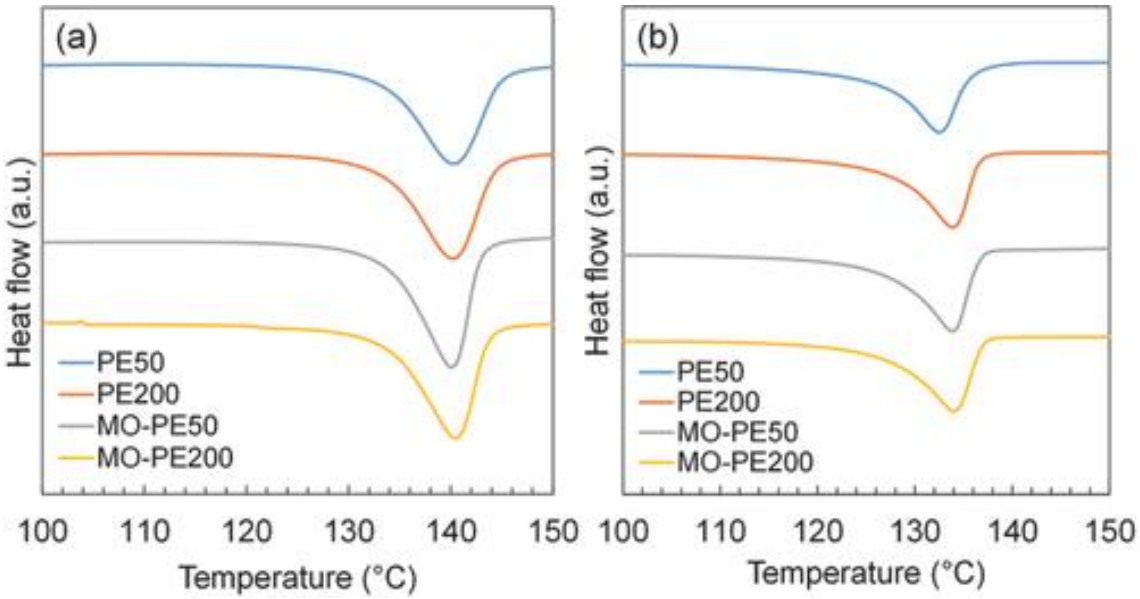

Figure 8 Melting endotherms of obtained UHMWPE samples in a) the nascent form and b) the melt-crystallized form

It can be seen that the nascent UHMWPE melted around 140–140.6°C, while the T_m value was reduced to 132.5 – 133.9°C in the second heating. This phenomenon and the obtained T_m values were consistent with those reported by Rastogi *et al.* [44] for nascent and melt-crystallized UHMWPE having the molecular weight of 4.5×10^6 g mol^{-1}. The higher T_m value of nascent UHMWPE with respect to that of melt-crystallized UHMWPE was explained by differences in the crystal topology. In the case of the nascent form

having tight folds, the melting requires cooperative melting of several chain stems that are connected by tight folds to adopt the random coil state [44].

The MO modification suppressed excessive agglomeration of catalyst particles in heptane, which led to a dramatic improvement in the morphology of the UHMWPE products. As displayed in Figure 9a, b, the appearance of the UHMWPE samples changed from the agglomerated coarse bodies for the unmodified catalysts (see Figure 4a, b) to independent particles. This improvement allowed us to measure the particle size distribution of UHMWPE samples based on light scattering (Figure 10). The derived particle sizes (D_{50} in Table 3) were found to be more or less consistent with the theoretically derived values (a deviation in MO-PE200 plausibly came from the broad particle size distribution of MO-Cat200 in heptane). Figure 9c, d represents the surface morphology of the UHMWPE particles. The presence of the fibrillar morphology suggested that the catalyst particles were composed by the agglomeration of smaller particles (multigrained structure) and the agglomeration was hard to be disintegrated in the polymerization. This observation was consistent with the light scattering results that the catalyst particles in heptane were not of primary particles even though the MO modification suppressed the excessive agglomeration.

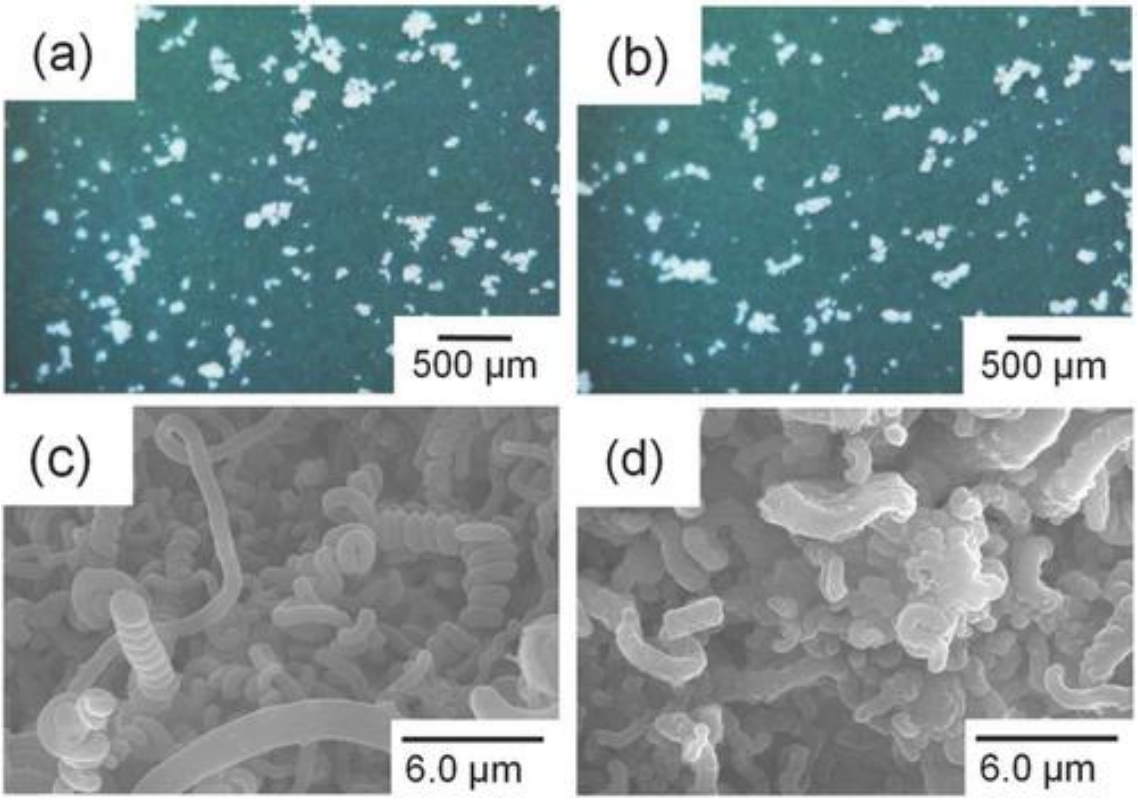

Figure 9 Optical and SEM images of obtained UHMWPE samples:

a,c) MO-PE50 and b,d) MO-PE200

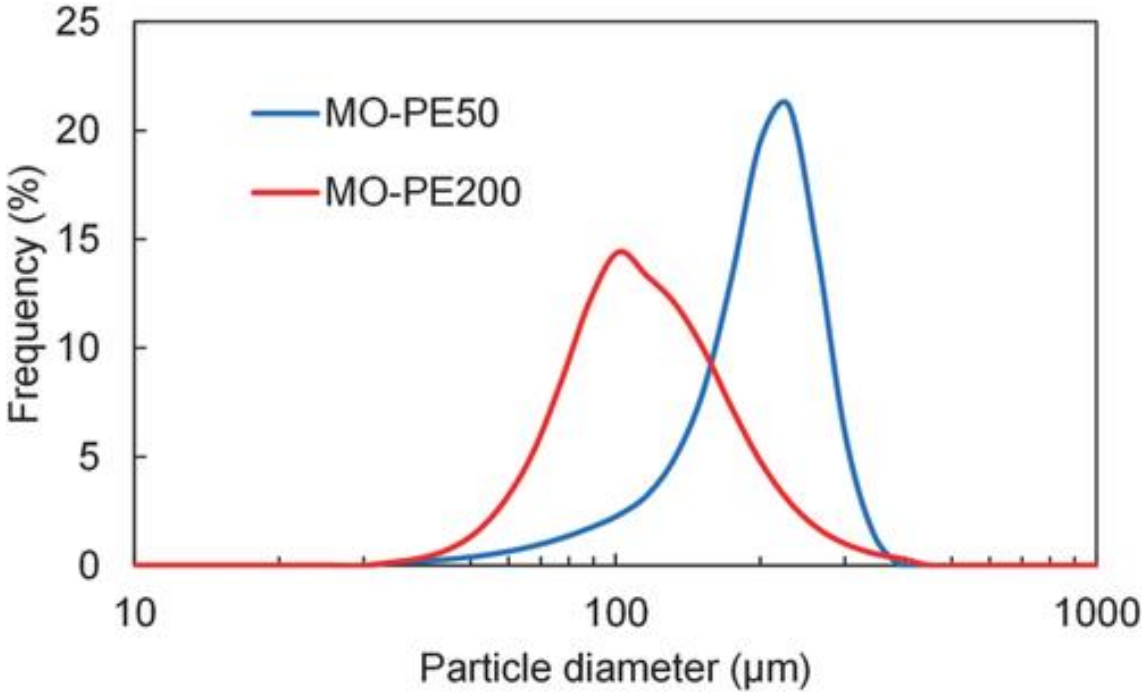

Figure 10 Particle size distribution of the UHMWPE samples obtained from MO-Cat50 and MO-Cat200

2.4. Conclusions

In this chapter, the performance of $MgO/MgCl_2/TiCl_4$ core–shell catalysts was investigated in ethylene polymerization, especially in terms of the production of UHMWPE particles. Owing to the nonporous and nonfragmental features, the $MgO/MgCl_2/TiCl_4$ core–shell catalysts provided a linear dependence of the ethylene polymerization activity on the catalyst surface area that was controlled by the size of MgO nanoparticles. The obtained PE possessed molecular weights classified as UHMWPE, while their morphology was not of independent particles due to severe agglomeration of the catalyst particles in the polymerization medium. The modification of MgO surfaces with MO partly suppressed the agglomeration of the resultant catalyst particles. The polymerization using the MO-modified catalysts successfully afforded UHMWPE particles. Thus, the present chapter proposes an alternative catalyst system for the production of UHMWPE particles, which is advantageously featured with the synthetic simplicity and a dramatically reduced Cl content.

Reference

[1] E. J. Dil, S. Pourmahdian, M. Vatankhah, F. A. Taromi, *Polym. Bull.*, **2010**, *64*, 445–457.

[2] R. Jamjah, G. H. Zohuri, J. Vaezi, S. Ahmadjo, M. Nekomanesh, M. Pouryari, *J. Appl. Polym. Sci.*, **2006**, *101*, 3829–3834.

[3] A. Dashti, S. A. Ramazani, Y. Hiraoka, S. Y. Kim, T. Taniike, M. Terano, *Polym. Int.*, **2009**, *58*, 40–45.

[4] T. Taniike, V. Q. Thang, N. T. Binh, Y. Hiraoka, T. Uozumi, M. Terano, *Macromol. Chem. Phys.*, **2011**, *212*, 723–729.

[5] G. Fink, B. Tesche, F. Korber, S. Knoke, *Macromol. Symp.*, **2001**, *173*, 77–88.

[6] T. Taniike, T. Funako, M. Terano, *J. Catal.*, **2014**, *311*, 33–40.

[7] P. S. Umare, R. Antony, K. Gopalakrishnan, G. L. Tembe, B. Trivedi, *J. Mol. Catal. A Chem.*, **2005**, *242*, 141–150.

[8] L. Xu, Y. F. Huang, J. Z. Xu, X. Ji, Z. M. Li, *RSC Adv.*, **2014**, *4*, 1512–1520.

[9] S. Gu, T. Mogi, M. Konno, *J. Colloid Interface Sci.*, **1998**, *207*, 113–118.

[10] W. Hou, T. B. Lloyd, *J. Appl. Polym. Sci.*, **1992**, *45*, 1783–1788.

[11] K. J. Kim, *Powder Technol.*, **2005**, *154*, 156–163.

[12] H. Matsuyama, M. Teramoto, M. Kuwana, Y. Kitamura, *Polymer*, **2000**, *41*,

8673–8679.

[13] I. Cuffiani, U. Zucchini, US Patent 5500397 A, **1996**.

[14] N. H. Friederichs, US Patent 20110269925 A1, **2011**.

[15] T. J. Kidd, V. F. Q. Norambuena, T. B. Mikenas, V. E. Nikitin, V. A. Zakharov, US Patent 20100143719 A1, **2010**.

[16] L. Sinthusai, R. Strauss, S. Thumsuruk, A. I. Anan, US Patent 9617357 B2, **2017**.

[17] Y. J. E. Ramjoie, S. A. Sergeev, M. Vlaar, V. A. Zakharov, G. D. Bukatov, US Patent 7947788 B2, **2011**.

[18] Y. Nakayama, N. Matsukawa, J. Saito, H. Bando, Y. Sonobe, K. Michiue, M. Mitani, T. Fujita, **2009**.

[19] M. Suga, M. Kioka, T. Kobayashi, A. Kato, M. Endo, US Patent 4972035 A, **1990**.

[20] P. Chammingkwan, V. Q. Thang, M. Terano, T. Taniike, *Top. Catal.*, **2014**, *57*, 911–917.

[21] T. Taniike, P. Chammingkwan, M. Terano, *Catal. Commun.*, **2012**, *27*, 13–16.

[22] T. Taniike, P. Chammingkwan, V. Q. Thang, T. Funako, M. Terano, *Appl. Catal. A Gen.*, **2012**, *437–438*, 24–27.

[23] M. Thommes, K. Kaneko, A. V. Neimark, J. P. Olivier, F. Rodriguez-Reinoso, J.

Rouquerol, K. S.W. Sing, *Pure Appl. Chem.*, **2015**, *87*, 1051–1069.

[24] H. D. Chanzy, J. F. Revol, R. H. Marchessault, A. Lamandé, *Colloid Polym. Sci.*, **1973**, *251*, 563–576.

[25] E. M. Ivan'kova, L. P. Myasnikova, V. A. Marikhin, A. A. Baulin, B. Z. Volchek, *J. Macromol. Sci. Part B*, **2001**, *40*, 813–832.

[26] Z. Ye, S. Zhu, W. J. Wang, H. Alsyouri, Y. S. Lin, *J. Polym. Sci. Part B Polym. Phys.*, **2003**, *41*, 2433–2443.

[27] A. Kalita, I. R. Kamrupi, B. Pokhrel, S. K. Dolui, *J. Appl. Polym. Sci.*, **2012**, *125*, 2539–2548.

[28] K. Kageyama, J. Tamazawa, T. Aida, *Science*, **1999**, *285*, 2113–2115.

[29] R. O. Feuge, M. B. Pepper, R. T. O'Connor, E. T. Field, *J. Am. Oil Chem. Soc.*, **1951**, *28*, 420–426.

[30] N. U. Soriano, V. P. Migo, M. Matsumura, *Chem. Phys. Lip.*, **2003**, *126*, 133–140.

[31] H.T. Zhang, X.H. Chen, *Nanotechnology*, **2005**, *16*, 2288–2294.

[32] M. Klokkenburg, J. Hilhorst, B. H. Erné, *Vib. Spectrosc.*, **2007**, *43*, 243–248.

[33] I. Shancita, H. H. Masjuki, M. A. Kalam, S. S. Reham, S. A. Shahir, *Energy & Fuels*, **2016**, *30*, 4790–4805.

[34] P. Li, C. Liu, L. Zhang, S. Zheng, Y. Zhang, *Ultrason. Sonochem.*, **2017**, *34*, 938–946.

[35] S.B. Kumari, V.K. Rao, *Int. J. Pure Appl. Zool.*, **2016**, *4*, 262–270.

[36] J. Sivasankari, S. Selvakumar, K. Sivaji, S. Sankar, *J. Alloys Compd.*, **2014**, *616*, 51–57.

[37] P. J. Thistlethwaite, M. L. Gee, D. Wilson, *Langmuir*, **1996**, *12*, 6487–6491.

[38] Y. Tao, *J. Am. Chem. Soc.*, **1993**, *115*, 4350–4358.

[39] W. Q. Gong, A. Parentich, L. H. Little, L. J. Warren, *Colloids Surf.*, **1991**, *60*, 325–339.

[40] F.X. Perrin, V. Nguyen, J.L. Vernet, *J. Sol-Gel Sci. Technol.*, **2003**, *28*, 205–215.

[41] Y. Ren, K. Iimura, T. Kato, *Langmuir*, **2001**, *17*, 2688–2693.

[42] R. Urlaub, U. Posset, R. Thull, *J. Non. Cryst. Solids*, **2000**, *265*, 276–284.

[43] D.C.L. Vasconcelos, V.C. Costa, E.H.M. Nunes, A.C.S. Sabioni, M. Gasparon, W.L. Vasconcelos, *Mater. Sci. Appl.*, **2011**, *02*, 1375–1382.

[44] S. Rastogi, D.R. Lippits, G.W.H. Höhne, B. Mezari, P.C.M.M. Magusin, in:, J. Phys. Condens. Matter, IOP Publishing, **2007**, p. 205122.

Chapter 3

Nano-dispersed Ziegler-Natta catalysts for 1 μm-sized ultra-high molecular weight polyethylene particles

Abstract

A catalytic approach to synthesize microfine ultra-high molecular weight polyethylene (UHMWPE) particles was proposed based on the exploitation of nano-sized catalysts. By utilizing MgO nanoparticles as a core material, a Ziegler-Natta-type $MgO/MgCl_2/TiCl_4$ core-shell catalyst with the particle size in a nano-range scale was prepared in a simple preparation step. The organic modification of MgO surfaces prior to catalyzation prevented agglomeration and facilitated the full dispersion of catalyst particles at a primary particle level for the first time. The nano-dispersed catalysts successfully afforded a direct access to UHMWPE having the particle size in the range of 1-2 μm at a reasonable activity. Extremely fine polymer particles yielded several advantages, especially at a significantly lower fusion temperature in compression molding.

3.1. Introduction

Polyethylene (PE) having a molecular weight over 1-1.5 × 10^6 g mol^{-1}, termed as ultra-high molecular weight polyethylene (UHMWPE), equips a range of advantages over commodity high-density PE (HDPE), such as high abrasion resistance, excellent impact toughness, good corrosion and chemical resistance, resistance to cyclic fatigue and radiation, and self-lubricating ability [1]. As a result, it has been highly demanded in numerous applications, especially under harsh environment. While a number of catalysts have been developed and disclosed (non-supported or supported metallocene, fluorinated-oxide supported chromium, etc [2–8], the industrial production of UHMWPE is dominantly owed by heterogeneous Ziegler-Natta catalysts, $MgCl_2/TiCl_4$. Prohibitively high melt viscosity of UHMWPE necessitates direct processing of as-synthesized reactor powder, in which the initial morphology of UHMWPE powder is retained in the final product to be a cause of abrasive wear and ultimate failure [9–11].

Various methods have been proposed to improve the processability of UHMWPE. This includes the addition of low molecular weight PE [12] or liquid paraffin [13] as a processing aid. However, some or considerable losses of the beneficial properties of UHMWPE are accompanied due to the dilution with the low molecular weight component and shear degradation in the extruder [12]. Catalytic approaches have been also adopted

to produce UHMWPE featured with enhanced flow characteristics and drawability. These methods target at minimizing the density of polymer chain entanglement as it restricts the mobility of polymer. Ethylene is polymerized under a condition that a single polymer chain crystallizes without overlapping with the others. This requires diluted active sites and low temperature for the crystallization, especially polymerization using a diluted molecular catalyst for a spatial distance between growing alkyl chains sufficiently far to allow chain folding into individual crystals as soon as they come out [14,15]. Recently, a compartmentalization concept has been applied to a heterogeneous catalyst to provide the spatial distance between the growing chains. For example, Li et al. employed polyhedral oligomeric silsesquioxane (POSS) as a spacer in a fluorinated bis(phenoxyimine)Ti dichloride/SiO_2 catalyst system [16]. POSS was bonded to a methylaluminoxane-activated SiO_2 surface, and this became a horizontal spacer to compart the neighboring active sites and disallow an overlap of polymer chains. Another work from the same group showed that POSS can capture $MgCl_2$ through its hydroxyl groups to form nano-sized aggregates that served as a spacer in a $TiCl_4/MgCl_2/SiO_2$ catalyst system for the synthesis of weakly entangled UHMWPE with enhanced flow properties [17].

The simplest yet effective route to improve processability of UHMWPE is to

control/reduce the size of polymer particles as building blocks [18–20]. Though several processes, such as emulsion polymerization and thermally induced phase separation, are commonly applied to access polymer fine particles [21,22], these processes are hardly applicable to UHMWPE owing to the catalyst deactivation in the presence of a polar solvent as well as the limitation of polymer dissolution in a common organic solvent. Consequently, a direct approach to obtain fine particles in catalyzed olefin polymerization is most preferred. Known as replication phenomena [23,24], the particle size and its distribution of UHMWPE reactor powder are determined by those of the catalysts employed, in which the final polymer particle size is roughly proportional to $Y^{1/3}\ D_{Cat}$, where Y and D_{Cat} represent the polymer yield per gram-catalyst and the size of catalyst particles, respectively. Considering not only the essential requirement for a low impurity level in the obtained polymer, but also the factor of 1/3 for Y, the range of the polymer particle size controllable by the polymer yield is quite limited. Hence, minimizing the catalyst particle size without scarifying the activity and morphological integrity during polymerization is essential. In general, Ziegler-Natta catalysts possessing particle sizes around 5-20 μm are used to produce commodity grades of UHMWPE having particle sizes of 100-300 μm. Whilst, microfine particles (*e.g.* below 80 μm) can be accessed by catalysts with the sizes of a few-to-several micrometers [25].

A number of preparation protocols have been developed to access a Ziegler-Natta catalyst possessing a small particle size. However, most of the processes necessitate complicated chemical formulas as well as technically demanding processes. For example, a multistep process is typically required for the preparation of Mg solution precursors, and subsequent precipitation/titanation to form morphologically controlled solid particles [26–28]. In some cases, a high speed shearing either during the formation of a solid support or after forming a solid catalyst [25,29] is further required to bring the particle size down to a few-to-several micrometers. To escape from an elaborate preparation process, the development of catalyst preparation protocol to access small catalyst particles in a simple manner is still highly desired. Especially, a Ziegler-Natta catalyst with the particle size in a nano-range scale is expected to facilitate the greatest advantage for $Y^{1/3}$ D_{Cat}.

A simple protocol for the preparation of a Ziegler-Natta nanocatalyst was developed by our laboratory using MgO nanoparticles as a core material [30–32]. In this catalyst system, catalyzation proceeds on the surfaces of MgO cores: The chlorination using $TiCl_4$ converts MgO outermost surfaces into a thin $MgCl_2$ overlayer, and simultaneously immobilizes $TiCl_4$ on $MgCl_2$ via chlorine bridges to form a core-shell $MgO/MgCl_2/TiCl_4$ catalyst in one step. The catalyst possesses a similar active site

nature to a typical Ziegler-Natta catalyst, thus being active for olefin polymerization. In chapter 2, I have successfully applied the core-shell $MgO/MgCl_2/TiCl_4$ catalyst for the synthesis of UHMWPE with a reasonable activity [33]. However, it was found that the size of polymer particles did not reflect the nano-sized nature of the catalyst particles. The key issue was found at the dispersion of nanoparticles: MgO was poorly dispersed in a non-polar solvent due to its hydrophilic nature, hence causing the agglomeration of catalyst particles. While an organic modification of MgO surfaces helped to alleviate the dispersion problem, the removal of the organic modifier from MgO surfaces by $TiCl_4$ prevented the exploitation of nano-sized features for polymer particle control. In this chapter, I attempted to screen a variety of organic modifiers to access truly nano-dispersed Ziegler-Natta catalyst particles. By a careful selection of the organic modifier, a catalyst with the dispersion at a nano level was attained for the first time, which enabled the direct synthesis of extremely fine UHMWPE particles featured with several advantages in compression molding.

3.2. Experimental

3.2.1 Materials

MgO nanoparticles with the mean particle size of 50 nm (Wako Pure Chemical Industries Ltd.), 100 nm (Alfa-Aesar), and 200 nm (Wako Pure Chemical Industries Ltd.) were used after dehydration at 160°C under vacuum for 2 h. Titanium tetrachloride ($TiCl_4$) and kerosene of research grade were used as received. Sorbitan monooleate ($C_{24}H_{44}O_6$, donated by Kao Co.), sorbitan sesquioleate ($C_{33}H_{60}O_{6.5}$, donated by Kao Co.), methyl oleate ($C_{19}H_{36}O_2$, Tokyo Chemical Industry Co., Ltd.), and polyoxyethylene alkylamine ($RN(C_2H_4O)_x(C_2H_4O)_y$, donated by NOF Co.) were used for the organic modification of MgO surfaces (the chemical structures are given in Figure 1 in the supplementary information). *n*-Heptane was used after dehydration by passing through a column of molecular sieve 4A, followed by N_2 bubbling for 2 h. Ethylene of polymerization grade was purchased from Hokurikuekikasangyou Co., Ltd. and used as received. Triethylaluminium (TEA, donated by Tosoh Finechem Co.) was used after dilution in heptane. A precipitation-based Ziegler-Natta catalyst (denoted as R-Cat, D_{50} = 7.95 μm, donated by IRPC Public Co., Ltd.) was used as a reference catalyst in ethylene polymerization.

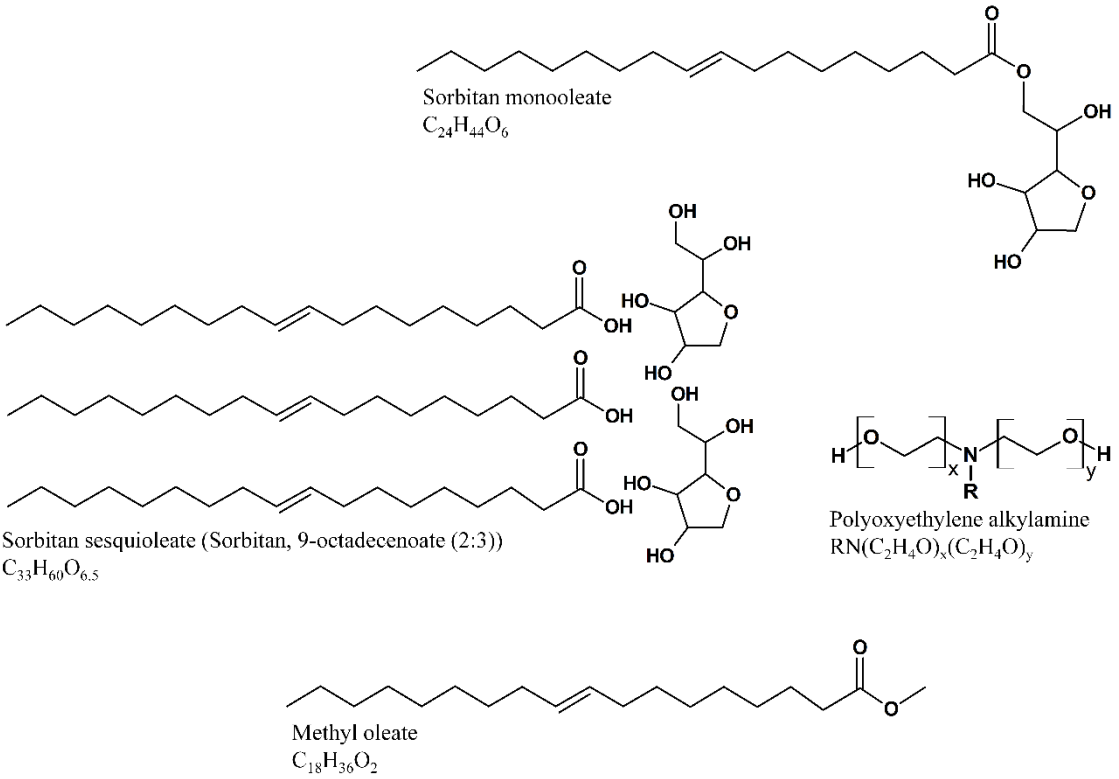

Figure 1 Chemical structures of organic modifiers

3.2.2 Surface Modification of MgO and Catalyst Preparation

To a suspension of 10 g of dehydrated MgO powder in 25 mL of kerosene, 8 mL of an organic modifier was added. The mixture was heated at 160°C for 1 h under stirring at 250 rpm. The product was repetitively washed with heptane to yield organically modified MgO. The samples were named as X-MgOY, where X corresponded to the type of the organic modifier (sorbitan monooleate = SM, sorbitan sesquioleate = SS, methyl oleate = MO, and polyoxyethylene alkylamine = PA), and Y corresponded to the particle size of employed MgO.

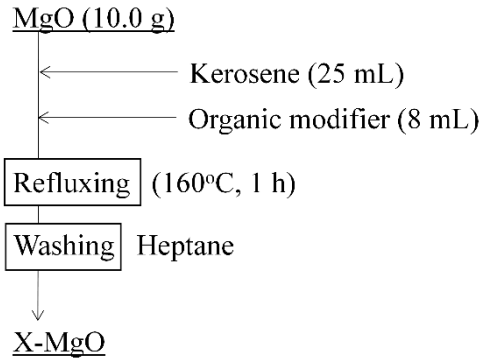

Scheme 1 Preparation of treated MgO

2.0 g of PA-MgO was treated with 30 mL of $TiCl_4$ in 100 mL of heptane at the reflux temperature for 1 h. Thus obtained catalyst was repetitively washed with heptane and kept as a slurry in heptane. The samples were named as PA-Cat50, PA-Cat100, and PA-Cat200. Reference catalyst samples were also prepared from pristine MgO powder having the particle size of 50 and 200 nm according to the same procedure. The samples were named as Cat50 and Cat200, respectively.

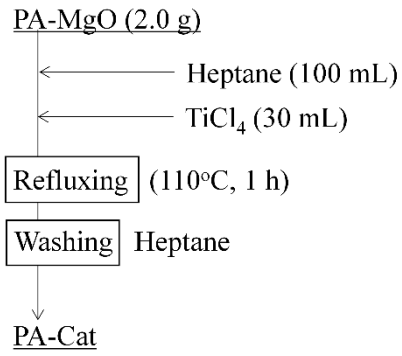

Scheme 2 Catalyst preparation

3.2.3 Polymerization

Ethylene polymerization was performed in a 1 L stainless steel reactor equipped with a mechanical stirrer rotating at 500 rpm. After sufficient N_2 replacement, 500 mL of heptane as a polymerization medium and 1.0 mmol of TEA as an activator were introduced. The solution was then saturated with 0.8 MPa of ethylene at 70°C for 30 min. 10 mg of a catalyst was injected to start polymerization. The polymerization was carried out at 70°C under 0.8 MPa of ethylene pressure for 2 h. Thus obtained polymer was filtered and dried in vacuum at 60°C for 6 h.

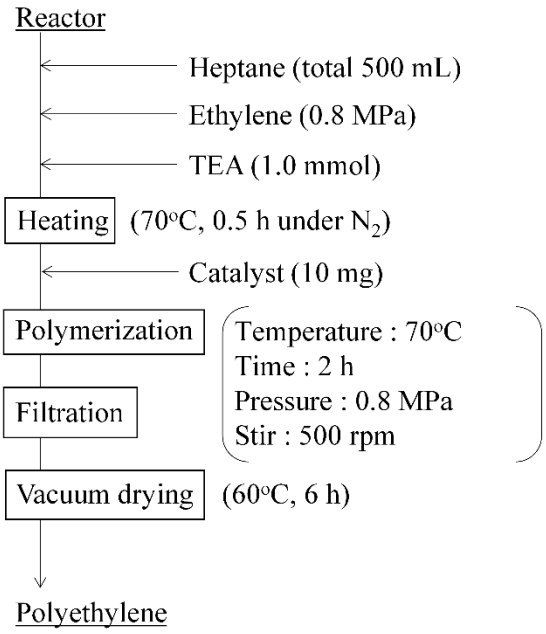

Scheme 3 Polymerization condition

3.2.4 Characterization

Images of MgO nanoparticles were recorded on a transmission electron microscope (TEM, Hitachi H-7100) operated at an accelerating voltage of 100 kV. MgO powder was dispersed in ethanol, drop-casted on a copper grid, and naturally dried. The particle size distribution profiles of MgO and catalyst samples were acquired from light scattering (Horiba Partica LA-950V2). The measurements were done in a suspension form using heptane as a medium unless stated. The particle size was expressed as D_{10}, $D_{50,}$ and D_{90}, which corresponded to the particle size at 10%, 50% and 90% of the cumulative volume distribution. A relative span factor (RSF) was calculated based on **Equation (1)**:

$$\text{RSF} = \frac{D_{90} - D_{10}}{D_{50}} \quad (1)$$

The presence of the organic modifier on MgO surfaces was observed by attenuated total reflectance infrared spectroscopy (ATR-IR, Perkin Elmer Spectrum 100 FT-IR) in the range of 4000-500 cm^{-1}. The Ti content of a catalyst was determined by ultraviolet-visible spectrometry (UV-vis, Jasco V670). 50 mg of the catalyst was dissolved in an aqueous solution of hydrochloric acid and sulfuric acid. After that, 200 μL of hydrogen peroxide (35% aqueous solution) was added. The Ti content was determined based on the intensity of the absorption band at 410 nm[34].

The particle size of polymer reactor powder was acquired by light scattering using ethanol as a medium. The observed particle size was compared with the theoretical size estimated according to **Equation (2)**:

$$D_{PE} = \left(\frac{d_{Cat}}{d_{PE}} Y\right)^{\frac{1}{3}} D_{Cat} \quad (2)$$

where d_{Cat} and d_{PE} are the densities of the catalyst and polymer, respectively. Y is the polymerization yield in g-PE g-Cat^{-1}. D_{PE} and D_{Cat} are the particle sizes of the polymer and catalyst, respectively. This equation assumes that one polymer particle is formed per one catalyst particle without disintegration of the catalyst particle during polymerization. The particle size of polymer in a dry form was also measured based on image analysis of vacuum-dispersed powder using a VD-3200nano particle size analyzer (JASCO). A vacuum-type dispersion unit allowed the dispersion of polymer particles on a glass plate in a dry state, and the particle characteristics were acquired by an automatic image analysis using Pro image analysis software. The viscosity-average molecular weight (M_v) of polymer was determined based on ASTM D4020. This method is widely used to acquire the molecular weight of UHMWPE as it is nearly impossible to apply gel permeation chromatography due to restriction of solution flow and shear-induced chain scission in the column. The viscosity of a dilute polymer solution in decahydronaphthalene was measured at 135°C using an Ubbelohde-type

viscometer, and M_v was derived from the intrinsic viscosity of polymer ([η]) according to **Equation (3)**:

$$M_v = 5.37 \times 10^4 [\eta]^{1.37} \quad (3)$$

The melting temperature (T_m) and crystallization temperature (T_c) of polymer were acquired using a differential scanning calorimeter (DSC, Mettler Toledo DSC 822). As-obtained reactor powder was heated to 180°C at the heating rate of 10 °C/min under N_2 flow. T_m of polymer for the nascent form was obtained from the melting endotherm in the first heat cycle. After holding at 180°C for 10 min, the sample was cooled down to 50°C at the cooling rate of 10 °C/min to acquire non-isothermal T_c. Thereafter, the second heat cycle was applied at the heating rate of 10 °C/min to obtain T_m for the melt-crystallized form.

3.2.5 Compression Molding

Reactor powder was molded into a 5 cm × 5 cm specimen with the thickness of 500 μm by compression molding using a flash picture-frame mold. A specified amount of reactor powder was filled into an aluminum chase sandwiched between two thin ferrotype plates and pressed with a contact pressure at room temperature for 5 min. Thereafter, the temperature was raised to a molding temperature and kept for 6 min before applying

full pressure of 20 MPa for additional 5 min. The specimen was then cooled to room temperature. Different molding temperatures in the range of 120 - 140°C were applied to observe the initiation of fusion. As-obtained reactor powder was also used to form a scratch resistant coat. On a 5 cm × 5 cm HDPE plaque, a specified amount of reactor powder was placed, followed by compression molding using the above-mentioned procedure at the molding temperature of 140°C.

3.3. Result and Discussion

A nano-sized Ziegler-Natta catalyst was developed based on the utilization of MgO nanoparticles as a core material. Since a non-polar solvent is required in catalyzation, full dispersion of MgO in the medium is essential to prevent the agglomeration of catalyst particles. As shown in Figure 2a, MgO50 was highly dispersible in ethanol with a sharp particle size distribution profile. The mode size was *ca.* 80 nm, and was small enough to be regarded as the dispersion of primary particles. Contrary, the same sample was poorly dispersed in heptane as demonstrated in the mode size of around 10 μm. Organic modifiers of various types in the group of non-ionic surfactants were applied for the surface modification (Figure 2a). It should be noted that these organic modifiers have a similar length of aliphatic chains, while different functional groups are present in the head group (see Figure 1). In all cases, the adsorption is expected to occur through hydrogen bonding between the functional group and hydroxyl groups available on MgO surfaces. Light scattering results showed that the treatment with the organic modifiers caused the shift of the particle size towards the primary particle size, while only polyoxyethylene alkylamine afforded fully dispersible MgO. These results indicated a different strength of the adsorption, in which multiplicity of anchoring groups is important to attain the strong adsorption.

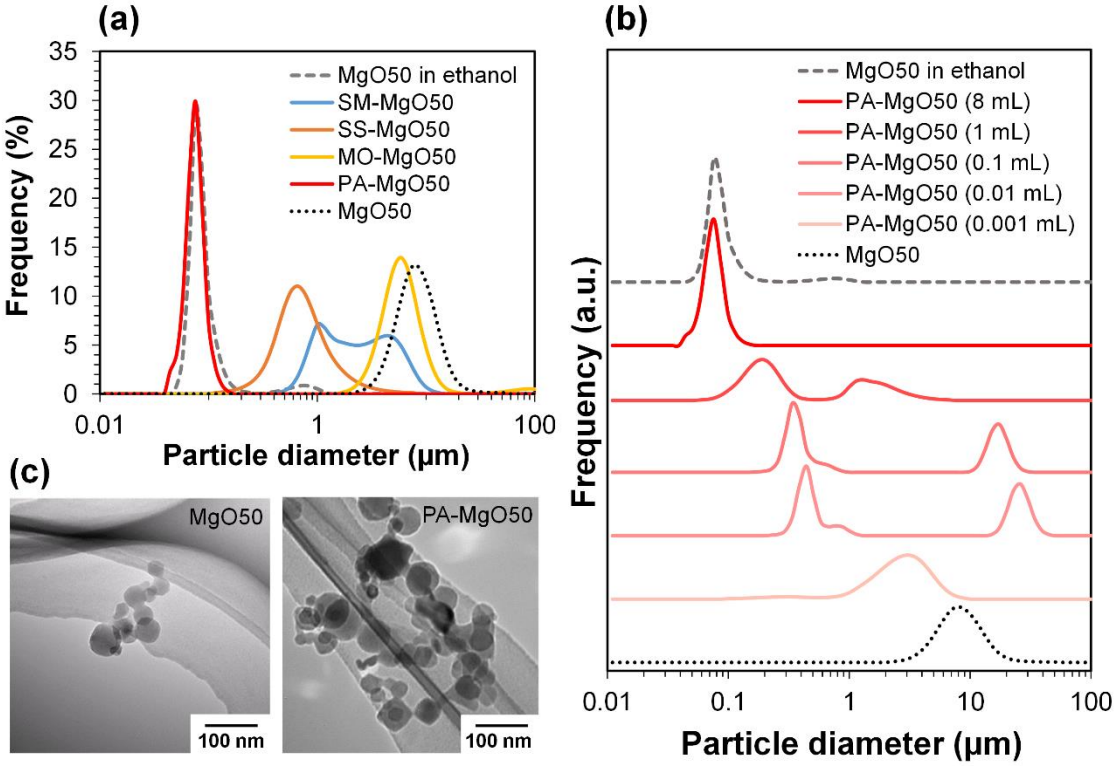

Figure 2 Particle size distribution profiles of MgO50 before and after treating with different types of organic modifiers (a), and different amounts of polyoxyethylene alkylamine (b). The analysis was conducted as a suspension in heptane unless stated. TEM images of pristine MgO50 and PA-MgO50 (c)

Figure 2b and Table 1 show the light scattering results of MgO50 that was treated with different amounts of polyoxyethylene alkylamine. The increase in the addition amount from 0.001 to 1 mL caused a change in the particle size distribution profile in a non-uniform way: Unimodal and bimodal distribution profiles appeared. However, the particle size always shifted towards the primary particle size, and this was true for the particle size in the first mode of the bimodal distribution. By further increasing the

amount of polyoxyethylene alkylamine to 8 mL, MgO nanoparticles became fully dispersed at a primary particle level. These resulted implied that polyoxyethylene moiety helped to eliminate the attraction force among nanoparticles and/or to endow nanoparticles with surface hydrophobicity, in which a full surface coverage was essential for the homogenous dispersion of primary particles. TEM images in Figure 2c confirmed that a polygonal morphology of MgO nanoparticles was well-preserved after the surface modification.

Table 1 Particle characteristics of organically modified MgO

Sample	Particle size[a] (μm)			RSF[b]
	D_{10}	D_{50}	D_{90}	
MgO50	4.48	7.58	13.0	1.12
PA-MgO50 (0.001 mL)	1.08	2.50	4.54	1.38
PA-MgO50 (0.01 mL)	0.354	0.699	27.9	39.4
PA-MgO50 (0.1 mL)	0.283	0.492	19.2	39.5
PA-MgO50 (1 mL)	0.119	0.230	2.00	8.18
PA-MgO50 (8 mL)	0.054	0.070	0.088	0.490
MgO50 in ethanol	0.061	0.077	0.120	0.766

[a] Analyzed by light scattering as a suspension in heptane unless stated; [b] Calculated based on **Equation (1)**.

ATR-IR spectra were acquired to confirm the presence of polyoxyethylene alkylamine

on MgO surfaces (Figure 3). In the spectrum of MgO50, a sharp peak at 3700 cm^{-1} indicates the presence of physisorbed water, which also accompanies the OH bending at 1632 cm^{-1} [35,36]. The bands between 1300-1500 cm^{-1} are assigned to the O-C-O vibration from CO_2 impurity adsorbed on MgO surfaces in different modes of the adsorption [37,38]. The band at 849 cm^{-1} is ascribed to the C=O vibration of the bidentate carbonate complex of CO_2 [38,39]. In the spectrum of PA-MgO50, new bands belonging to the organic modifier were observed. The peaks at 2959, 2925, and 2856 cm^{-1} are assigned to the asymmetric stretching of CH_3, asymmetric stretching of CH_2, and symmetric stretching of CH_2 from the aliphatic chain, respectively [40]. A broad band around 1085 cm^{-1} corresponds to the asymmetric C-O-C stretching of the repeating -O-CH_2-CH_2-O- units of polyoxyethylene [41], while an intense peak at 1460 cm^{-1} comes from both of the CO_2 adsorption [36] and the CH_2 deformation bending [40].

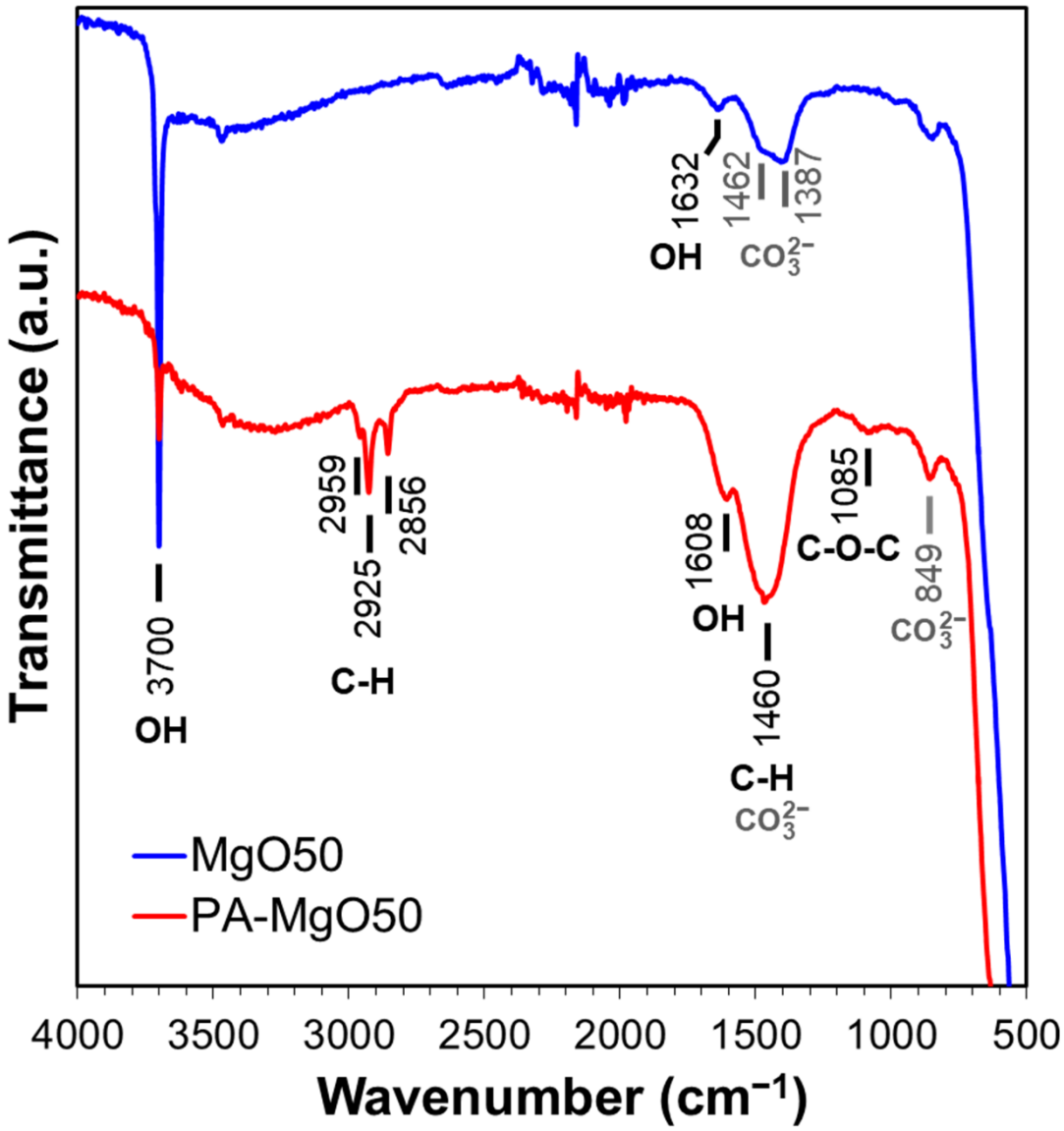

Figure 3 ATR-IR spectra of PA-MgO50, referenced to pristine MgO50

Figure 4a illustrates the light scattering results of PA-MgO50 and MgO50 before and after catalyzation. The particle characteristics are also summarized in Table 2 In the case of pristine MgO, the catalyzation further promoted the agglomeration, where a second peak in the particle size distribution profile appeared at around 100 μm (Cat50).

As mentioned earlier, such a severe agglomeration was originated from poor dispersion of MgO in a non-polar solvent. Suspended nanoparticles were electrostatically agglomerated. Once a thin layer of $MgCl_2$ was formed, the agglomeration further progressed and became irreversible due to an enhanced attraction arising from an ionic character and/or the formation of a hard neck at the contact points. When the surface modification was applied (PA-Cat50), the agglomeration during catalyzation could be fully prevented due to the presence of adlayer. We also attempted to apply the same procedure to MgO nanoparticles having different particle sizes and the results showed that all of the catalysts became fully dispersible at the primary particle level (Figure 4b). Hence, the proposed method offered an access to nano-dispersed Ziegler-Natta catalysts, whose size could be easily controlled through the size of original MgO nanoparticles.

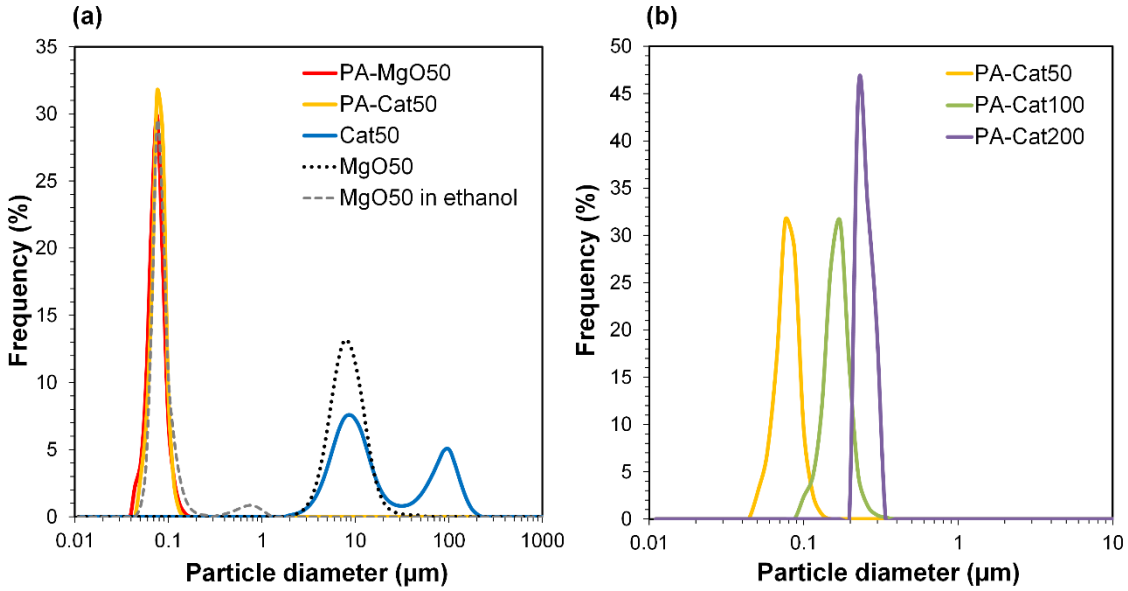

Figure 4 Particle size distribution profiles for MgO50 and before and after catalyzation (a), and those for catalyst samples prepared from organically modified MgO having different particle sizes (b)

Table 2 Particle characteristics of catalysts

Sample	Particle size[a] (μm)			RSF[b]
	D_{10}	D_{50}	D_{90}	
PA-Cat50	0.058	0.073	0.090	0.438
PA-Cat100	0.118	0.153	0.191	0.477
PA-Cat200	0.203	0.230	0.279	0.330
Cat50[c]	5.02	11.3	98.3	8.25
Cat200[c]	3.32	5.95	10.0	1.12

[a]Analyzed by light scattering as a suspension in heptane; [b]Calculated based on **Equation (1)**; [c]Prepared from pristine MgO.

The polymerization performance of the nano-dispersed catalysts was examined and

compared with reference catalysts (Cat50, Cat200, and R-Cat). In Table 3, the Ti content and the polymerization activity increased with the decrease in particle size of MgO for both of the modified and non-modified catalyst systems. However, it could be recognized that the activities for the modified catalysts were at maximum halved from that of non-modified ones. Considering that the particle size distribution profile of the nano-dispersed catalysts was maintained at the primary particle level, it was most plausible that the organic modifier retained on the surfaces during chlorination. The presence of electron donating groups as well as steric restriction upon chlorination might restrict the activity. Nonetheless, it must be mentioned that the catalyst efficiency per Ti content of PA-Cat50 was higher than that of a typical precipitation-based Ziegler-Natta catalyst (R-Cat), while the Cl content in the resultant polymer was estimated to be an order of a magnitude lower due to the Cl existence only in the thin $MgCl_2/TiCl_4$ catalytic layer (below 2 nm) [32]. Simplicity in the catalyst preparation featured with the reasonable activity as well as a reduced Cl residue in polymer powder made nano-dispersed $MgO/MgCl_2/TiCl_4$ catalysts promising for an industrial application.

Table 3 Polymerization results

Sample	Ti content[a] (wt%)	Activity[b] (g-PE g-Cat^{-1})	Polymer particle characteristics		
			D_{50}[c] (μm)	RSF[d]	Theoretical size[e] (μm)
PA-Cat50	0.76	3200	77.3	0.564	1.67
PA-Cat200	0.33	68	171	0.370	1.46
Cat50	0.47	6240	711	1.01	324
Cat200	0.17	420	633	0.870	69
R-Cat[f]	2.5	7900	147	0.686	212[g]

[a]Determined based on UV-vis spectroscopy; [b]Polymerization conditions: Ethylene pressure = 0.8 MPa, heptane = 500 mL, TEA = 1.0 mmol, catalyst = 10 mg, T = 70 °C, t = 2 h; [c]Analyzed by light scattering as a suspension in ethanol; [d]Calculated based on **Equation (1)**; [e]The theoretical polymer particle size was calculated based on **Equation (2)**. The densities of polymer and the catalysts were set to 0.97 g cm^{-3} for UHMWPE and 3.65 g cm^{-3} for MgO, respectively. The catalyst particle size in **Equation (2)** was set to the D_{50} value acquired from light scattering (*cf.* Table 2); [f]A precipitation-based Ziegler-Natta catalyst (D_{50} = 7.95 μm) was supplied from IRPC Public Co., Ltd; [g]The density of R-Cat was set at 2.32 g cm^{-3} for $MgCl_2$.

The morphology of polymer reactor powder was observed either by an optical microscope or SEM, depending on the particle characteristics. In the absence of the surface modification, as-obtained polymer powder apparently exhibited chunk-like and non-free-flow characteristics (PE50 and PE200). Optical microscope images of these samples show a coarse body of heavily agglomerated structures (Figure 5a, b). Contrary, free-flow polymer powder was obtained for the modified catalysts. SEM images

(Figure 5c, d) show that the particle sizes for PA-PE50 and PA-PE200 were much smaller than those obtained from the non-modified system. Microscopically, each particle was composed of a random agglomeration of many small particles. On the other hand, R-Cat gave polymer with a popcorn-like morphology, which is typical for a multigrain catalyst (Figure 5e) [42]. The particle sizes were acquired by light scattering in ethanol (Figure 6a) and the results are compared with the theoretical sizes. From Table 3, R-Cat gave polymer with a smaller particle size as compared to the theoretical size. Bearing in mind that that Equation (2) assumes a dense sphere for both of the catalyst and polymer particles, the deviation between the observed and theoretical sizes for R-Cat was originated from its porous structure rather than the disintegration of the catalyst or polymer particles during polymerization, *i.e.* the apparent density of the catalyst particles is lower than 2.32 g cm^{-3}, which was assumed for the $MgCl_2$ crystal. In the case of the non-modified catalysts (Cat50 and Cat200), the particle sizes were found to be 2-10 times greater than the theoretical sizes, indicating that further agglomeration proceeded during the polymerization. On the other hand, the deviation became unusually large for the modified catalyst system. Considering the dispersion stability of PA-Cat50 and PA-Cat200 in heptane, it was unlikely that the catalyst particles re-agglomerated during the polymerization. Rather, the plausible scenario was at the difficulty of polymer particles

to be dispersed in ethanol against electrostatic force. In order to confirm this idea, a different mean of the dispersion was adopted. Figure 6b depicts a microscope image of dry powder (PA-PE50), which was physically dispersed and collected on a glass plate. The observed image evidenced the presence of very small particles that are well-separated from each other. Indeed, the particle size measurement based on the image analysis of vacuum-dispersed powder unveiled a much smaller particle size than that observed from light scattering (Figure 6c). PA-PE50 exhibited D_{50} of 1.7 μm with a narrow range of particle size distribution and particle solidity. From the particle shape analysis, PA-PE50 generally composed of two types of particles, the distorted sphere and round shape. The former was found to be dominant with the range of the particle size close to the theoretical value (*ca.* 1 μm). It was believed that these distorted polymer particles were produced from primary catalyst particles, while some of them merged into a rounder shape with a bigger size during polymerization. In the case of R-PE, the polymer particles were also disintegratable due to a multigrain nature of the catalyst. This result is consistent with patent literature, where the popcorn-shape UHMWPE particles could be physically separated into fine particles by high speed shearing treatment [25]. However, it could be noticed that the particle size distribution for R-PE was much broader than that of PA-PE50 and a major portion of particles was not disintegratable only by

vacuum dispersion. These results evidenced that $MgO/MgCl_2/TiCl_4$ catalysts with nano-level dispersion allowed a direct access to microfine reactor powder.

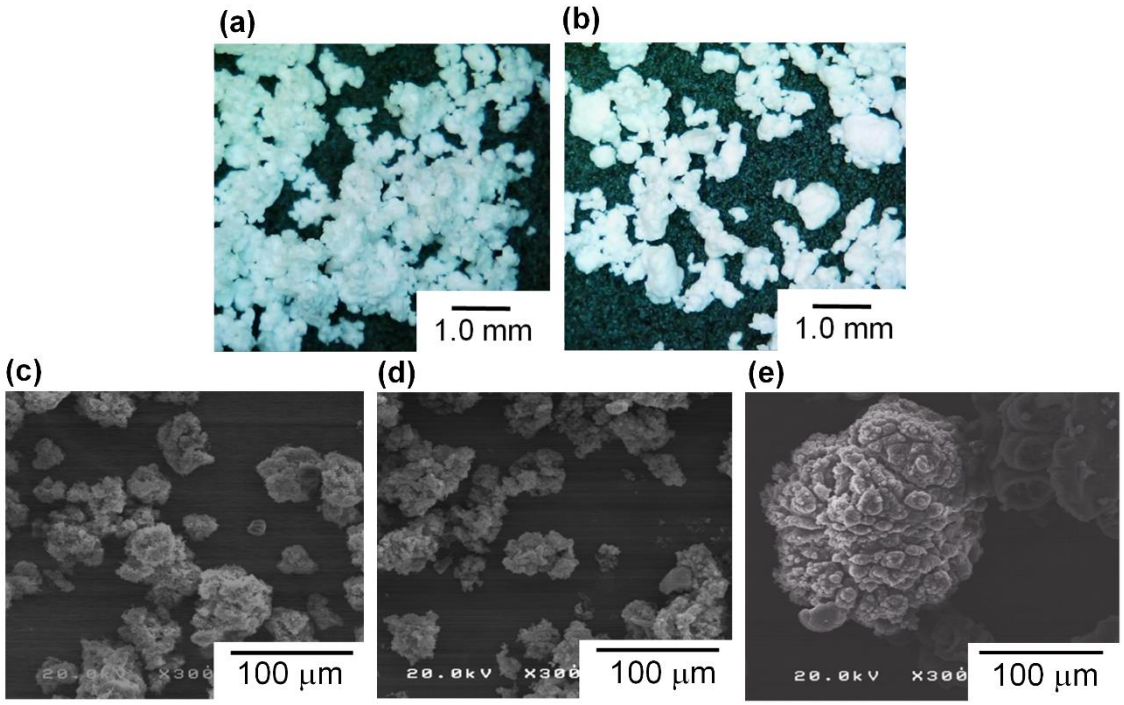

Figure 5 Morphology of polymer reactor powder: Microscope images of PE50 (a), and PE200 (b). SEM images of PA-PE50 (c), PA-PE200 (d), and R-PE (e)

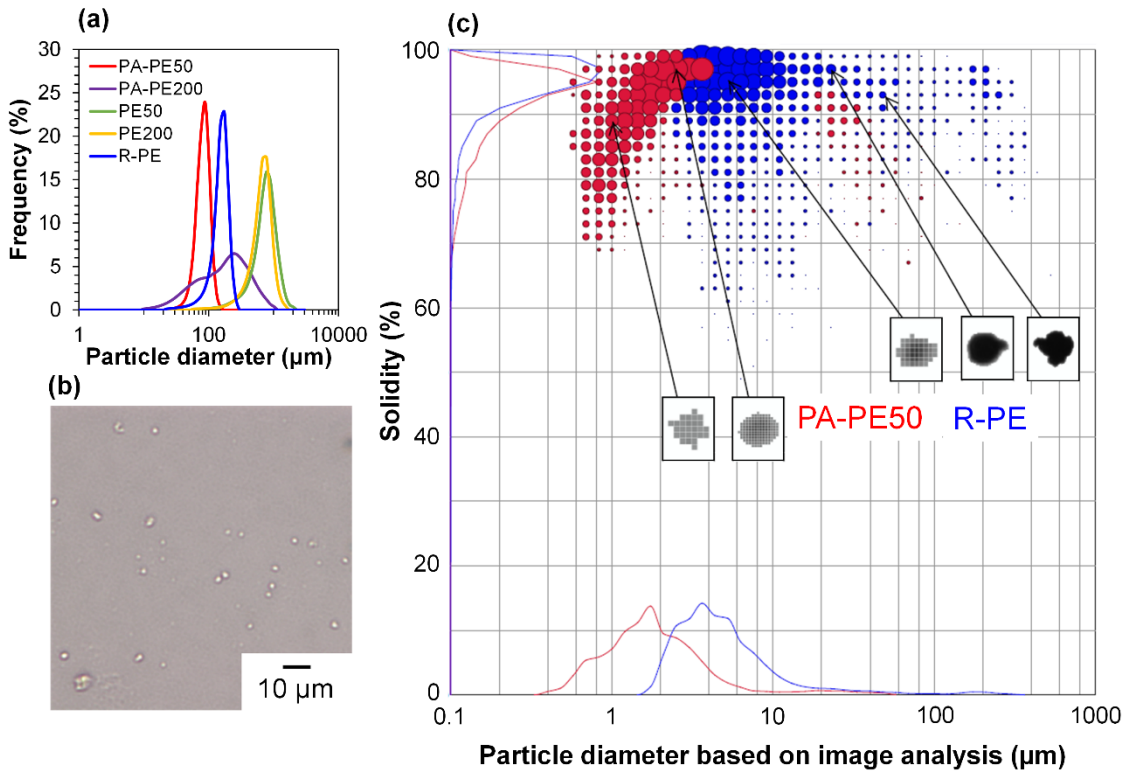

Figure 6 Polymer particle characteristics: Particle size distribution profiles of polymer reactor powder in ethanol (a), microscope image of PA-PE50 dispersed on a glass plate (b), and particle characteristics based on an image analysis of vacuum-dispersed polymer particles (c)

Table 4 summarizes the DSC results. The melting temperature (T_m) of as-obtained reactor powder (nascent form) was in the range of 140 - 143°C, while the T_m value was reduced to 132 - 135°C in the second heating (melt-crystallized form). The obtained values are consistent with literature reported for nascent and melt-crystallized UHMWPE having the molecular weight of 4.5×10^6 g/mol [43,44]. In fact, the M_v values of polymer powder obtained from PA-Cat50 and R-Cat were measured as 3.7×10^6 and 4.4

× 10^6 g mol^{-1}, respectively. These results confirmed that the nano-dispersed $MgO/MgCl_2/TiCl_4$ catalysts enabled the production of PE having the molecular weight in the range of ultra-high molecular weight similar to a typical Ziegler-Natta catalyst. A higher T_m value for the nascent form with respect to that for the melt-crystallized form was explained by the difference in crystal topology, where the cooperative melting of several lamellae is required for the nascent form to adopt the random coil state [44]. The crystallinity (X_c) and the crystallization temperature (T_c) for all of the samples were found to be in a similar range, and these values are typical for UHMWPE produced by Ziegler-Natta-type catalysts (Table 4) [17,45–47].

Table 4 DSC results

Sample	First heating (50 to 180°C)			Cooling (180 to 50°C)		Second heating (50 to 180°C)		
	T_m (°C)	ΔH_m (J g^{-1})	X_c[a] (%)	T_c (°C)	ΔH_c (J g^{-1})	T_m (°C)	ΔH_m (J g^{-1})	X_c[a] (%)
PA-PE50[b]	142.6	177.5	61.3	119.9	127.5	135.5	136.1	47.0
PA-PE200	140.2	173.6	60.0	120.4	141.4	135.0	139.1	48.1
PE50	140.2	185.0	63.9	122.6	125.4	132.5	150.7	52.1
PE200	140.2	192.3	66.5	121.8	140.9	133.7	149.4	51.7
R-PE[c]	142.8	176.5	61.0	119.2	137.7	135.8	143.1	49.4

[a]$\Delta H_{100\%}$ = 289.3 J g^{-1} (ASTM F2625); [b]M_v = 3.7 × 10^6 g mol^{-1}; [c]M_v = 4.4 × 10^6 g mol^{-1}.

In order to examine the processability of polymer reactor powder produced from the nano-dispersed catalyst, PA-PE50 was compressed into specimens at different molding temperatures. As shown in Figure 7, PA-PE50 started to fuse at 120°C as evidenced by the translucent region. On the other hand, R-PE required the molding temperature at least 140°C to start fusion. In general, the fusion of polymer powder involves physical processes such as melting, coalescence of particles, and crystallization [48]. In the case of the crystallization, the DSC results for the cooling (Table 4) revealed that PA-PE50 and R-PE samples have almost an identical crystallization temperature as well as a comparable crystallinity in the second heating. Hence, a significant difference in the crystallization behavior is unlikely. In regards to the polymer melting, though the applied molding temperatures were below T_m of polymer in the nascent form, a fraction of polymer might be already melted. Additional DSC measurements were conducted on the annealed samples to identify any differences for this fraction. The annealing temperature of 135°C was selected due to the following reasons: i) Both of the PA-PE50 and R-PE samples melted around this temperature in the second heating, and ii) this temperature represented the upper limit to obtain a clear disparity of the appearance between the two samples. Figure 8 shows the DSC curves of PA-PE50 and R-PE after being annealed at 135°C for 60 min. The melting peaks for the nascent and melt-

crystallized forms are also given as references. In the case of the annealed samples, a shoulder appeared in addition to the melting peak for the nascent form. This shoulder was related to the detachment of chains from the surfaces [44], which indicated that a part of crystals already melted under the processing condition. However, judging from a comparable DSC profile for both of the samples, it was concluded that PA-PE50 and R-PE possessed a similar melting behavior at the applied molding temperature. Considering the similarity in the molecular weight, crystallinity, melting and crystallization behaviors, a lower fusion temperature for PA-PE50 as compared to R-PE was most plausibly originated from the coalescence among particles. Though the coalescence of PA-PE50 particles could not be visually observed by an optical microscope due to too small particles, it is believed that the fine structure of PA-PE50 provided a larger contact interface to promote the fusion across the interface during compression molding. Additionally, a smaller size of voids between adjacent primary polymer particles might accelerate the process of compaction by shortening the flow path for particle sliding or elastic flow to complete the void filling step in molding.

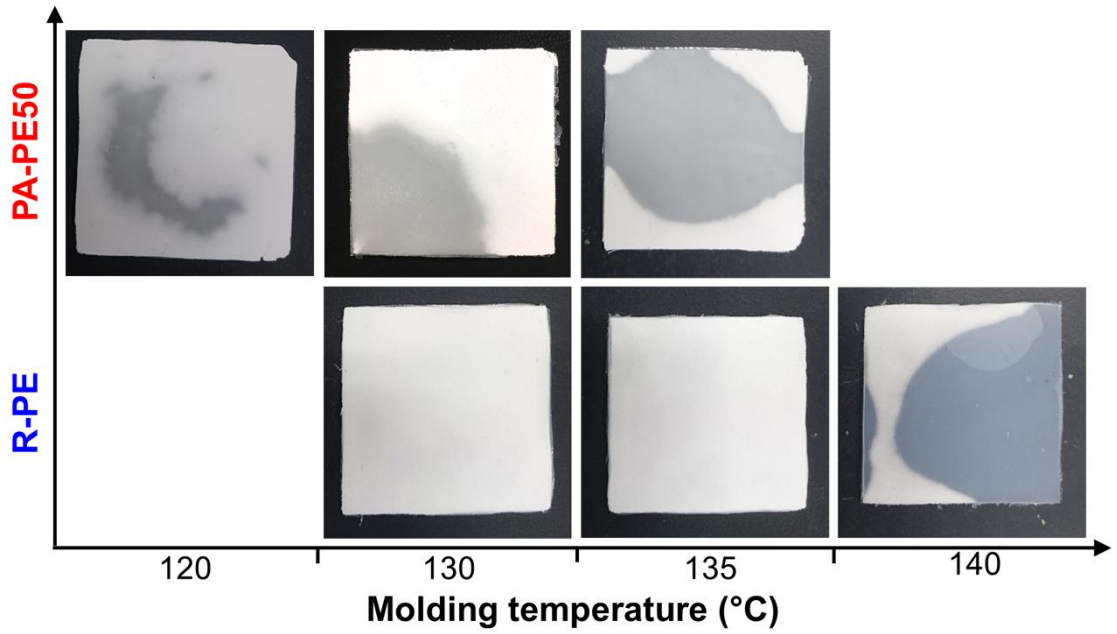

Figure 7 Compression-molded polymer reactor powder at different temperatures

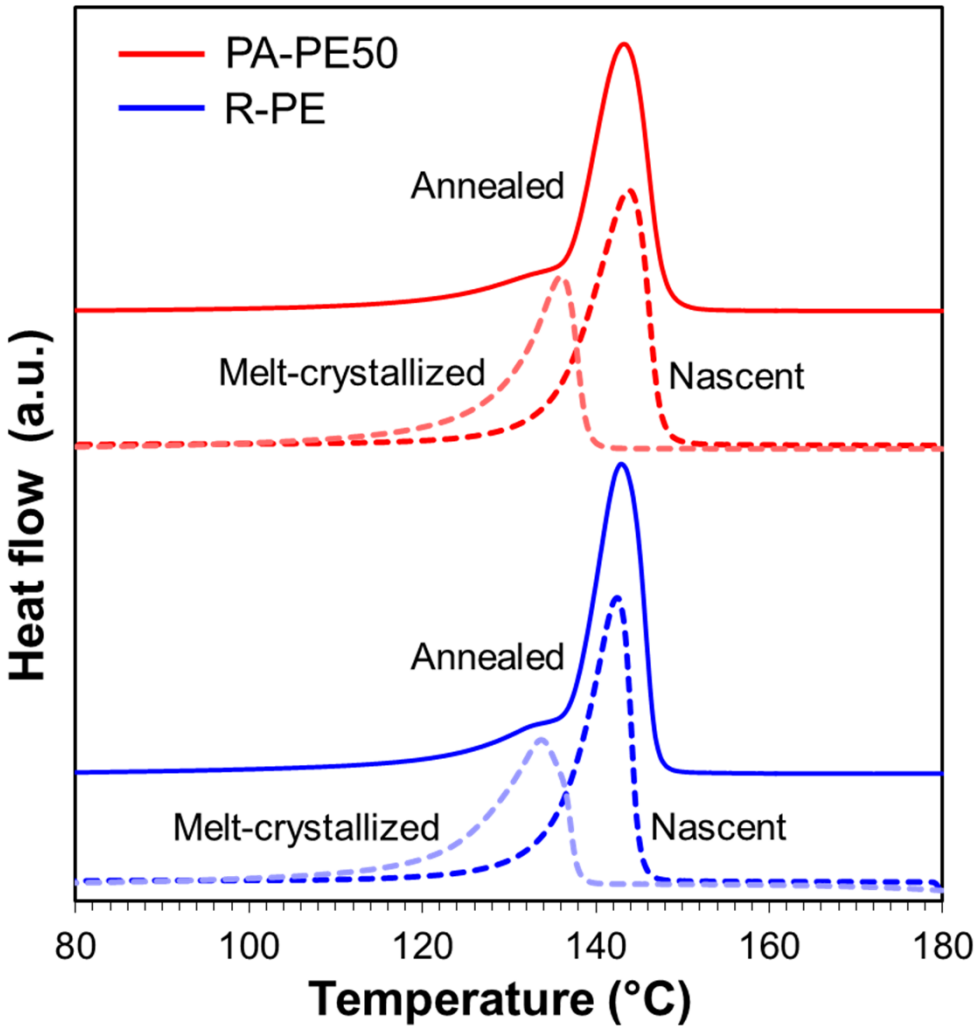

Figure 8 Melting behavior of polymer reactor powder after being annealed at 135°C for 60 min. Dashed lines are melting behavior for nascent and melt-crystallized forms as references

As-obtained reactor powder was also used to form a scratch resistant coat on a HDPE plaque by compression molding. The appearance of the specimens and the microscopic view of the surface after introducing a scratch are illustrated in Figure 9a, b. It should

be noted that the scratch was simply introduced using tweezers at an equivalent angle and force to preliminary observe the damage of the surface. As can be seen in Figure 9b, parabolic tracks were clearly visible for the original surface of HDPE. Contrary, coating the surface with both of PA-PE50 and R-PE powder noticeably introduced the scratch resistant property. In the case of PA-PE50 coating, no trace of the scratch was visible on the surface, while tiny parabolic tracks were observed for R-PE coating. The finished surface was also found to be much smoother for PA-PE50 than for R-PE. These results suggested that the fine structure of PA-PE50 allowed a better consolidation to improve the surface properties at a given processing temperature.

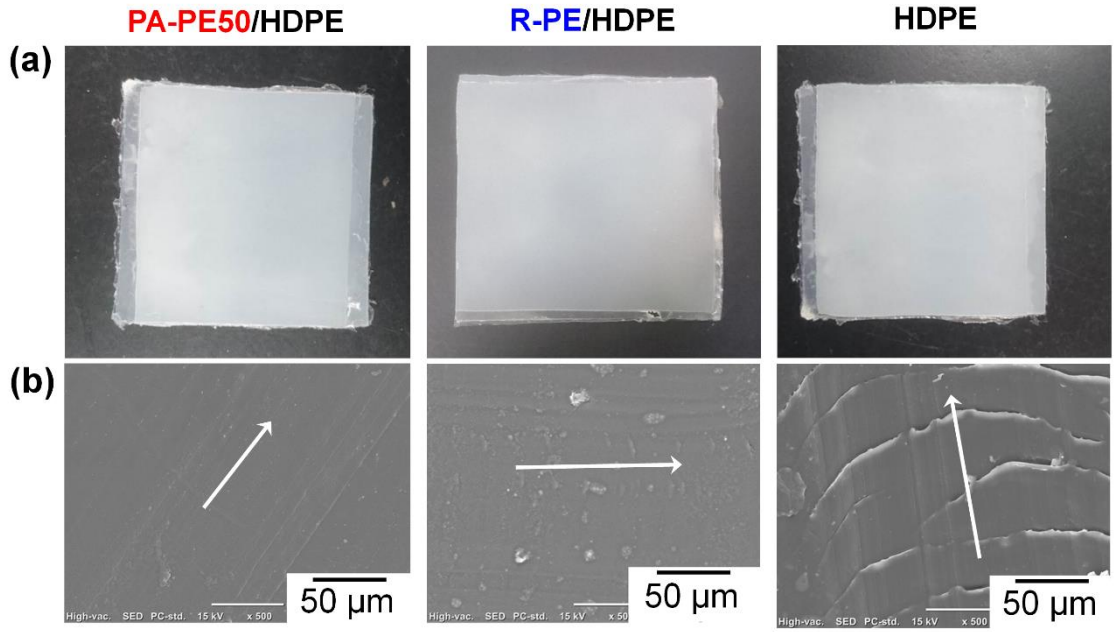

Figure 9 Scratch resistant of UHMWPE-coated HDPE: Appearance of specimens (a), and SEM images after the scratch test (b). The arrows indicate the scratch direction

To the end, a potential of the nano-dispersed Ziegler-Natta catalyst is discussed in terms of the industrial process scale-up. The catalyst synthesis is comprised of two simple steps: A dispersion step (modification of MgO nanoparticles with an appropriate surfactant) and a catalyzation step ($TiCl_4$ treatment of the modified MgO nanoparticles). MgO nanoparticles are not only producible by a variety of methods including the sol-gel, hydro/solvothermal, and even physical methods, but also widely commercially available. The choice of a proper surfactant is also done easily: Aprotic and neutral surfactants to accommodate with the $TiCl_4$ treatment. Judging from the availability of the starting

materials and the simplicity of the processes, facile scale-up is highly expected. The resultant catalyst can be used in a slurry polymerization process, similar to other Ziegler-Natta catalysts for the UHMWPE production, where the dispersibility of the nano-sized catalyst must be profitable in uniform feeding and polymerization. On the other hand, an electrostatic interaction for the fine UHMWPE powder and expected low bulk density may be a focus of a future research.

3.4. Conclusions

A catalytic approach to produce fine polymer particles was proposed based on the exploitation of a nano-sized catalyst. In this work, a truly nano-dispersed Ziegler-Natta catalyst was firstly synthesized. The modification of MgO surfaces by a proper organic modifier improved the dispersion of MgO in a hydrocarbon solvent, so as to facilitate the formation of truly nano-dispersed MgO/$MgCl_2$/$TiCl_4$ core-shell catalysts. In ethylene polymerization, the MgO/$MgCl_2$/$TiCl_4$ catalysts afforded UHMWPE with the activity viable in an industrial point of view with a substantial reduction of the Cl content in the resultant polymer. Moreover, the polymer particle size measured based on a dry dispersion method was found to be in the range of 1-2 μm in agreement to the theoretical estimate. These extremely fine UHMWPE particles yielded several advantages in processing, such as a significantly lower fusion temperature and an improved consolidation in compression molding. In conclusion, the proposed approach facilitated several promising advantages in the production of UHMWPE, including simple preparation protocol, Cl-free, and direct access to microfine particles featured with better processability at a lower temperature.

Reference

[1] S. M. Kurtz, The UHMWPE Handbook, **2004**.

[2] H.G. Alt, A. Köppl, *Chem. Rev.*, **2000**, *100*, 1205–1221.

[3] S. Matsui, T. Fujita, *Catal. Today*, **2001**, *66*, 63–73.

[4] R. Furuyama, J. Saito, S. ichi Ishii, M. Mitani, S. Matsui, Y. Tohi, H. Makio, N. Matsukawa, H. Tanaka, T. Fujita, *J. Mol. Catal. A Chem.*, **2003**, *200*, 31–42.

[5] M.S. Weiser, R. Mülhaupt, in:, Macromol. Symp., Wiley-Blackwell, **2006**, pp. 111–116.

[6] R.L. Jones, M. Armoush, *Macromol. Symp.*, **2009**, *283–284*, 88–95.

[7] R.L. Jones, M.Z. Armoush, T. Harjati, M. Elder, A.A. Hummel, J. Sullivan, *Inorganica Chim. Acta*, **2010**, *364*, 275–281.

[8] S. Mihan, L. Koelling, H. Vogt, D. Lilge, H. -F. Enderle, H. -J. Nitz, L. Lukesova, U.S. Patent 20110218309A1, **2011**.

[9] D.F. Farrar, A.A. Brain, *Biomaterials*, **1997**, *18*, 1677–1685.

[10] P. Smith, J. Visjager, T. Tervoort, U.S. Patent 8063175B2, **2011**.

[11] P. Bracco, A. Bellare, A. Bistolfi, S. Affatato, *Materials (Basel).*, **2017**, *10*, 791.

[12] T. Takahashi, H. Fujii, M. Nishiyama, U.S. Patent 5422061A, **1995**.

[13] S. Liu, F. Wang, J. Chen, Y. Cao, *Int. J. Polym. Anal. Charact.*, **2015**, *20*, 138–

149.

[14] A. Pandey, Y. Champouret, S. Rastogi, *Macromolecules*, **2011**, *44*, 4952–4960.

[15] S. Rastogi, Y. Yao, S. Ronca, J. Bos, J. Van Der Eem, *Macromolecules*, **2011**, *44*, 5558–5568.

[16] W. Li, H. Yang, J. Zhang, J. Mu, D. Gong, X. Wang, *Chem. Commun.*, **2016**, *52*, 11092–11095.

[17] W. Li, L. Hui, B. Xue, C. Dong, Y. Chen, L. Hou, B. Jiang, J. Wang, Y. Yang, *J. Catal.*, **2018**, *360*, 145–151.

[18] E. Baumgaertner, U.S. Patent 3847888A, **1974**.

[19] K.S. Han, J.F. Wallace, R.W. Truss, P.H. Geil, *J. Macromol. Sci. Part B*, **1981**, *19*, 313–349.

[20] A. Barnetson, P.R. Hornsby, *J. Mater. Sci. Lett.*, **1995**, *14*, 80–84.

[21] H. Ogawa, A. Ito, K. Taki, M. Ohshima, *J. Appl. Polym. Sci.*, **2007**, *106*, 2825–2830.

[22] A. Rudin, P. Choi, The Elements of Polymer Science & Engineering, Elsevier Science, **2012**.

[23] T. Taniike, V.Q. Thang, N.T. Binh, Y. Hiraoka, T. Uozumi, M. Terano, *Macromol. Chem. Phys.*, **2011**, *212*, 723–729.

[24] J.B.P. (João B.P.. Soares, T.F. (Timothy F.. McKenna, Polyolefin Reaction Engineering, Wiley-VCH, **2012**.

[25] M. Suga, M. Kioka, T. Kobayashi, A. Kato, M. Endo, US Patent 4972035 A, **1990**.

[26] I. Cuffiani, U. Zucchini, US Patent 5500397 A, **1996**.

[27] D. Bilda, L. Boehm, U.S. Patent 6114271A, **2000**.

[28] T. J. Kidd, N. V. F. Quiroga, T. B. Mikenas, V. E. Nikitin, V. A. Zakharov, WO2008058749, **2010**.

[29] Y. Nakayama, N. Matsukawa, J. Saito, H. Bando, Y. Sonobe, K. Michiue, M. Mitani, T. Fujita, US Patent 7601423 B2, **2009**.

[30] T. Taniike, P. Chammingkwan, V.Q. Thang, T. Funako, M. Terano, *Appl. Catal. A Gen.*, **2012**, *437–438*, 24–27.

[31] T. Taniike, P. Chammingkwan, M. Terano, *Catal. Commun.*, **2012**, *27*, 13–16.

[32] P. Chammingkwan, V.Q. Thang, M. Terano, T. Taniike, *Top. Catal.*, **2014**, *57*, 911–917.

[33] Y. Bando, P. Chammingkwan, M. Terano, T. Taniike, *Macromol. Chem. Phys.*, **2018**, *219*, 1800011.

[34] T. Taniike, T. Funako, M. Terano, *J. Catal.*, **2014**, *311*, 33–40.

[35] L. Todan, T. Dascalescu, S. Preda, C. Andronescu, C. Munteanu, D.C. Culita, A. Rusu, R. State, M. Zaharescu, *Ceram. Int.*, **2014**, *40*, 15693–15701.

[36] P. Li, C. Liu, L. Zhang, S. Zheng, Y. Zhang, *Ultrason. Sonochem.*, **2017**, *34*, 938–946.

[37] Y. Fukuda, K. Tanabe, *Bull. Tjhe Chem. Soc. Japan*, **1973**, *46*, 1616–1619.

[38] K. Teramura, T. Tanaka, H. Ishikawa, Y. Kohno, T. Funabiki, *J. Phys. Chem. B*, **2004**, *108*, 346–354.

[39] Y. Yanagisawa, K. Takaoka, S. Yamabe, *J. Phys. Chem.*, **1995**, *99*, 3704–3710.

[40] N.B. Colthup, L.H. Daly, W. S.E., Introduction to Infrared and Raman Spectroscopy, Academic Press, Inc., New York, **1975**.

[41] K. Tanaka, A. Igarashi, "Determination of Nonionic Surfactants" in Handbook of Detergents. Part C, Analysis, Waldhoff, H., and Spilker, R. (Florida; CRC Press), **2005**.

[42] Y. V. Kissin, V.P. Marin, P.J. Nelson, *J. Polym. Sci. Part A Polym. Chem.*, **2017**, *55*, 3832–3841.

[43] S. Rastogi, D.R. Lippits, G.W.M. Peters, R. Graf, Y. Yao, H.W. Spiess, *Nat. Mater.*, **2005**, *4*, 635–641.

[44] S. Rastogi, D.R. Lippits, G.W.H. Höhne, B. Mezari, P.C.M.M. Magusin, *J. Phys.*

Condens. Matter, **2007**, *19*, 205122.

[45] Y.L. Joo, O.H. Han, H.K. Lee, J.K. Song, *Polymer*, **2000**, *41*, 1355–1368.

[46] R. Schaller, K. Feldman, P. Smith, T.A. Tervoort, *Macromolecules*, **2015**, *48*, 8877–8884.

[47] V.A. Tuskaev, S.C. Gagieva, D.A. Kurmaev, N.A. Kolosov, E.S. Mikhaylik, E.K. Golubev, A.I. Sizov, S. V. Zubkevich, V.G. Vasil'ev, G.G. Nikiforova, M.I. Buzin, O.A. Serenko, B.M. Bulychev, *Polymers (Basel).*, **2018**, *10*, 2.

[48] S. Hambir, J.P. Jog, *Bull. Mater. Sci.*, **2000**, *23*, 221–226.

Chapter 4

Preparation of Multigrained MgO-Supported Ziegler-Natta Catalyst via Spray Dry Method

Abstract

Improvement handling of Ziegler-Natta nanocatalyst was proposed based on Bottom-up catalyst design utilizing aggregation. Spherical catalyst secondary particles of 6 - 7 μm were prepared using MgO particles whose aggregation was controlled by spray drying as a carrier. The morphology of MgO nanoparticles changed to $Mg(OH)_2$ plate due to water. Catalytic secondary particles synthesized about 40 μm polymer particles. The polymer particles had the morphology of wool balls in which coiled polymers were agglomerated. As with fine polymer particles, the polymer particles could be compression molded at low temperature. The particle size of the catalyst and polymer particles could be increased while maintaining the characteristics of the fine polymer.

4.1. Introduction

Miniaturization of catalyst particles makes it possible to increase the surface area per unit weight and to make effective use of materials [1,2]. Owing to large specific surface area and, the nanoparticles are widely used in various fields unique characteristics like to the quantum size effect [3]. On the other hand, when the particle size is reduced, the adhesion force between particles cannot be ignored, resulting in aggregation and deterioration of fluidity. By supporting the nanoparticles on inert supports such as silica and alumina, while problem of operation is solved. Activity and selectivity of the reaction can be controlled by changing the morphology of the catalyst support. Hence, many researches on catalyst morphology have been conducted. There are several ways to control the catalyst morphology. For example, a top-down method of mechanically pulverizing small and a bottom-up method of growing crystals in a solution [4]. Recently, various structures have been made using nanoparticles as building blocks, and various properties are given to catalyst particles. For preparing the structures, various methods such as freeze-drying, mechanical grinding, spray drying, thermal decomposition, supercritical fluid, emulsion, *etc.* have been reported [5]. Spray drying is a method of evaporating the solvent of atomized droplets to form secondary particles and is used for dry foods, medicines, fertilizers and so on. Various structured particles

such as donut-type, porous-type, hollow-type, agglomerated particles were reported on metal oxides [6].

Also in the Ziegler-Natta catalyst, the morphology of catalyst particles changes according to the preparation method, thereby affecting the reaction kinetics and the morphology of the polymer [7]. For example, the catalyst prepared by the co-grinding method is indefinite morphology, exhibits high initial activity and low duration of activity. On the other hands, the catalyst prepared by the dissolution-precipitation method and chemical reaction method is better morphology, exhibits low initial activity and high duration of activity. Therefore, a number of researches have been conducted on the influence of the catalyst particle morphology on the morphology of resultant polymer powder to prevent undesirable fluidization due to fine polymer particles as well as fouling of the reactor by coagulation of particles [8,9].

$MgCl_2$, used as a catalyst support, is essential not for controlling the morphology of the catalyst particle but also to situating titanium chloride in the octahedral position making electron donation. The morphology of a carrier is controlled by precipitating $MgCl_2$ dissolved in alcohol [10], chlorinating magnesium ethoxide with titanium tetrachloride to prepare $MgCl_2$ [11] and others. The catalyst particles obtained by the precipitating method are spherical having a large bulk density and having almost no pores. In the

method of magnesium ethoxide method, particles having a lower bulk density and having pores are obtained. In these preparation methods, particle diameter, pore structure and the like can be controlled by precisely manipulating the preparation conditions, but $MgCl_2$ is brittle, deliquescent and easily coagulates.

Also, there is some supports synthesis example of the catalyst for olefin polymerization using spray drying. A method of evaporating a solvent at high temperature using an alcohol solution in which $MgCl_2$ is dissolved, a method of ejecting and crystallizing in low-temperature nitrogen, and the like. However, the shape of the obtained support is not so good, and since the particle size distribution is broad, it causes destruction or collapse of the particles [12]. Also, there are examples in which nonporous silica secondary particles are prepared by spray drying as a carrier of a metallocene catalyst [13].

A core-shell Ziegler-Natta nanocatalyst was prepared using MgO nanoparticles as support. The catalyst is obtained by chlorinating MgO with titanium tetrachloride and forming a $MgCl_2/TiCl_4$ catalyst layer on the MgO core [14,15]. Also, by treating MgO with a surfactant before preparing the catalyst, the catalyst was dispersed in a nonpolar solvent, and ultrahigh molecular weight polyethylene was successfully atomized [16,17]. The catalyst handling is difficult because it is nano-sized. The spray dryer can

agglomerate the particles and prepare spherical secondary particles. In this chapter, to improve handling of the catalyst by increasing the catalyst particle diameter while maintaining the molding properties of micro size polymer particles by agglomerating the nanocatalyst.

4.2. Experimental

4.2.1. Materials

MgO nanoparticles with the mean particle size of 50 nm (Wako Pure Chemical Industries Ltd.) were used after dehydration at 160°C under vacuum for 2 h. Titanium tetrachloride ($TiCl_4$) of research grade was used as received. *n*-Heptane was used after dehydration by passing through a column of molecular sieve 4A, followed by N_2 bubbling for 2 h. Ethylene of polymerization grade was purchased from Hokurikuekikasangyou Co., Ltd. and used as received. Triethylaluminium (TEA, donated by Tosoh Finechem Co.) was used after dilution in heptane.

4.2.2. Catalyst Preparation

50 nm of MgO was added in methanol or deionized water to obtain uniform suspensions at 2 g/L. Spray drying of these suspensions was carried out to prepare the secondary particles of MgO conditions were: inlet temperature = 140°C, feed rate = 500 mL/h, atomization air pressure = 250 kPa, and blower rate = 0.6 m^2/min. MgO secondary particles were obtained. The MgO secondary particles were dried at 150°C under nitrogen flow. Thereafter, 0.2 g of obtained MgO powder was reacted with 30 mL of $TiCl_4$ at 140°C for 2 h under a nitrogen atmosphere. The obtained solid was washed

with heptane and kept as a slurry in heptane.

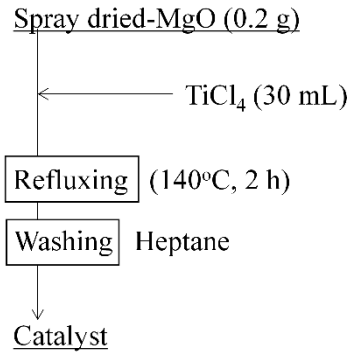

Scheme 1 Catalyst preparation

4.2.3. Polymerization

Ethylene polymerization was performed in a 1 L stainless steel reactor equipped with a mechanical stirrer rotating at 500 rpm. After sufficient nitrogen replacement, 500 mL of heptane as a polymerization medium and 1.0 mmol of TEA as an activator were introduced. The solution was then saturated with 0.8 MPa of ethylene at 70°C for 30 min. 10 mg of a catalyst was injected to start the polymerization. The polymerization was carried out at 70°C under 0.8 MPa of ethylene pressure for 2 h. Thus obtained polymer was filtered and dried in vacuum at 60°C for 6 h.

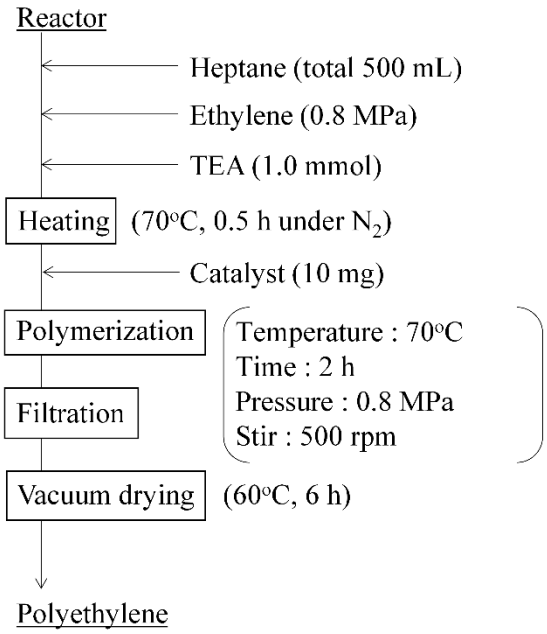

Scheme 2 Polymerization condition

4.2.4. Compression Molding

Reactor powder was molded into a 5 cm × 5 cm specimen with the thickness of 500 μm by compression molding using a flash picture-frame mold. A specified amount of reactor powder was filled into an aluminum chase sandwiched between two thin ferrotype plates and pressed with a contact pressure at room temperature for 5 min. Thereafter, the temperature was raised to a molding temperature and kept for 6 min at 130°C before applying full pressure of 20 MPa for additional 5 min. The specimen was then cooled to room temperature.

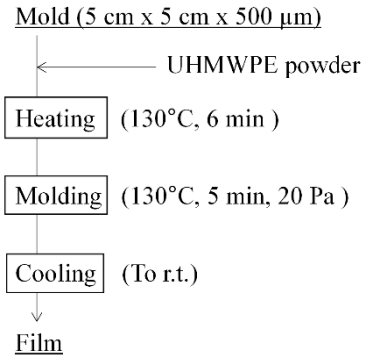

Scheme 3 Conditions for compression molding

4.2.5. Characterization

The morphology of MgO, catalyst, and polymer particles was observed by scanning electron microscopy (SEM, Hitachi S-4100) operated at an accelerating voltage of 20 kV. SEM samples were prepared by dropping a suspension of samples in ethanol or heptane to carbon tape and subsequently subjected to Pd–Pt sputtering for 100 s before the measurement. The thermal decomposition behavior of MgO soaked in water or methanol were studied by differential scanning calorimeter (DSC, Mettler Toledo DSC 822) and thermo gravimetry (TG, Rigaku Thermo plus EV02 TG 8121) analysis in a temperature range of 200 – 500°C with heating rate of 5 °C/min under nitrogen flow. The particle size and the particle size distribution of MgO and catalyst samples were analyzed by light scattering (Horiba Partica LA-950V2) in a suspension form using ethanol or heptane as a solvent. The particle size was reported as D_{10}, D_{50}, and D_{90},

which corresponded to the particle size at 10%, 50%, and 90% of the cumulative volume.

The particle size distribution was reported as a relative span factor (RSF) [18] calculated based on

$$\mathrm{RSF} = \frac{D_{90} - D_{10}}{D_{50}} \quad (1)$$

The Ti content of the catalyst was analyzed by ultraviolet–visible spectrometry (UV–vis, Jasco V670). The catalyst (50 mg) was dissolved in an aqueous solution of hydrochloric acid and sulfuric acid. Thereafter, 200 μL of hydrogen peroxide was added to form a peroxotitanium complex that exhibited the absorption band at 410 nm. The Ti content was determined based on the intensity at 410 nm, using an externally acquired standard curve.

4.3. Results and Discussion

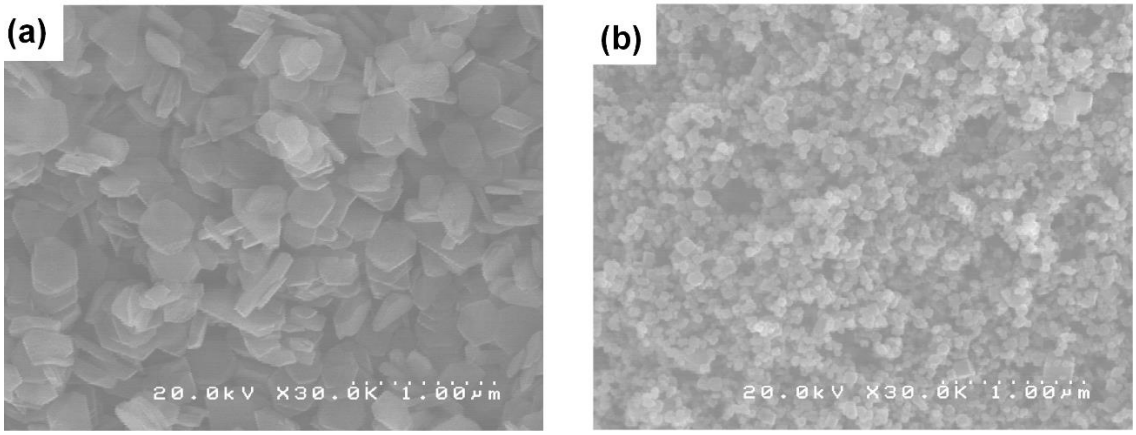

Figure 1 SEM images of a) MgO soaked in water and b) methanol for 6 h

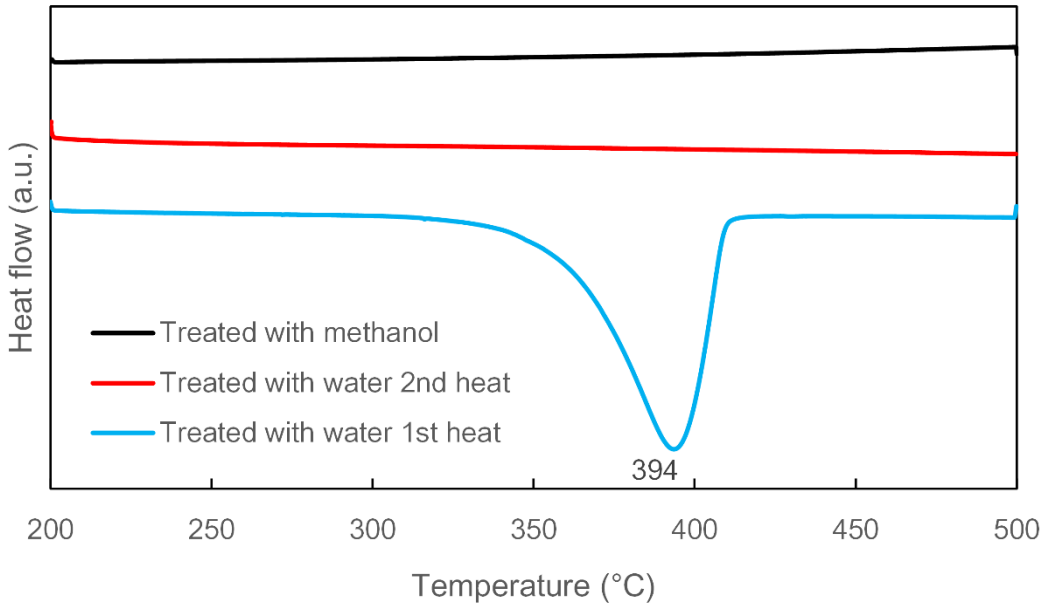

Figure 2 DSC curves of MgO powder soaked in water and methanol at the temperature range of 200 – 500°C with a heating rate of 5 °C/min

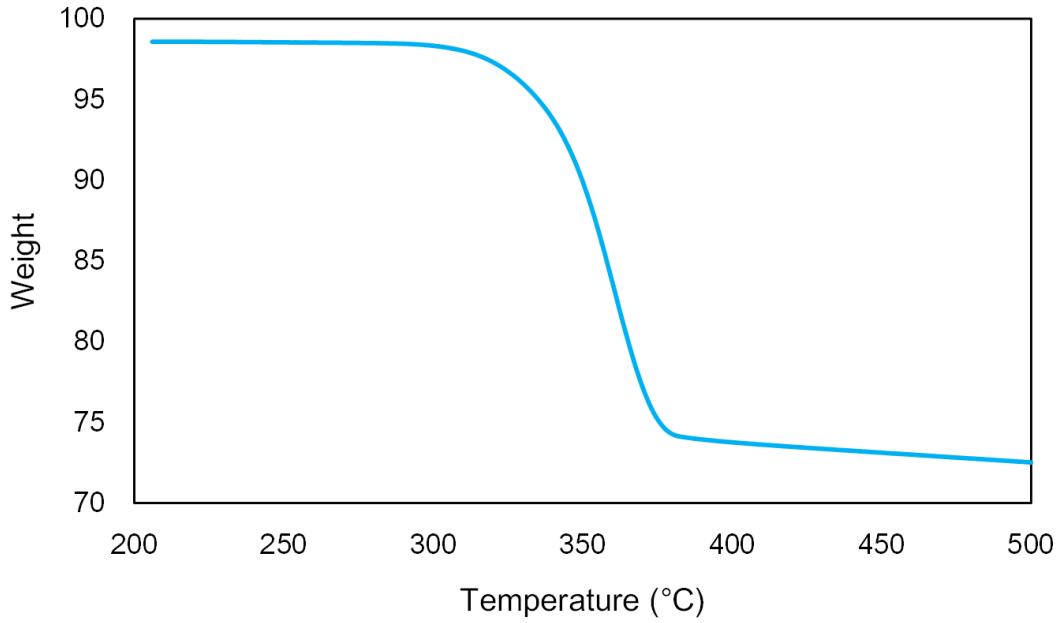

Figure 3 TG curves of MgO powder soaked in water at the temperature range of 200 – 500°C with a heating rate of 5 °C/min

50 nm MgO nanoparticles were soaked in water for several hours at normal temperature and pressure. Figure 1 illustrates the SEM images of MgO nano particles soaked in water or methanol for 6 h. The originally cubic morphology of MgO turned in to a plate-like morphology (Figure 1). The DSC and TG measurement were carried out to analyze the thermal decomposition behavior of the MgO nano particles soaked in water. The DSC curve of the MgO particles soaked in water showed one endothermic peak at 394°C (Figure 2). As shown in the Figure 3, weight loss from 98.6% to 72.5% was confirmed in the temperature range of 300 - 400°C. This weight loss is the process of

decomposition with dehydration from $Mg(OH)_2$ to MgO. In decomposition of $Mg(OH)_2$, it is generally known that there are some differences in weight loss due to differences in synthesis method and structure of $Mg(OH)_2$ [19,20]. This indicates that a phase transformation from $Mg(OH)_2$ to MgO occurred [21]. It is known that MgO changes to $Mg(OH)_2$ under microwave irradiation [22]. In this case, the morphology of $Mg(OH)_2$ is also plate-like.

$$MgO_{(s)} + H_2O_{(l)} \rightarrow MgOH^{+}_{(ads)} + OH^{-}_{(aq)} \rightarrow Mg(OH)_{2(s)}$$

It was considered that a high surface energy of MgO nanoparticles spontaneously induced the same conversion in water

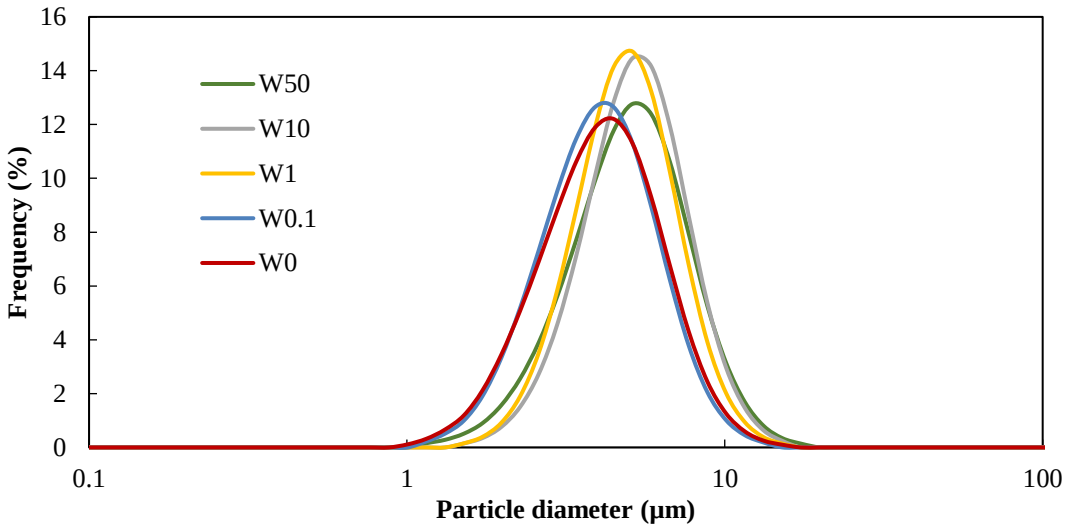

Figure 4 Particle size and its distribution of spray dried MgO particles

Table 1 Synthesis and characteristics of spray dried MgO particles

	H_2O/MeOH ratio (v/v)	Yield (%)	D_{10} (μm)	D_{50} (μm)	D_{90} (μm)	RSF
W50	50/50	13	2.61	4.72	7.97	1.14
W10	10/90	7.4	2.97	4.91	7.83	0.99
W1	1/99	6.7	2.79	4.57	7.31	0.99
W0.1	0.1/99.9	6.1	2.14	3.77	6.39	1.13
W0	0/100	5.3	2.10	3.85	6.62	1.17

The objective was to control catalyst morphology by changing ratio water and methanol. In addition, the presence or absence of the effect of partial adhesion with MgO and $Mg(OH)_2$ was confirmed. Particle size and its distribution were measured with light scattering using ethanol as a dispersion solvent. Figure 4 illustrates the light scattering results of spry dry to prepare secondary particles. All samples showed a unimodal peak, indicating that aggregation was controlled by spray drying. As shown in Table 1, there was no significant change in particle size when the concentrations of water and methanol were changed. On the other hand, the yield increased as the concentration of water increased. Morphology of particles becomes a plate-like particle due to reacting with water is increased particle size. Hence, it is thought that the yield is due to the loss of small particles.

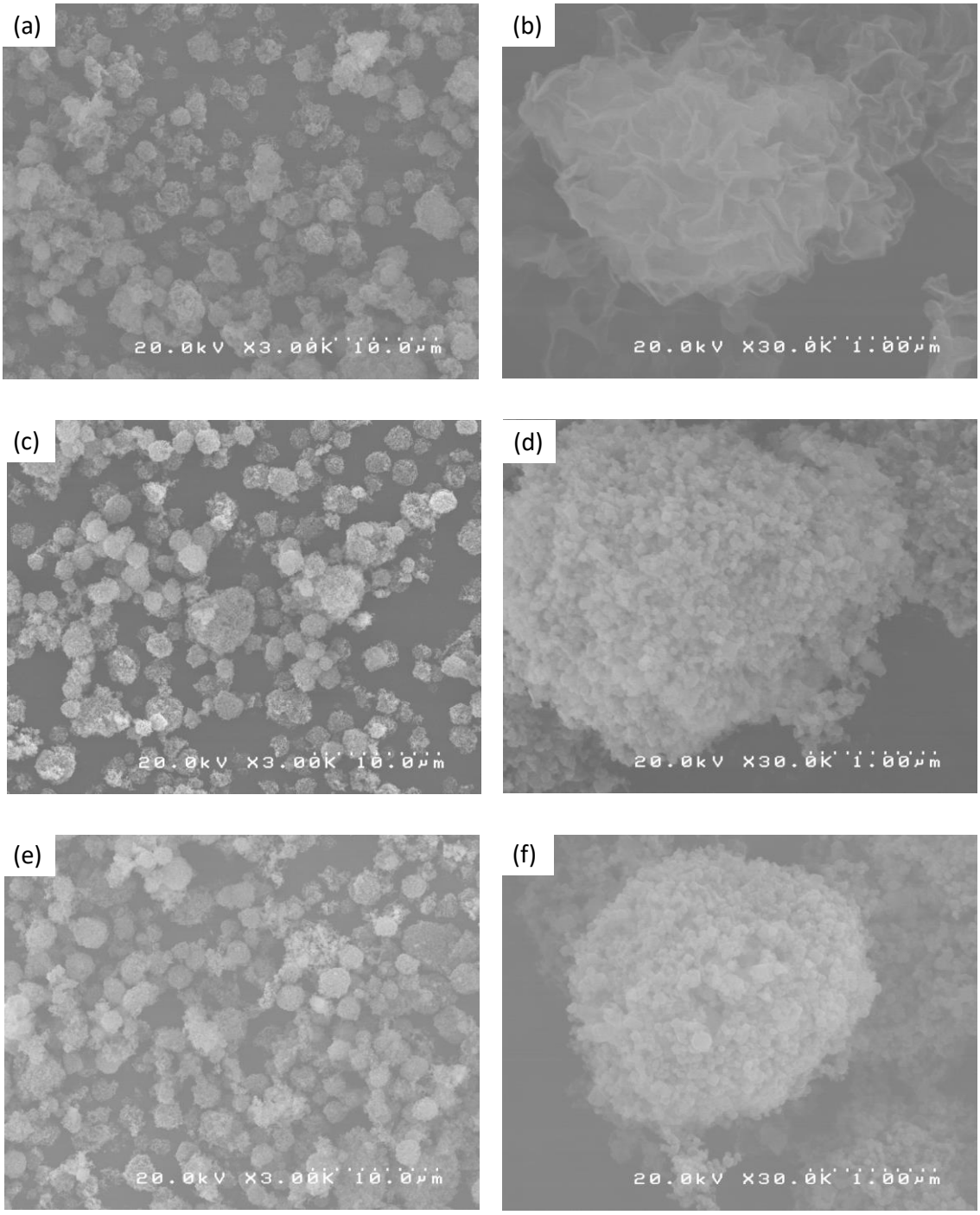
(a)
20.0kV X3.00K 10.0μm
(b)
20.0kV X30.0K 1.00μm
(c)
20.0kV X3.00K 10.0μm
(d)
20.0kV X30.0K 1.00μm
(e)
20.0kV X3.00K 10.0μm
(f)
20.0kV X30.0K 1.00μm

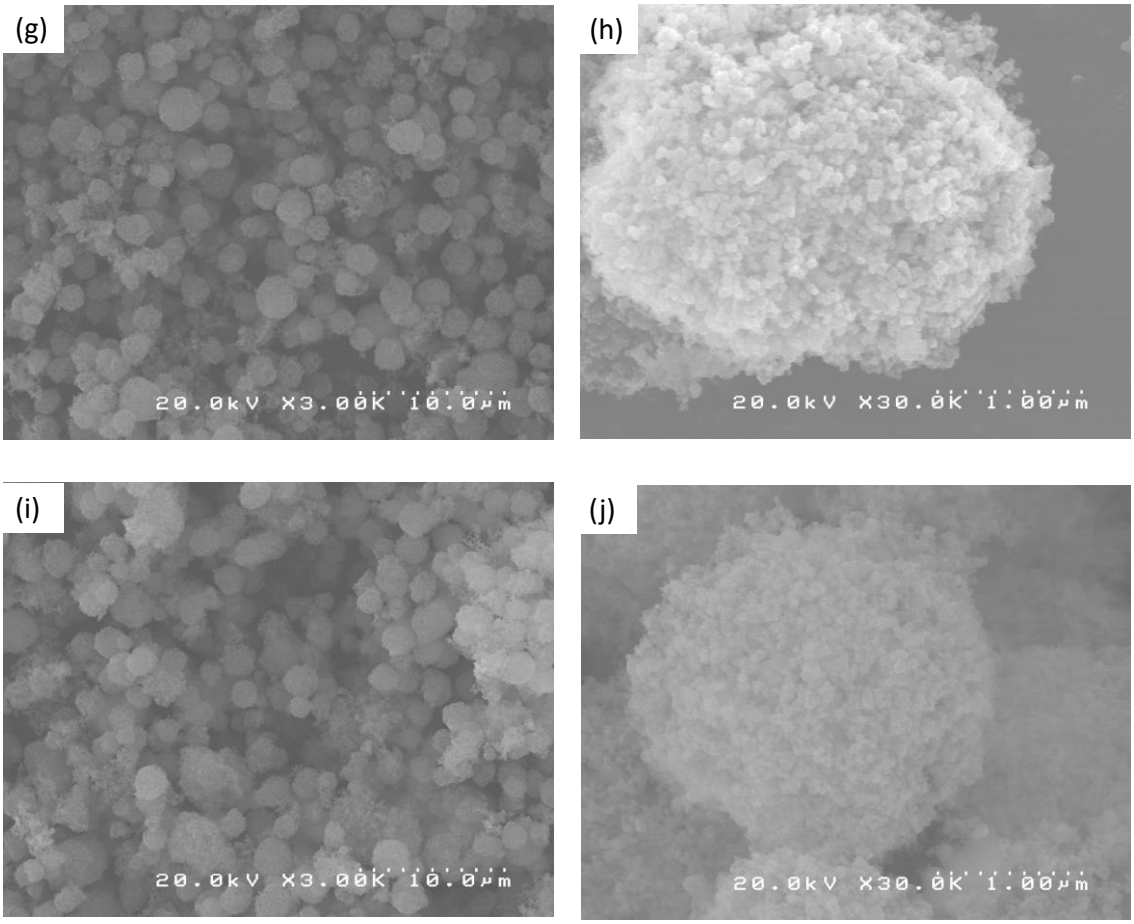

Figure 5 SEM images of spry dry MgOs; a,b) W50, c,d)W10, e,f)W1, g,h)W0.1 i,j)W0

Morphology of MgO secondary particles was observed using SEM images (Figure 5). The spherical secondary particles could be obtained using spray dry method (Figure 5acegi). In the case of a solvent using 50% water, the morphology of the original primary particles was completely lost, where plate-like $Mg(OH)_2$ were aggregated to form nano flowers morphology (Figure 5b). It was confirmed that the particles aggregated with maintaining the morphology of MgO primary particles with a solvent having water of

10% or less (Figure 5dfhj). It appears that the secondary particle morphology is collapsed as the moisture content increases.

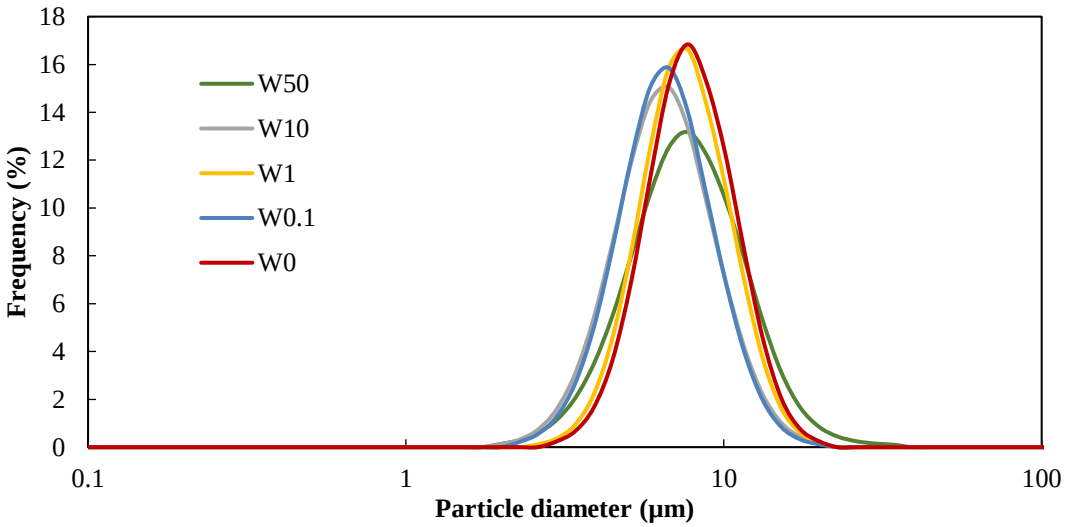

Figure 6 Particle size and its distribution of catalyst particles

Table 2 Result of catalyst preparation

	Ti cont. (wt%)	D_{10} (μm)	D_{50} (μm)	D_{90} (μm)	RSF
W50	0.62	4.13	7.12	12.15	1.13
W10	0.54	3.78	6.07	9.73	0.98
W1	0.55	4.60	7.01	10.74	0.88
W0.1	0.58	3.92	6.11	9.58	0.93
W0	0.64	4.81	7.30	11.13	0.86

In the Figure 6, the results of light scattering measurement of particles after catalyst preparation are shown. All samples showed a unimodal peak as in the Figure 4. Thus, it was shown that extreme morphological disintegration did not occur during catalyst preparation. As shown in Table 2, the particle size of the catalyst became large after catalyst preparation. Titanium content showed almost the same value in all samples. RSF of catalyst particles became smaller than before catalyst preparation except for the W50. It is believed that unstable morphology particles were removed by catalyst washing. On the other hand, there was no change in RSF of W50. It seems that it is fragile because the particle morphology is round and spiny of plate.

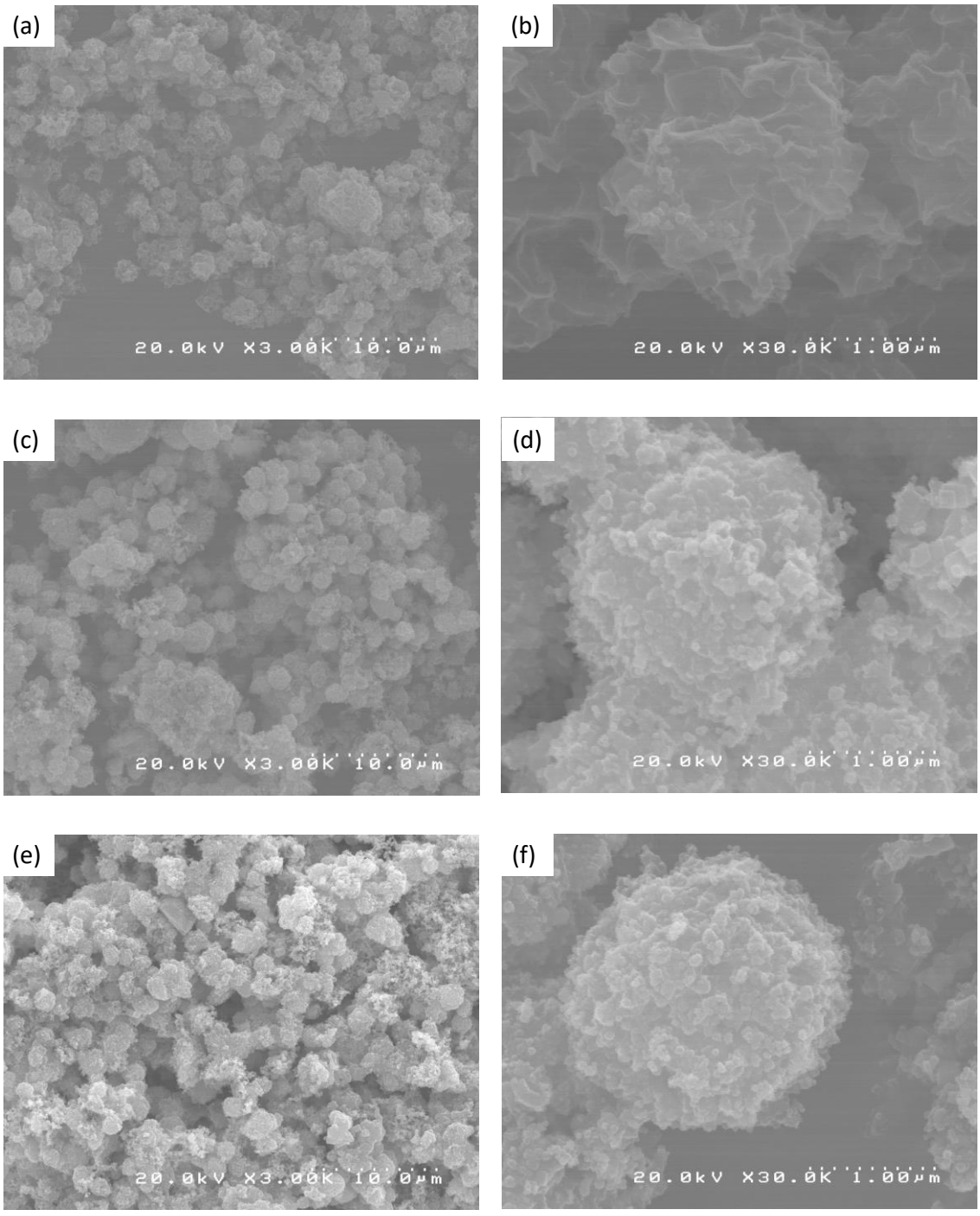
(a)
20.0kV X3.00K 10.0μm
(b)
20.0kV X30.0K 1.00μm
(c)
20.0kV X3.00K 10.0μm
(d)
20.0kV X30.0K 1.00μm
(e)
20.0kV X3.00K 10.0μm
(f)
20.0kV X30.0K 1.00μm

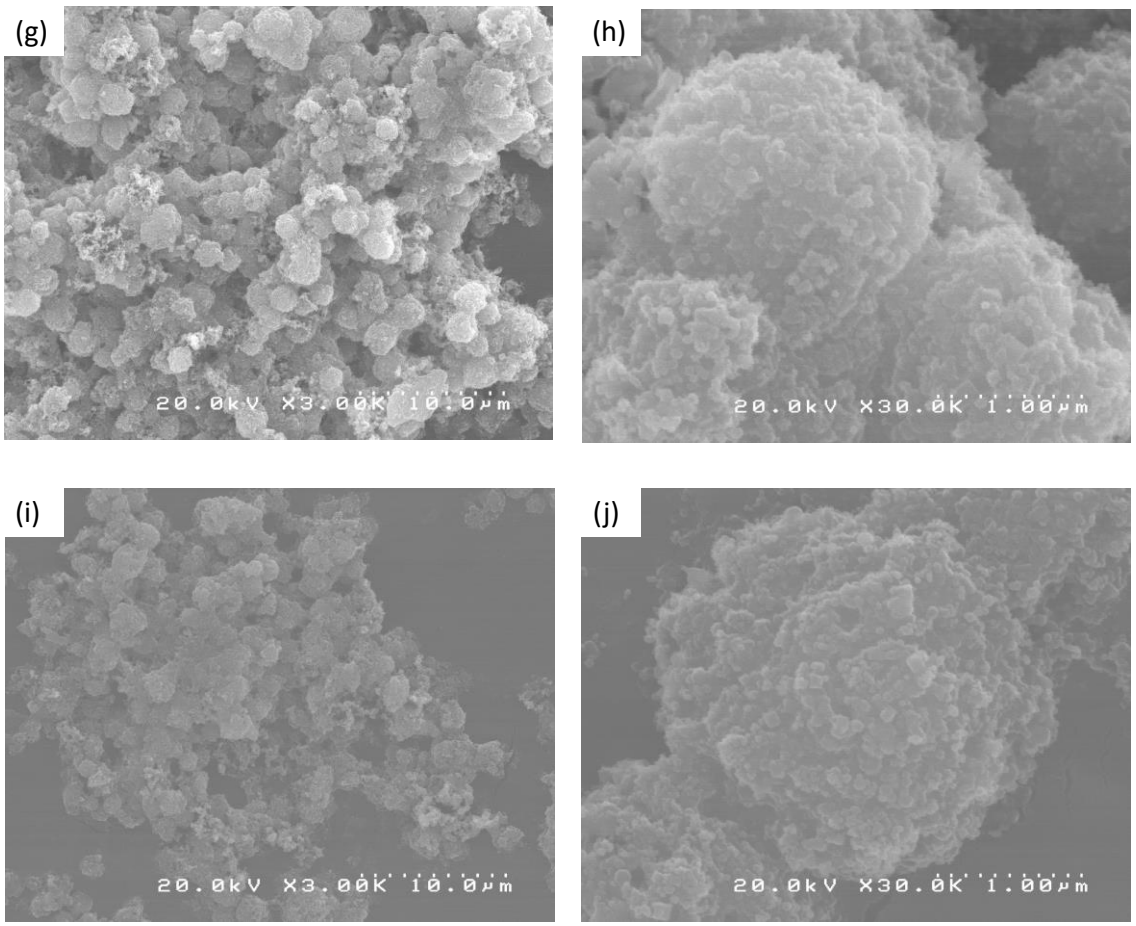

Figure 7　SEM images of Catalyst powders; a,b) W50, c,d)W10, e,f)W1, g,h)W0.1 i,j)W0

The SEM images in Figure 7 show the morphology of secondary particles after catalyst preparation. The particle morphology of the catalyst did not change significantly before and after preparation. Hence, it was possible to prepare two types of catalysts having different morphologies.

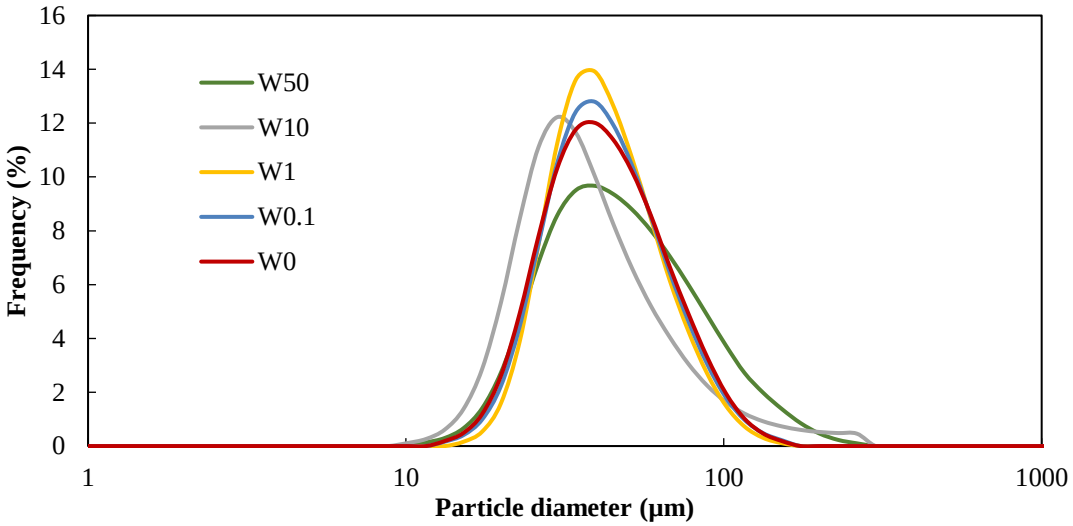

Figure 8　Particle size and distribution of PE particle

Table 3　Result of polymerization

	Yield (g-PE/g-Cat.)	BD (g/mL)	D_{10} (μm)	D_{50} (μm)	D_{90} (μm)	RSF
W50	316	0.100	22.8	42.5	93.4	1.66
W10	222	0.104	19.6	32.7	73.4	1.64
W1	349	0.087	24.4	38.3	67.0	1.11
W0.1	338	0.089	23.5	38.6	69.9	1.20
W0	301	0.097	23.0	38.7	71.1	1.24

As shown in Figure 8, the results of the light scattering measurement showed a unimodal peak in all the samples as well as the support and the catalyst. In the Table 3, there was no significant difference in yield or particle size. It was shown that magnesium hydroxide can be used as a catalyst support in the ethylene polymerization. It was

confirmed that $Mg(OH)_2$ can be used catalyst support as well as MgO. Particles with a large proportion of water have increased RSF. It is considered that the catalyst particles are easily broken.

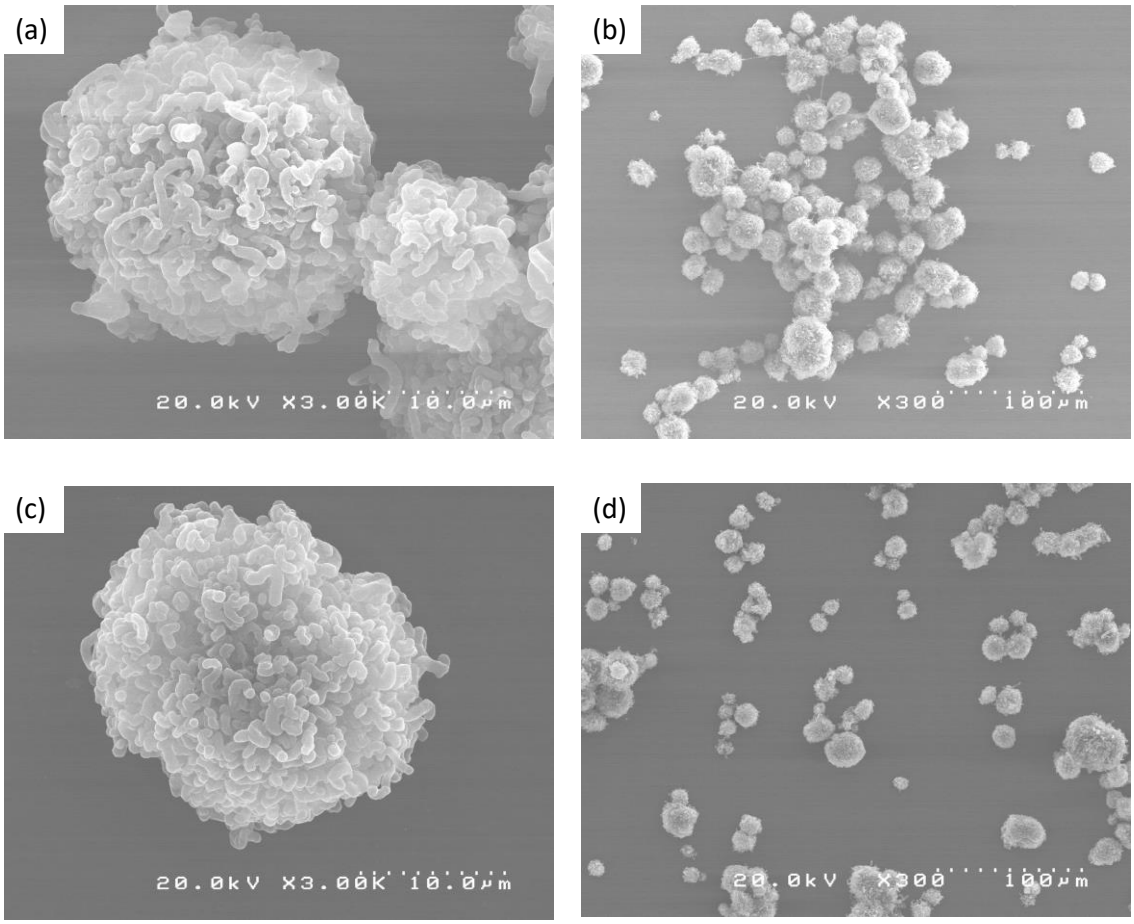

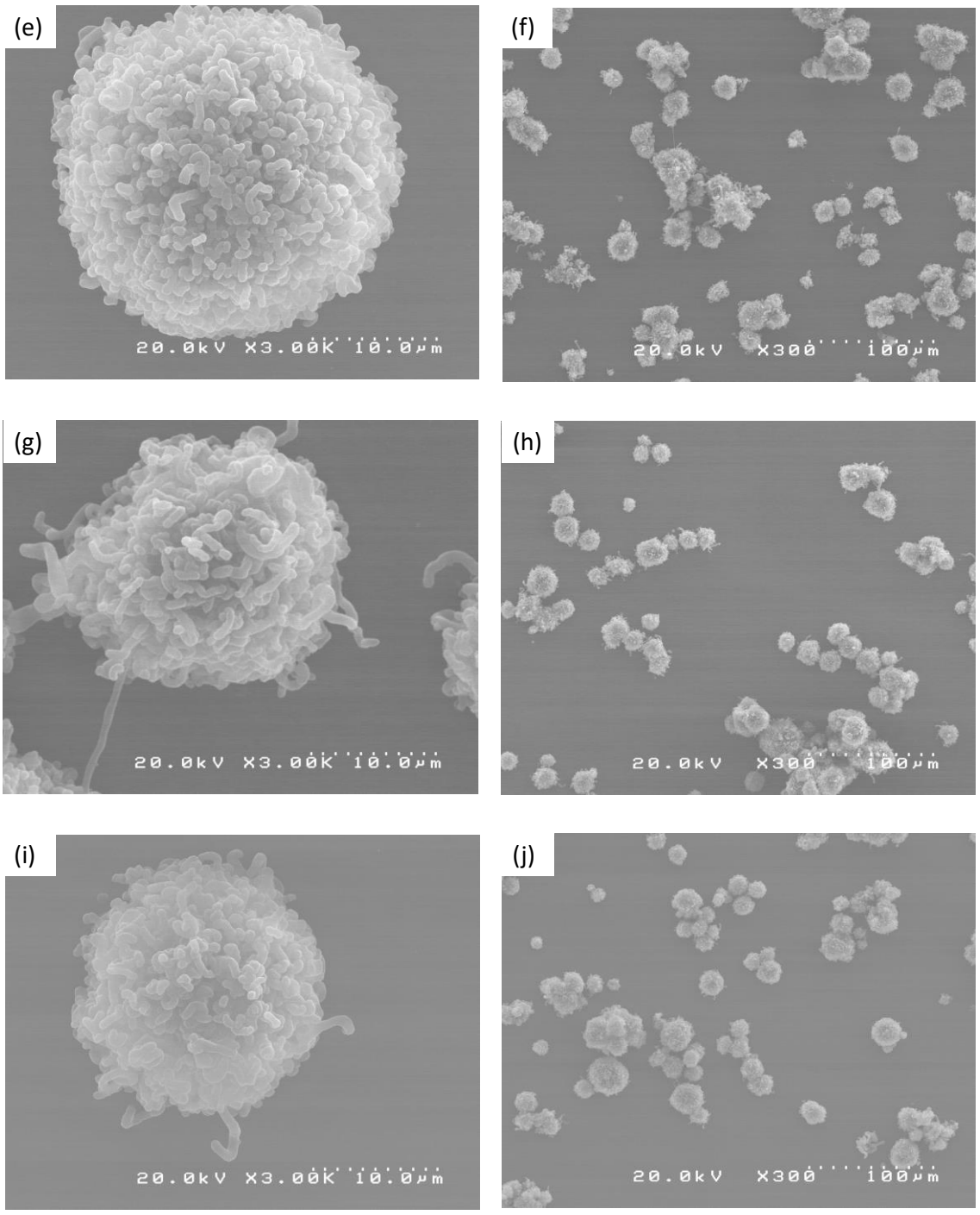

Figure 9 SEM images of PE powders; a,b) W50, c,d)W10, e,f)W1, g,h)W0.1 i,j)W0

Two kinds of catalyst morphology, nano flower type catalyst and multigrain type catalyst, were used for ethylene polymerization (Figure 7). However, in each of the obtained all polymer morphology, the coiled polymer was agglomerated into a spherical shape as shown in Figure 9. In addition, the thickness of the polymer coil was almost the same. Therefore, it is difficult to explain by forming a polymer coil by extrusion from between aggregate particles. Hence, there is a maybe that polymer coils are growing long from one active point.

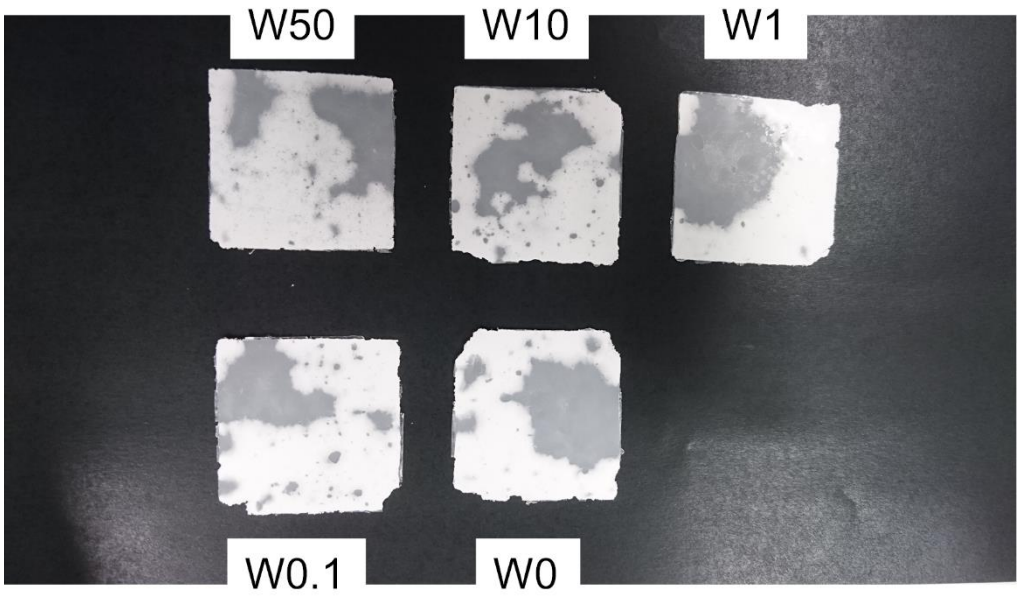

Figure 10 PE films molded at 130°C

Compression molding was performed at 130°C using UHMWPE particles synthesized this time. In the Figure 10, it was confirmed that fusion of particles was started at low temperature like the 1-2 μm UHMWPE particles prepared in Chapter 3. It is thought that this is because the coiled polymer was sufficiently thin.

4.4. Conclusions

In this chapter, MgO nanoparticles were agglomerated by spray drying to prepare secondary particles in a controlled manner for improving handling of catalyst particles. The obtained secondary particles were used to prepare $MgO/MgCl_2/TiCl_4$ core shell Ziegler-Natta catalysts and their performance was investigated in ethylene polymerization, especially for the production of UHMWPE particles. When MgO nano particles were soaked in water for 6 h, which turned into $Mg(OH)_2$ plates. The objective was to control the morphology of catalyst by changing the ratio of water and methanol in spry dry method. In the case of 50% water, plate-like $Mg(OH)_2$ were aggregated to form nano flower morphology. On the other hand, water of 10% or less, it was confirmed that the MgO nano particles aggregated to form multigrained morphology. The structure prepared by spray drying kept its integrity during preparation of the catalyst. Two kinds of catalyst morphology, nano flower type catalyst and multigrain type catalyst, were prepared. As a result of the polymerization, the obtained polymer did not replication the catalyst morphology. All of the obtained polymer particles were spherical in shape, but had a morphology like a wool ball with coiled polymer aggregated, despite using different morphology type catalysts. Fusion of the obtained polymer at low temperature was confirmed as in Chapter 3. The particle size of catalyst particles and polymer particles

could be increased while maintaining the same characteristics of UHMWPE as in Chapter 3. From this, it was considered that the ease of handling of the particles could be improved.

Reference

[1] A.N. Shipway, E. Katz, I. Willner, *ChemPhysChem*, **2000**, *1*, 18–52.

[2] M.-C. Daniel, D. Astruc, *Chem. Rev. (Washington, DC, United States)*, **2004**, *104*, 293–346.

[3] C. Sönnichsen, T. Franzl, T. Wilk, G. Von Plessen, J. Feldmann, *New J. Phys.*, **2002**, *4*, 93–93.

[4] C.L. De Castro, B.S. Mitchell, in:, Synth. Funct. Surf. Treat. Nanoparticles, **2002**, pp. 1–350.

[5] S.Y. Lee, L. Gradon, S. Janeczko, F. Iskandar, K. Okuyama, *ACS Nano*, **2010**, *4*, 4717–4724.

[6] A. B. D. Nandiyanto, K. Okuyama, *Adv. Powder Technol.*, **2011**, *22*, 1–19.

[7] A. Dashti, S.A.A. Ramazani, Y. Hiraoka, S.Y. Kim, T. Taniike, M. Terano, in:, Macromol. Symp., Wiley-Blackwell, **2009**, pp. 52–57.

[8] A. Dashti, S. A. Ramazani, Y. Hiraoka, S. Y. Kim, T. Taniike, M. Terano, *Polym. Int.*, **2009**, *58*, 40–45.

[9] R. Jamjah, G. H. Zohuri, J. Vaezi, S. Ahmadjo, M. Nekomanesh, M. Pouryari, *J. Appl. Polym. Sci.*, **2006**, *101*, 3829–3834.

[10] Mario Ferraris, Francesco Rosati, Sandro Parodi, Enzo Giannetti, Giuseppe

Motroni, E. Albizzati, US 4399054, **1983**.

[11] M. Kioka, N. Kashiwa, JP 2537506, **1996**.

[12] K. Yucca, Y. Petri, JP 0516311, **1993**.

[13] C. F. Hohenesche, K. K. Unger, T. Eberle, *J. Mol. Catal. A Chem.*, **2004**, *221*, 185–199.

[14] T. Taniike, P. Chammingkwan, M. Terano, *Catal. Commun.*, **2012**, *27*, 13–16.

[15] P. Chammingkwan, V.Q. Thang, M. Terano, T. Taniike, *Top. Catal.*, **2014**, *57*, 911–917.

[16] P. Chammingkwan, Y. Bando, M. Terano, T. Taniike, *Front. Chem.*, **2018**, *6*, 524.

[17] Y. Bando, P. Chammingkwan, M. Terano, T. Taniike, *Macromol. Chem. Phys.*, **2018**, *219*, 1800011.

[18] T. Taniike, T. Funako, M. Terano, *J. Catal.*, **2014**, *311*, 33–40.

[19] L. Kumari, W.Z. Li, C.H. Vannoy, R.M. Leblanc, D.Z. Wang, *Ceram. Int.*, **2009**, *35*, 3355–3364.

[20] X. Ma, H. Ma, X. Jiang, Z. Jiang, *Mater. Res. Bull.*, **2014**, *56*, 113–118.

[21] W. Yang, Z. Zhu, J. Shi, B. Zhao, Z. Chen, Y. Wu, *Powder Technol.*, **2017**, *311*, 206–212.

[22] J. M. Hanlon, L. B. Diaz, G. Balducci, B. A. Stobbs, M. Bielewski, P. Chung, I. Maclaren, D. H. Gregory, *CrystEngComm*, **2015**, *17*, 5672–5679.

Chapter 5

General Conclusion

5.1. General Summary

In this thesis, synthesis of ultrahigh molecular weight polyethylene (UHMWPE) particles was attempted using Ziegler-Natta catalyst with magnesium oxide as a carrier. The results are summarized below.

In Chapter 1, structure, properties and applications of polyethylene, history, and development of olefin polymerization catalysts, the structure of $MgCl_2$ support, particle growth and polymer morphology control, and the chain entanglement of UHMWPE were mentioned based on the objectives of this dissertation.

In Chapter 2, UHMWPE was synthesized using $MgO/MgCl_2/TiCl_4$ core-shell catalysts. The catalyst preserved the morphology of MgO nanoparticles. As a result of the ethylene polymerization, the catalyst surface area and the ethylene polymerization activity showed a linear relationship. On the other hand, since the catalyst particles were agglomerated in the polymerization solvent, the particle size of the obtained UHMWPE was coarse. It was possible to partially disperse the catalyst particles in the polymerization solvent by MgO surface treatment with methyl oleate. The small size UHMWPE particles were obtained using methyl oleate modified catalysts. Thus, the present chapter 2 proposes an alternative catalyst system for the production of UHMWPE particles, which is advantageously featured with synthetic simplicity and a dramatically

reduced Cl content.

In Chapter 3, $MgO/MgCl_2/TiCl_4$ core-shell catalysts were attempted to improve agglomeration to synthesize UHMWPE fine particles. In this chapter, a truly nano-dispersed Ziegler-Natta catalyst was first synthesized. It was possible to highly disperse the catalyst in the polymerization solvent by treating the surface of MgO with an organic modifier. It was confirmed that UHMWPE fine particles synthesized using the catalyst are comparable in particle diameter estimated from the particle size of the catalyst and polymerization activity and that the particle diameter of UHMWPE can also be controlled through the particle size of MgO. Smaller UHMWPE fine particles as compared with conventional products while maintaining high catalytic activity were achieved. The UHMWPE fine particles had a lower fusion temperature than synthesized with typical catalyst, and the molded article showed high scratch resistance.

In Capter4, an attempt was made to control catalyst agglomeration to facilitating the handling of the catalyst nanoparticle. Spherical catalyst secondary particles could be obtained by using spray drying. Morphological change of MgO nanoparticles to $Mg(OH)_2$ plate was confirmed with water in the suspension solution. The catalyst particles maintained the morphology before preparation as in Chapter 2 and 3. Polymer particles having a spherical morphology like a wool ball in which the coil polymer was aggregated

were achieved. The polymer particles were fused at a low temperature as Chapter 3. It was possible to synthesize large spherical polymer particles with the same properties as in Chapter 3 with the catalyst secondary particles agglomerated using spray drying.

5.2. Conclusion

UHMWPE has excellent characteristics such as high impact strength, sliding property and abrasion resistance. However, due to its high melt viscosity, it is difficult to process by a conventional molding method, and it is processed by a particular molding method. In this molding method, layered peeling due to no uniform structure and defective bonding of particle interfaces due to pores is a problem. Therefore, fine particles with a fine particle shape are required. Further, since it cannot be pelletized and polymerized powder is directly used for molding, the form of polymerized powder directly affects the molded article. Hence, morphological control of polymerized powders is important. Many polyolefins including UHMWPE is synthesized by Ziegler-Natta catalyst. In order to prevent fouling due to crushing and agglomeration of particles during polymerization, much research has been done on the influence of catalyst morphology on polymerized powder. Conventional catalyst preparation methods are difficult to operate, and in particular, there have been few examples of synthesis of nano-sized catalyst

particles. Therefore, there is no example of synthesizing microparticles of UHMWPE directly from the catalyst. This study was able to control the catalyst particle diameter by the support particle size by using MgO nanoparticles as a carrier and synthesized primary particles of nm size directly. Since the catalyst can be easily obtained only by treating MgO nanoparticles with $TiCl_4$, the catalyst preparation process is largely simplified. Also, since only the outermost surface of the MgO particles is catalyzed, the Cl component can be remarkably reduced as compared with the conventional catalyst. The particle diameter of the UHMWPE particles synthesized by the catalyst primary particles is several μm, which is far smaller than the industrially synthesized degree of 70-200 μm. Hence, reduction of molding temperature accompanying decrease of fusion temperature of particles and improvement of physical properties by reduction of gaps between particles could be achieved. On the other hand, by adjusting agglomeration of primary particles as a structural unit by a spray dry method, a bottom-up design that controls the morphology of secondary particles was made possible. The synthesized UHMWPE particles had the same molding processability as polymer particles of several μm. Hence, the findings obtained in this study will contribute to the expanded use of UHMWPE.

Achievements

Publications

Original Articles

[1] "Synthesis of Ultrahigh Molecular Weight Polyethylene Using MgO/$MgCl_2$/$TiCl_4$ Core–Shell Catalysts"

Yusuke Bando, Patchanee Chammingkwan, Minoru Terano, Toshiaki Taniike

Macromolecular Chemistry and Physics, **2018**, *219*, 1800011.

[2] "Nano-Dispersed Ziegler-Natta Catalysts for 1 μm-Sized Ultra-High Molecular Weight Polyethylene Particles"

Patchanee Chammingkwan, Yusuke Bando, Minoru Terano, Toshiaki Taniike

Frontiers in Chemistry, **2018**, *6*, 524.

Patent

[1] “A Method to Produce a Well-dispersed MgO Nanoparticle-Based Ziegler-Natta Catalyst, and Usage in Producing Ultra High Molecular Weight Polyethylene” Taniike Toshiaki, Chammingkwan Patchanee, Bando Yusuke, Strauss Roman, Sinthusai Likhasit

WO 2018/123070 A1

Presentations

International Conference

[1] "Fabrication of Ultra-High Molecular Weight Polyethylene Fine Particles by $MgO/MgCl_2/TiCl_4$ Core-Shell Nanocatalyst"

Yusuke Bando, Patchanee Chammingkwan, Minoru Terano, Toshiaki Taniike

Asian Polyolefin Workshop 2015 and World Polyolefin Congress 2015, Tokyo, Japan, November, 23-27, 2015.

[2] "Ultra-High Molecular Weight Polyethylene Micro-fine Particles Synthesis Using $MgO/MgCl_2/TiCl_4$ Core-Shell Nanocatalysts"

Yusuke Bando, Patchanee Chammingkwan, Minoru Terano, Toshiaki Taniike

Asian Polyolefin Workshop 2017, Tianjin, China, October, 23-27, 2017

Acknowledgment

I would like to express my deepest gratitude to Associate Professor Dr. Toshiaki Taniike who offered continuing support and constant encouragement. I would also like to thank Assistant Professor Dr. Patchanee Chammingkwan whose opinions and information have helped me very much throughout the production of this study. I wish to express my gratitude to laboratory members for their kind encouragement. I appreciate Tosoh Finechem Co. for the donation of the reagent. This research was conducted under the financial support of the IRPC Public Company Limited. Finally, I am deeply grateful to Professor Dr. Minoru Terano gave me a kindly support.

Yusuke Bando

Taniike Laboratory,
School of Materials Science,
Japan Advanced Institute of Technology

March 2019

Sub-theme report

Influence of material properties such as viscosity and density on flow mark

by

Yusuke BANDO

Supervisor for sub-theme: Tetsuya TADANO

(KOJIMA Industries Corporation)

Supervisor for sub-theme in JAIST: Prof. Tatsuo KANEKO

School of Materials Science

Japan Advanced Institute of Science and Technology

September 2018

1. Introduction

Polypropylene(PP) is one of general purpose plastics consists of only of hydrogen and carbon that does not contain any harmful substances such as chlorine and aromatic compounds. Therefore, recycling and reusing are more straightforward than other materials, and they are low environmental impact materials. Also, since its characteristics as a material are inexpensive, lightweight, high melting point, high chemical resistance, high strength, excellent mechanical properties, and high moldability, the application range is used automotive parts, package, and containers. It has been demanded further development of PP material in the future as well[1].

In general, most of the PP is produced using Ziegler-Natta catalyst. Numerous attempts through catalyst modification have been made so far for improving a PP ability such as activity and tacticity to produce PP of good quality such as morphology and strength at low cost and mass production. Therefore, compared to the industrialized 1950's catalyst, the activity was 50 times or more, and the tacticity was improved from 90% to 99%. However, the required performance of PP have been diversified; correspondence has become difficult. Most of the PP materials have been developed to make them flexible in many industrial applications by copolymerization which is polymerizing two or more kinds of monomers, polymer alloy which is technology to mix

different polymers and polymer composite which is techniques of adding inorganic compounds, *etc*. as fillers. Therefore, PP composite materials have been actively studied alongside the development of the catalyst[2−5].

PP composite materials are prepared by melt-mixing with rubber component and filler in ethylene propylene rubber and used in various scenes as parts of automobiles and home appliances due to their excellent mechanical properties. Recently, it has been used for large products such as bumpers and console side panels, and surface appearance is required in addition to mechanical properties. There are various improper appearances, such as haze, heat mark, silver streak, weld line, flow mark and so on, but flow marks have been a problem from long before, especially for long flow length products.

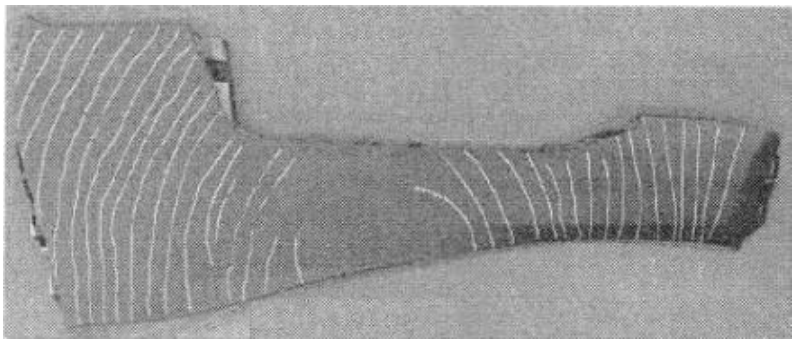

Figure 1 flow mark of the molded article.

It is well known that the flow mark is a striped pattern caused by the flow of the resin, such as a record stripe flow mark formed by flowing like a resin wavily waves, an anti-phase flow mark formed by vibration of resin flow and an in-phase flow mark formed by

a molten resin popping out. There is a study that visualized inside of the mold, and the flow of the resin is observed, it is indicated that the occurrence of flow marks is due to the flow front of the resin at the injection is flowing in an unstable condition[6]. In general, it is said that flow marks are hard to appear in resins with large die swell, but the detailed corrective action is not known[7−10].

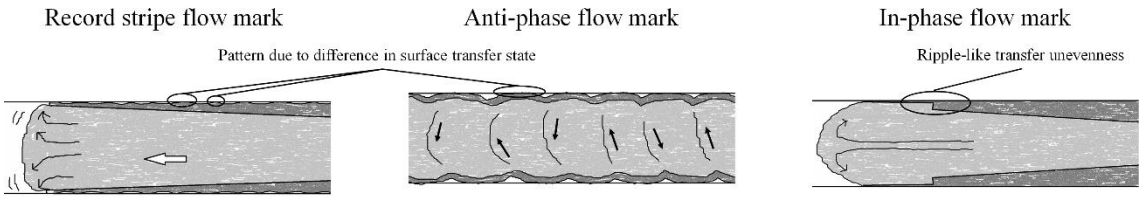

Figure 2 Types of flow marks

In this report, the flow mark of the test pieces which are prepared using four types of PP pellets, five types of rubber and talc was observed to investigate the physical properties most affecting flow mark in existing materials.

2. Experimental

2.1. Materials

PP Pellets, rubber, and talc were used things provided by the company. The physical properties of PP pellets and rubber shown in Tabele1, 2 and Figure 1.

Table 1 Information on PP pellet.

	Swell ratio	M_W	Molecular weight distribution
PP A	1.35	307,000	7.29
PP B	1.44	311,000	7.23
PP C	1.39	344,000	8.60
PP D	1.70	482,000	18.7

Table 2 Information on rubber.

	Density (g/cm^3)	Melt index (g/10 min)	Mooney viscosity (ML)	Durometer hardness (A-)	T_m (°C)	T_g (°C)	Flexural modulus（MPa）	Tensile strength（MPa)
Rubber A	0.864	13.0	4.00	63	56.0	-55.0	7.30	2.40
Rubber B	0.902	1.00	20.0	89	99.0	-31.0	81.5	24.8
Rubber C	0.87	1.00	24.0	73	60.0	-52.0	13.1	9.80
Rubber D	0.87	30.0	2.00	72	65.0	-54.0	10.5	2.80
Rubber E	0.902	30.0	2.00	88	96.0	-36.0	72.0	11.3

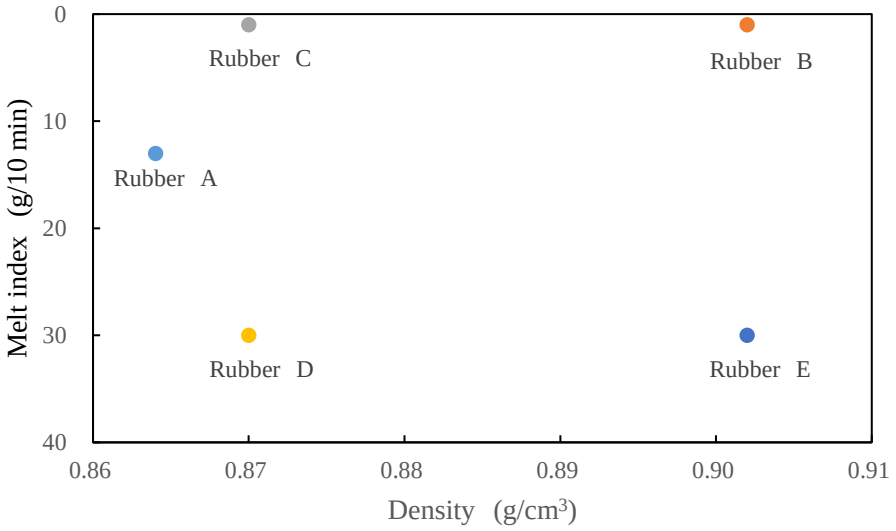

Figure 3 The relationship on rubber between melt index and density.

2.2. Analysis of PP pellets and rubber

The rate of propylene and ethylene in PP pellets was determined using ATR-IR. The percentage of propylene and ethylene was determined by using a calibration curve from the intensity ratio of the propylene-derived peak (ca. 974 cm^{-1}) and ethylene-derived peak (ca. 721 cm^{-1})[11]. The rubber component content was determined to separate the rubber component in the PP pellet. The rate of propylene and ethylene in the extracted rubber component was also established in the same manner as PP pellets. Extraction of the rubber component was carried out as follows. 5 g of PP pellets, 250 mL of xylene and 0.03 wt% of dibutylhydroxytoluene as a stabilizer are introduced into a flask equipped with a condenser. After that, heating under reflux is carried out using a mantle heater. PP pellet was utterly dissolved in xylene, and then the xylene solution is allowed

to cool down to room temperature overnight, and the precipitated white powder was separated and recovered by a centrifugal separator. Rubber components are precipitated from the remaining xylene solution using acetone as a poor solvent and classified. The obtained resin component and rubber component were heated at 60 °C for 2 hours to dry, and the amount of rubber added was determined.

2.3. Sample preparation and characterization

Test piece and dumbbell specimen were prepared using an injection molding machine. Materials were compounded at a ratio of PP 72% rubber 78% talc 20%. The molding was carried out at 200°C of molding temperature, 40°C of mold temperature, and 200 mm/s of a resin speed. Charpy impact test and tensile test were carried out using a dumbbell specimen to characterize physical property evaluation. The flow mark on the surface of the test piece was observed by measuring the gloss of three places, right and left, and center. As shown in Figure 3 and Equation (1), the average value of the difference between the peak top and peak bottom of the measured gloss value was set to ΔG.

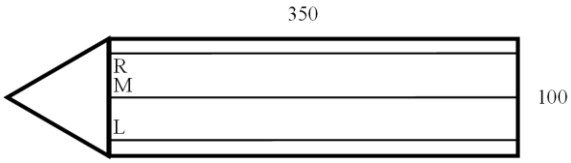

Figure 4　Test pieces.

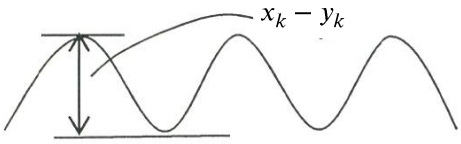

x : Glossy part (Top)
y : Cloudy part (Bottom)

Figure 5　Gloss on the surface of flow mark.

$$\Delta G = \sqrt{\frac{\sum_{k=1}(x_k - y_k)^2}{n}} \quad \text{.....Eq. (1)}$$

3. Results and discussion

Sample A, B, C, and D were prepared to add rubber A and talc to PP A, B, C, and D, respectively, and molded at an injection speed of 60%, and then ΔG was measured.

Table 3　Result of flow mark observation using gloss.

	ΔG	ΔG'(150-250 mm)	Number of flow marks (10 cm^{-1})
Sample A	4.45	5.00	5
Sample B	1.55	1.18	7
Sample C	3.93	3.41	5
Sample D	1.35	0.483	11

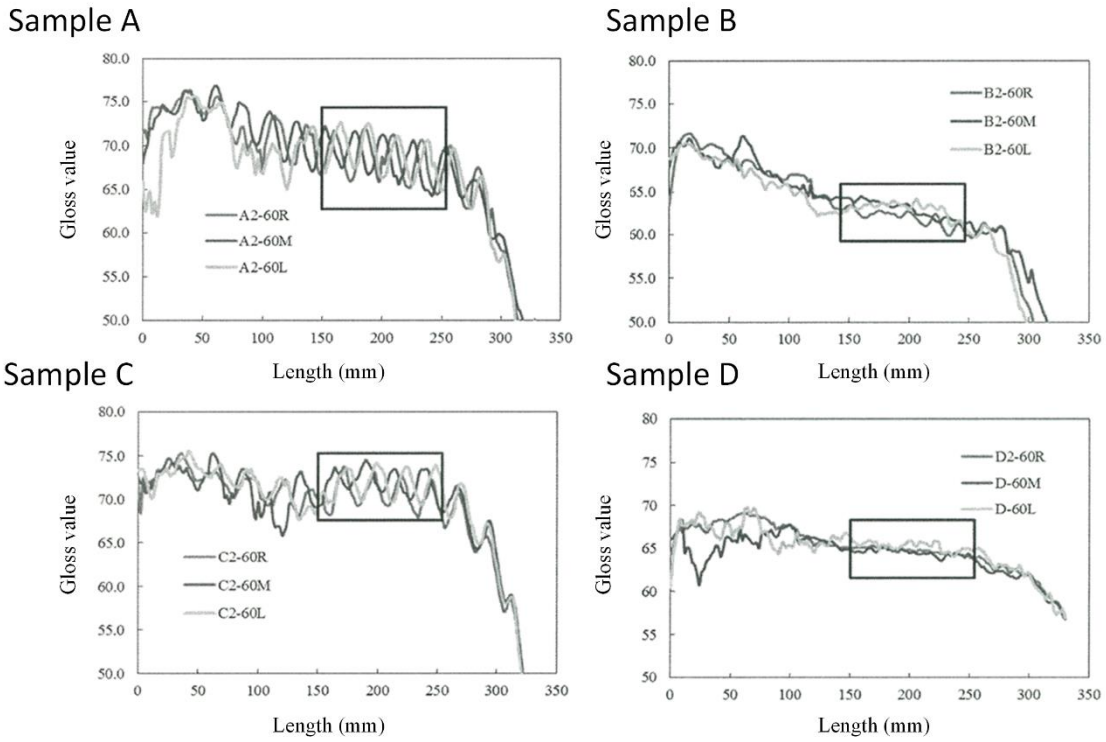

Figure 6 Gloss on the surface of flow mark.

In Figure 4, the gloss value near the gate is unstable on all sample. However, there was no significant turbulence seen from the beginning to the end of the flow mark on the appearance. Therefore, it decided to use a range of 150-250 mm for evaluation as ΔG' which is numerically stable. Sample D had the smallest ΔG', and flow mark could not be observed.

Next, injection molding was carried out while changing the injection speed to 30% and 90%.

Table 4　Effect of injection speed.

	Injection speed (%)	ΔG’
Sample A	30	4.05
	60	5.00
	90	3.86
Sample B	30	1.46
	60	1.18
	90	0.993
Sample C	30	4.99
	60	3.41
	90	3.00
Sample D	30	0.544
	60	0.483
	90	0.751

In sample A, B, and C, ΔG' decreases as the injection speed increases. On the other hand, in sample D, ΔG' increased with injection speed rises. However, flow mark could not be observed in any test pieces on sample D.　This is because the amplitude of the measured wave of sample D was small compared to others.

Table 5 Effect of PP pellet physical properties.

	ΔG	Charpy (kJ/m^2)	MVR (cm^3/min)	PP pellet				
				Swell ratio	M_W	Molecular weight distribution	Rubber amount (wt%)	Ethylene amount* (%)
Sample A	5.00	36.5	28.2	1.35	307,000	7.29	17.2	42.4
Sample B	1.18	16.6	27.5	1.44	311,000	7.23	12.8	65.6
Sample C	3.41	44.7	18.4	1.39	344,000	8.60	16.7	44.4
Sample D	0.483	4.70	65.7	1.70	482,000	18.7	6.97	30.8

* Amount of ethylene in rubber

The Charpy value of material D is almost the same as generally untreated PP. Sample D has the highest swell ratio, and dispersion degree is the lowest ΔG'. The reason for this is considered that sample D is good liquidity due to the swell is high, and the molecular weight distribution is wide. Therefore, it is considered that flow marks are less likely to appear ones with low viscosity. In sample B, the ethylene ratio in EPR is the largest and ΔG' is low.

Injection molding was carried out by changing the addition amount of rubber A.

Table 6　Effect of rubber amount.

	ΔG'
x0.50	4.51
x1.0	4.45
x2.0	5.38

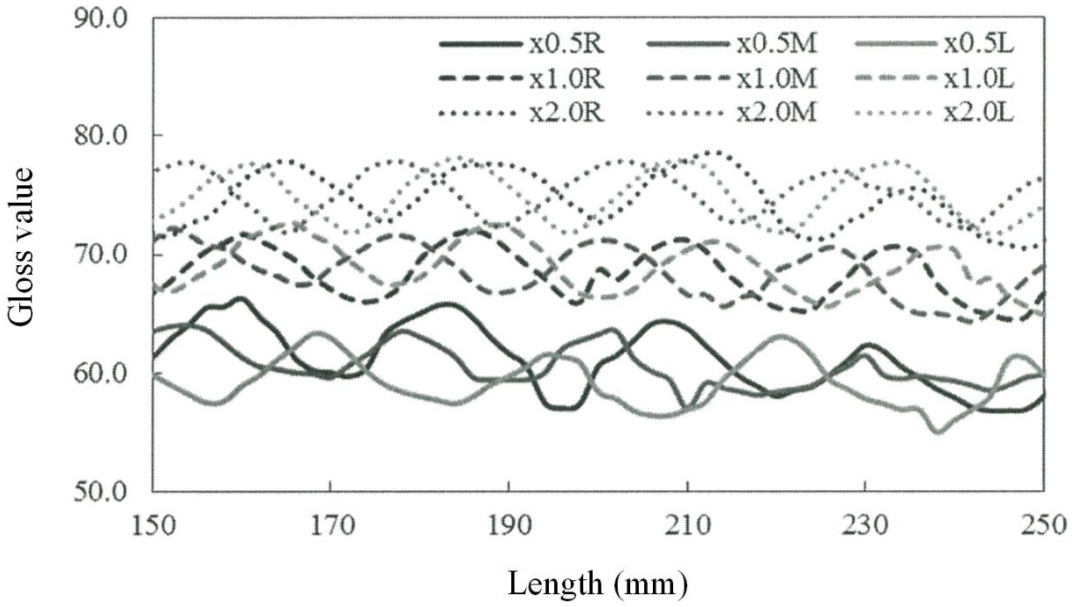

Figure 7　Gloss on the surface of flow mark.

Reducing the amount of rubber to be added reduces a certain amount of flow marks, but when the amount exceeds a certain amount, the effect is reduced.

Table 7　Effect of rubber physical properties.

	ΔG'
Rubber A	1.18
Rubber B	0.91
Rubber C	1.05
Rubber D	1.18
Rubber E	1.81

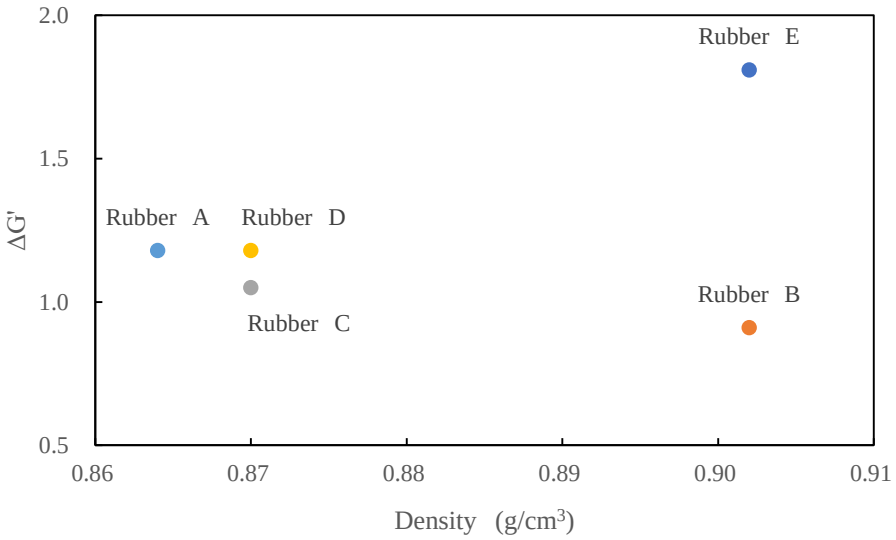

Figure 8　Relationship between rubber density and flow mark.

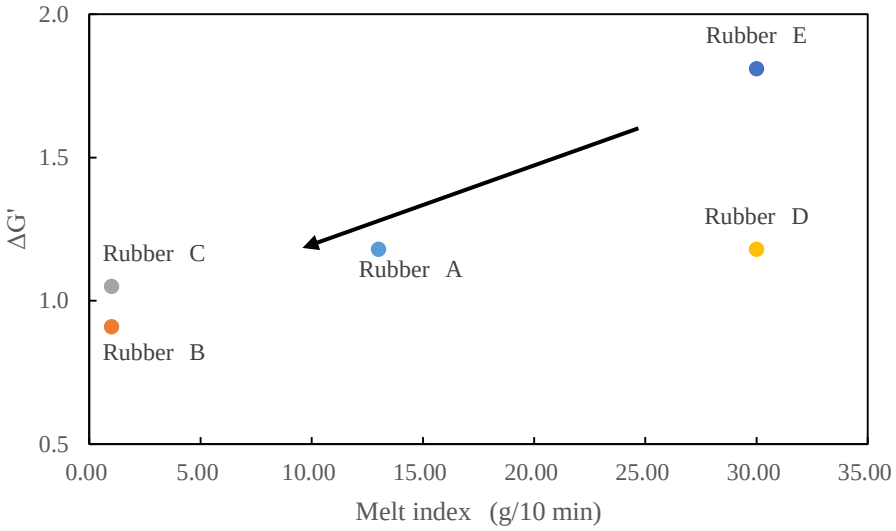

Figure 9 Relationship between rubber melt index and flow mark.

Finally, injection molding was carried out using five types of rubber with different density and melt index, and PP B. PP B was used because the mechanical properties are useful to some extent and ΔG' is small. Although rubber B has a high density, ΔG' is the lowest. It seems that the melt index has an influence on flow mark rather than density. The addition of rubber with a low melt index overall appears to be sufficient for flow mark. Rubber B was the most effective in this result.

4. Conclusion

Flow marks are affected by physical properties of PP and rubber to be added. In this study, flow marks are quantified by measuring the gloss value and evaluated. As a result of examination of the PP pellet series, it was found that the content of EPR is low and those with a large number of ethylene units are useful for reducing flow marks. It was found that as a rubber to be added, one having a low melt index (high molecular weight) is active.

5. Acknowledgment

The author greatly appreciates to Matsumoto, Tadano and Kurahashi in KOJIMA Industries Corporation, for many bits of help, advice and kind cooperation for the experiments. This work was kindly supported by all the members of KOJIMA Industries Corporation. The author is deeply grateful for the kind suggestion of Prof. Kaneko. Finally, the author profoundly appreciates to the president and representative director Kojima and Prof. Taniike for giving me a precious chance to work at KOJIMA Industries Corporation.

Reference

[1] Next Generation Polyolefin, Voll.11, Sankeisha, Japan, **2017**.

[2] H. Shi, T. Lan, T.J. Pinnavaia, *Chem. Mater.*, **1996**, *8*, 1584–1587.

[3] C.H. Wu, A.C. Su, *Polym. Eng. Sci.*, **1991**, *31*, 1629–1636.

[4] R. Zacur, G. Goizueta, N. Capiati, *Polym. Eng. Sci.*, **1999**, *39*, 921–929.

[5] S. Cheruthazhekatt, T.F.J. Pijpers, V.B.F. Mathot, H. Pasch, *Macromol. Symp.*, **2013**, *330*, 22–29.

[6] S. Owada, H. Yokoi, *AIP Conf. Proc.*, **2016**, *1713*, 040001.

[7] B. Patham, P. Papworth, K. Jayaraman, C. Shu, M.D. Wolkowicz, *J. Appl. Polym. Sci.*, **2005**, *96*, 423–434.

[8] K. Hirano, Y. Suetsugu, T. Kanai, *J. Appl. Polym. Sci.*, **2007**, *104*, 192–199.

[9] M. Yoshii, H. Kuramoto, T. Kawana, K. Kato, *Polym. Eng. Sci.*, **1996**, *36*, 819–826.

[10] H. Hamada, H. Tsunasawa, *J. Appl. Polym. Sci.*, **1996**, *60*, 353–362.

[11] S. Tanaka, N. Takeuchi, K. Takemoto, F. Nakamura, *Reports Cent. Cust. Lab.*, **2006**, 65–68.